Mechanistic insights into alpha-Synuclein neuronal toxicity: misfolding, serine phosphorylation and interactions with Rab GTPases

Dissertation

zur Erlangung des mathematisch-naturwissenschaftlichen Doktorgrades

"Doctor rerum naturalium"

der Georg-August-Universität Göttingen

vorgelegt von

Guowei Yin

aus Kunming, China

Göttingen, 2012

Mitglied des Betreuungsausschusses (Referent): Prof. Dr. Christian Griesinger
NMR-basierte Strukturbiologie, Max-Planck-Institut für biophysikalische Chemie

Mitglied des Betreuungsausschusses (Koreferent): Prof. Dr. Gerhard Braus
Mikrobiologie und Genetik, Georg-August-Universität Göttingen

Mitglied des Betreuungsausschusses: Prof. Dr. André Fischer
European Neuroscience Institute Göttingen

Mitglied des Betreuungsausschusses: Prof. Dr. Markus Zweckstetter
NMR-basierte Strukturbiologie, Max-Planck-Institut für biophysikalische Chemie

Tag der mündlichen Prüfung:

Affidavit

I hereby declare that this dissertation has been written independently and with no other sources and aids than quoted.

.....

Guowei Yin

Abstract

Alpha-Synuclein(αS), a protein abundant in presynaptic neurons, has been found as the major component of Lewy bodies, the neuronal inclusion identified as the hallmark of Parkinson's disease (PD). αS adopts intrinsically disordered conformation under physiological conditions and possesses a high propensity for assembling into oligomers and fibrils during the pathological process of PD. Although the pathology of PD is still elusive, several lines of evidence with respect to the neuronal toxicity, cellular physiology, and protein structure indicate that αS plays an important role in the development of PD and affects the normal cellular functions. In this dissertation we study the molecular mechanisms of serine phosphorylation, the interaction with Rab-GTPases and the aggregates structure of αS.

Phosphorylation is a major posttranslational modification of αS. Approximately 90% of αS in LB is phosphoylated at Ser129, but the pathological role of phosphorylation has still not been determined. Ser87 is also an important serine phosphorylation site located at NAC region. To understand the mechanisms of phosphorylation, we investigate phosphorylation kinetics and the effects of phosphorylation on αS aggregation. Real-time NMR spectroscopy is employed to study the phosphorylation kinetics of the Ser87 and Ser129 of αS. With the aid of the residue-specific resolution provided by NMR spectroscopy we reveal that the three familial mutations A30P, E46K, and A53T do not change the phosphorylation kinetics of Ser87 but slightly modify the kinetics of Ser129. At the same time, under the conditions of our assay, we also identify that PLK2 and PLK3 are capable of phosphorylating αS at Ser129 with high selectivity and efficiency. Furthermore, we find that phosphorylation

of Ser129 by PLK3 and the phosphorylation mimicking mutants (P128E/S129E and M127E/P128E/S129E) do not affect the aggregation propensity of αS.

Rab GTPases are important for the regulation of vesicle trafficking in eukaryotic cells. Rab1, Rab3a, and Rab8a were suggested to protect against αS-induced cellular toxicity in different model systems. Focusing on molecular mechanisms involved in the interplay between Rab proteins and αS, we firstly identify that both the GDP- and GppNHp-bound Rab8a bind to the C-terminus of αS. However, αS has a higher affinity to Rab8a(GDP) than Rab8a(GppNHp). Secondly, the positively charged C-terminal peptide of Rab8a is found to reproduce the binding of full-length Rab8a to αS, suggesting that a charge complementation between the C-terminal of both proteins is important for the interaction. Furthermore, we have assigned Rab8a in the GDP-bound state and find that in addition to the C-terminus the Switch I region of Rab8a serves as a binding site for the αS C-terminus. Since the conformation of switch regions is highly dependent on nucleotide binding, this finding elucidates the binding preference for the GDP-bound state. Furthermore, Rab8a enhances the aggregation of αS in both oligomerization and fibril formation. Rab1b and Rab3a do not bind to αS but they can also significantly enhance the fibril formation of αS. Taken together, our results demonstrate a tight interplay between αS and Rab proteins at the molecular level.

Furthermore, αS aggregates, namely oligomers and fibrils, are highly associated with PD pathology. We perform solution NMR based hydrogen/deuterium (H/D) exchange to detect the fibril core of E46K and A53T αS fibrils. These two mutations do not cause drastic changes to the fibril core structures in comparison to *wt*-αS and a conserved core region has been suggested for *wt*-αS and the three familial mutants. Furthermore, we optimize the H/D exchange method to detect the conformation of compounds-stabilized αS oligomers. Our results suggest that the compounds-stabilized oligomers do not contain strongly hydrogen-bonded regions.

Acknowledgements

I would like to thank Prof. Dr. Christian Griesinger for offering me this invaluable opportunity to undertake my thesis in this department for providing excellent facilities, research environment and continuous supports.

I would like to thank Prof. Dr. Markus Zweckstetter for his direct supervision, illuminating discussions, facilitation of knowledge transfer, and critical judgment throughout my thesis.

I would like to thank Prof. Dr. Gerhard Braus, Prof. Dr. Andre Fischer from the Georg-August-Universität Göttingen for their membership of my thesis committee and helpful suggestions during the committee meeting.

I am very grateful to Dr. Stefan Becker, Karin Giller and Sebastian Wolff for their preparations of alpha-Synuclein samples and help in the wet lab. I would thank Gerhard Wolf and Kerstin Overkamp for the HPLC manipulation and the peptide synthesis respectively. I would also thank our secretaries Mrs. Silberer and Mrs. Breiner, our IT system administrators Dr. Dirk Bockelmann and Jürgen Arve for their daily supports.

I would like to extend my thanks to Prof. Dr. Aymelt Itzen and Prof. Dr. Roger Goody from Max-Planck-Institute of Molecular Physiology, Dortmund for the continuous supply of the Rab protein samples and helpful suggestions in the project.

I would like to thank Prof. Dr. Tiago Fleming Outeiro from University Medical Center Göttingen for the collaboration in the Rab project and for accepting the request to be a member of my thesis defense committee. I would also like to thank Sibylle Eisbach, Tomás Lopes da Fonseca in the Outeiro's lab for the enjoyable experience of collaboration and our many discussions.

I would like to thank Prof. Dr. Hilal Lashuel, Katerina E. Paleologou, Martial K. Mbefo from EFPL, Lausanne, for the collaboration in the phosphorylation projects.

I would like to thank Dr. Dietmar Riedel and Gudrun Heim for recording the electron microscopy for me.

I would like to thank Sergey Ryazanov and María L. Orcellet for the nice collaborations and sharing the research experience. I would like to thank Dr. Min-kyu Cho and Dr. Hai-young Kim for introducing the projects to me at the beginning and sharing valuable experiences with me throughout the thesis process. I would like to thank Shengqi Xiang for the instruction of NMR experiments and wet lab and many helpful discussions. I would like to thank Dr. Nasrollah Rezaei-Ghaleh for help in biophysical analysis and NMR experiments. I would like to thank Rakhi Bajaj, Saskia Villinger and Han Sun for their help in my thesis writing.

I would like to thank my all the current and former colleagues in our department for their support and friendship.

I would like to also thank Prof. Micheal Hörner, Chiritina Bach, Christin Fischer and other persons in the GGNB team for their kind help and excellent organization of the course and academic activities.

Finally, I would like to thank my family. I would express my overwhelming gratitude to my parents for their untiring support and consideration. Thanks to my wife Yuhuan for her love and companionship, and for our son. Thanks finally to my grandfather who passed away last year for his lifelong encouragement and advice which will remain with me always.

Table of contents

Abbreviations

αS	Alpha-Synuclein
ATP	Adenosine-5'-Triphosphate
AmppNHp	5′-Adenylylimidodiphosphate
BEST	Band-selective Excitation Short-Transient
BSA	Bovine serum albumin
CK1	Casein kinase 1
CNS	Central nervous system
CSA	Chemical shift anisotropy
DA	Dopamine
DMSO	Dimethyl sulfoxide
DOSY	Diffusion ordered spectroscopy
DTT	Dithiotreitol
DLS	Dynamic light scattering
E. coli	*Escherichia coli*
ER	Endoplasmic reticulum
GDP	Guanosine diphosphate
GTP	Guanosine triphosphate
GuSCN	Guanidinium thiocyanate
H/D	Hydrogen/Deuterium
HSQC	Heteronuclear single quantum coherence
HPLC	High performance liquid chromatography
IPAP	In-phase-anti-phase
hr	hour

HSPs	Heat shock proteins
INEPT	Insensitive nuclei enhanced by polarization transfer
K_d	Dissociation constant
LB	Lewy body
LRRK2	Leucine-rich repeat kinases 2
NAC	Non-Aβ component of Alzheimer's disease amyloid plaques
NMR	Nuclear magnetic resonance
PD	Parkinson's disease
PDB	Protein data bank
PLKs	Polo-like kinases
PRE	Paramagnetic relaxation enhancement
pS129	Phsphorylated Ser129
Rab1b-δC	C-terminally truncated Rab1b (1-175)
Rab8a-δC	C-terminally truncated Rab8a (6-176)
Rh	Hydrodynamic radius
RDC	Residual dipolar coupling
SOFAST	band-Selective Optimized-Flip-Angle Short-Transient
ThT	Thioflavin-T
TROSY	Transverse relaxation optimized spectroscopy
wt	wild-type

1 Introduction

"*Involuntary tremulous motion, with lessened muscular power, in parts not in action and even when supported; with a propensity to bend the trunk forwards, and to pass from a walking to a running pace: the senses and intellects being uninjured.*"

– James Parkinson, *"An Essay on the Shaking Palsy"*, 1817.

The symptoms of what we now call Parkinson's disease were first described by the English apothecary surgeon James Parkinson in 1817 and named "maladie de Parkinson" or Parkinson's disease (PD) in 1861 by Jean-Martin Charcot, the founder of modern neurology. In today's aging society, PD is the second most common neurodegenerative disease after Alzheimer disease and approximately 7-10 millions people worldwide are living with PD (Statistics from Parkinson's disease foundation, "PDF").

In section 1.1, I will open with an overview of the Parkinson's disease and synucleinopathies will be exerted following the order "from bedside to bench" and accordingly the motivations of the research undertaken in this dissertation will be addressed. The focus of this dissertation upon protein α-Synuclein (αS) as one major cause of PD will be introduced in section 1.1.1 and 1.1.2 in terms of its pathological, biophysical, and structural characteristics. In section 1.2, the category of intrinsically disordered proteins (IDPs) will be described particularly in terms of its general structural features and the propensity of protein misfolding. To conclude this chapter, within the scope of this dissertation, the challenges for current research of PD pathologies with respect to α-Synuclein will be listed in section 1.3.

1.1 Parkinson's Disease and Synucleinopathies

1.1.1 Parkinson's disease overview

The occurrence of Parkinson's disease is strongly age-dependent (Lees et al, 2009). The average age of onset is about 65 years old and the incidence rises from 0.6%

at age 65–69 years old to 2.6–3.5% at age 85–89 years old (de Rijk et al, 2000). The onset of Parkinson's disease commonly presents with one or a few of the following motor-symptoms: impairment of dexterity, slight dragging of one foot, fatigue, stiffness, lugubrious stiff face, hangdog appearance, flexion of one arm with lack of swing, monotonous quality to speech, extreme slowing down (Hardy et al, 2009). These early symptoms are usually difficult to notice for patients and a delay of 2-3 years from first symptoms to diagnosis is common. Nonmotor symptoms (NMS) such as depress pain, hyposmia (loss of sense of smelling), disturbed sleep, and dysautonomia start to increase progressively in frequency and severity (Chaudhuri et al, 2006). In the late sages, Parkinson's disease is characterized by a masked and expressionless face, the monotonous, festinant, and slightly slurred speech, flexed simian posture with a severe pill rolling tremor of the hands (Hardy et al, 2009). Constipation, chewing and swallowing difficulties, drooling of saliva, and urge urinary incontinence are concomitant features.

The primary pathology of Parkinson's disease is progressive dopamingernic neuron loss in the substantial nigra of the midbrain. Several genes such as SNCA (PARK1), PARK2 (PARK2), PINK1 (PARK6), PARK7 (PARK7), LRRK-2(PARK8) have been implicated in this pathology, where the protein products of these genes are α-Synulcein, PARKIN, Serine/threonine-protein kinase PINK1, DJ-1, and Leucine-rich repeat serine/threonine-protein kinase 2 (Pankratz et al, 2004). Since 2009, a large-scale GWAS genomic screen has been applied to PD and several novel putative PD-associated genes have been identified as a marked progress in genome-wide studies of PD (Hardy, 2010; Nalls et al, 2011; Satake et al, 2009; Simon-Sanchez et al, 2009).

The dominant mechanism associated with dopaminergic neuronal loss is the Lewy body pathology. The Lewy body (LB), the hallmark of PD, is one type of neuronal inclusion deposited in the disease-associated neurons and is viewed as the cause of neuron death. The major component of LB are the amyloid fibrils formed through the aggregation of protein α-Synulcein (αS) (Spillantini et al, 1997), the protein product of the SNCA gene (Polymeropoulos et al, 1997). Therefore, it is crucial to study the roles of αS in the pathological scenario of PD in terms of its biochemical and biophysical natures, aggregation pathway, toxic mechanisms, pathological regulation factors *et al*.

This is the original motivation of this dissertation. Moreover, αS is not only present in PD, rather it also gets deposited into oligodendroglial cytoplasmic inclusions in multiple system atrophy (MSA) and into large axonal spheroids in a number of rarer neuroaxonal dystrophies (Halliday et al, 2011; Spillantini & Goedert, 2000). Thus, these 3 diseases caused by the abnormal inclusion formed by αS are grouped under the single category of synucleinopathies.

To date, PD is incurable, but oral drug administration improves the life quality and functional capacity of patients. The major PD treatment is dopamine replacement therapy which aims to increase the level of dompamines in the brain to compensate for the decreased levels caused by the neuronal loss. Levodopa (L-dopa) is one of most efficient and widely used drugs because it is the precursor of dopamine and able to pass through blood brain barrier (BBB) (Schapira et al, 2006). The catechol-O-methyltransferase (COMT) inhibitors and monoamine oxidase (MAO) inhibitors are two main drugs that also reduce the metabolism of L-dopa (Huynh, 2011), whilst ergot dopamine agonists are in another class of PD drugs that delay early onset of motor complication with high efficiency (Schapira et al, 2006). However, the application of these agents can not stop the dopaminergic neuron loss and the neurdegerative disorder and current drugs in markets and in clinical trials targeting αS are rare (Huynh, 2011; Schapira et al, 2006). Recent studies indicate that the inhibitors of COMT, entacapone and tolcapone, are able to block the fibril formation of αS (Di Giovanni et al, 2010). In July 2012, it was reported that the first therapeutic antibody of PD designed to clear αS stocked in the membranes and spread between the cells has been under clinical trial (Dolgin, 2012). This antibody has been proved to reduce the neuronal loss and improve the cognition in the transgenic mouse models and trials on human have now begun.

1.1.2 Research progress of α-Synuclein

Primary sequence of α-Synuclein

αS is an intrinsically disordered protein comprising of 140 amino acids (Polymeropoulos et al, 1997) that are mainly divided into 3 fundamental domains: N-terminal (1-60), NAC (61-95) and C-terminal (96-140) (Bisaglia et al, 2009) [Figure 1.1]. The N-terminal is amphipathic with high affinity to membrane. The middle NAC

region (non amyloid component) is a highly hydrophobic part of the protein and is located in the core region of amyloid fibrils, which is crucial in fibril formation. There are seven imperfect 11-mer repeats (XKTKEGVXXXX) spread through the N-terminal to NAC region. The total number and the conserved motif "KTKEGV" of these imperfect repeats have been implicated in lipid-binding (Davidson et al, 1998)and regulating aggregation (Kessler et al, 2003). The C-terminal is acidic which is enriched in negatively charged residues with a highly disordered conformation. 3 familial pathological mutations A30P, E46K and A53T identified in the different kindred are located at the N-terminal and are highly involved in functional and pathological modification.

Protein structures and biophysics of α-Synuclein aggregation

Structural insights into αS monomers reveal that αS is intrinsically disordered but not fully denatured. High resolution NMR data indicates that αS monomer possesses the transient long range interactions between N-terminal and C-terminal of αS and thereby stabilizes tertiary structure of the protein (Bertoncini et al, 2005b; Dedmon et al, 2005c). The structural ensembles of αS mapped by the paramagnetic relaxation enhancement measured by solution NMR indicate that the long-range interactions close the protein conformation and lock the hydrophobic NAC region into a state less accessible for the NAC of neighboring αS, which is considered as the auto-inhibition mechanism of the aggregation (Bertoncini et al, 2005b). Later studies reveal that the electrostatic interactions between two termini of αS also contributed to the intermolecular interactions between the N-terminal of one αS and the C-terminal of another in a head-to-tail manner (Wu & Baum), which is in concert with the *in vivo* observation by bimolecular fluorescence complementation(BiFC) (Outeiro et al, 2008). Recent studies have suggested that the endogenous αS directly isolated from the human living cells was mainly present as the helically folded tetramer (Bartels et al, 2011). The authors discussed that the protein recombination techniques and harsh conditions of sample purification for αS commonly adopted in the labs (Weinreb et al, 1996) might be harmful to to the retention of the native folded conformation of αS. However, a later study used the same conditions to generate the αS by isolating it from the living cells and found that the generated αS was still dominantly disordered in comparison to the

sample obtained through common recombination and purifications (Fauvet et al, 2012b). Thus the accumulated evidence confirms that the physiological conformation of αS should be disordered (Bertoncini et al, 2005b; Conway et al, 1998; Weinreb et al, 1996), but the α-helix propensity of αS N-terminus enables the protein to form the helix conformation under the certain conditions i.e. membrane binding.

The intrinsic disorder and the presence of highly hydrophobic NAC region determine a strong aggregation propensity of αS. The aggregation of αS can be generally divided into 3 phases: oligomerization, fibril growth and saturation (Fink, 2006). The aggregation pathway starting from αS monomers to the final fibrils deposited in the LB in plaques of PD patient brain is demonstrated in Figure 1.1.

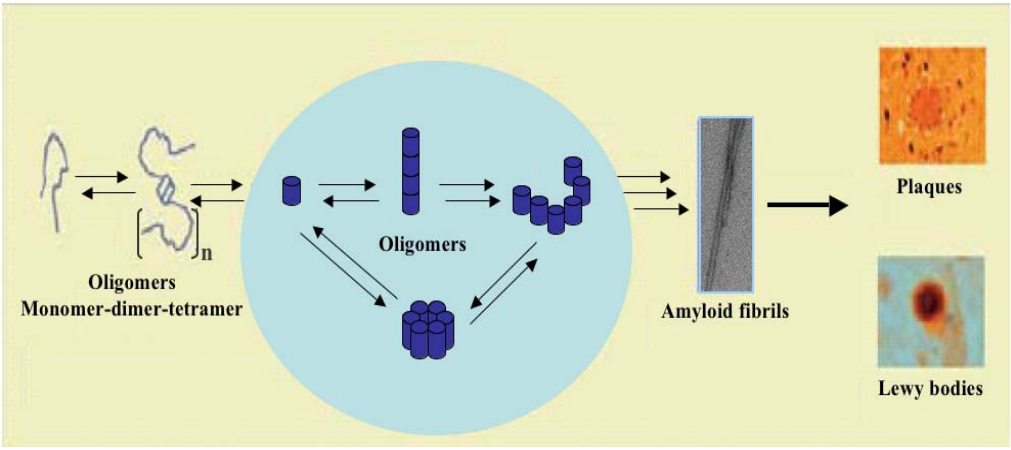

Figure 1.1 Aggregation pathway of α-Synuclein. The flowchart demonstrates the aggregation process of the oligomerization, fibrillization and deposition of LB (dark dots) observed at PD plaques. The figure is taken from (Lashuel & Lansbury, 2006).

The disordered αS monomers firstly associate with each other to form the oligomeric species. This process is kinetically defined as the nucleation period which is the rate determinating step for the whole aggregation process. The structural study of αS oligomers is of major interests and poses major challenges to understand αS neuronal toxicity. αS oligomers represent distinct shapes i.e. chain-like or annular observed by electron microscopy (EM) and atomic force microscopy (AFM) (Lashuel & Lansbury, 2006). The secondary structures of αS oligomers were indicated by CD as the β-sheet rich conformations. However, due to the nature of the aggregation intermediates i.e. structural heterogeneity and weak stability etc., αS oligomers until

now are still not characterized with high resolution. A recent study suggests that within the process of the oligomerization there is one conversion from the smaller sized oligomers to large sized oligomer and that the larger oligomers are toxic (Cremades et al, 2012). Moreover, SAXS data suggests that αS oligomers are finally assembled into fibrils with conserved size parameters, implying that mature αS oligomers act as the building blocks of αS fibrils (Giehm et al, 2011b).

As shown in figure 1.2, after the oligomerization, αS is finally assembled into the fibrils with well-defined morphorlogys. The phase from the ending of oligomerization to the final plateau phase is fibril growth which is kinetically defined as elongation. In this phase, the oligomers of αS are assembled into the protofilaments along the fibril axis direction and the protofilaments are further associated with each other to form the morphologically straight bundle or the twisted fibril. Since the amyloid fibrils of αS are stable and insoluble in water, they are readily separated and purified for further structural analysis. Therefore, the structures of the amyloid core region of αS have been well studied by high resolution methods such as ssNMR, solution NMR based H/D exchange, Mass spectrum, EPR *et al* (Chen et al, 2007; Cho et al, 2011; Comellas et al, 2011; Del Mar et al, 2005; Heise et al, 2008; Heise et al, 2005; Lemkau et al, 2012; Vilar et al, 2008). The boundaries of the fibril core region have been measured, where the core region has been extended from the NAC to ~ 37-97. However, there are discrepancies amongst the different reports regarding the locations and lengths of β-strands, involving factors such as sample preparation, the polymorphism of fibrils and different technique details of the experiments which should be taken into account to address the differences. Besides the fibril core, two termini of αS are mainly disordered. A recent report suggests that part of N-terminal residues are experiencing contact with the core region and are likely to be participating in the fibril formation (Lemkau et al, 2012). The C-terminal of αS still remains in a highly disordered nature in the fibrillar state.

Posttranslational modifications and phosphorylation

There are several posttranslational modifications (PTMs) such as phosphorylation, truncation, ubiquitination, nitration, and acetylation associated with LB formation in PD patient brains and transgenic animal models (Oueslati et al, 2010a). The effects of these PTMs of αS on the protein structure, aggregation propensity, neuronal toxicity and disease progression have not been determined. Most of PTMs are located at the C-terminus of αS. Phosphorylation is one major PTM of αS. Multiple sites such as Ser87, T92, Y125, S129, Y133, Y136 have been reported to be phosphorylated by the known kinases like CKI, PLKs, GRKs, LRRK2 *et al*. Truncation is another major PTM of αS. In LBs, the major truncation sites at the C-terminus are D115, D119, N122, Y133 and D135 (Anderson et al, 2006). Accumulating evidence suggests that the C-terminal truncations of αS enhance aggregation propensity and initiate the aggregation process by seeding both in *vivo* and in *vitro*(Hoyer et al, 2002; Li et al, 2005; Liu et al, 2005). The co-localization of ubiquitin with αS has been extensively found in LBs and Lewy neutrites (Gomez-Tortosa et al, 2000). The K12, K21 and K23 of αS have been identified as major sites responsible for ubiquitination in LBs (Anderson et al, 2006). In addition, other lysine residues are also able to be ubiquitinated *in vitro* and in cell cultures, which most of them are located at the N-terminus of αS (Nonaka et al, 2005; Rott et al, 2008). But the relationship between ubiquitination and degradation of misfoled αS by ubiquitin-mediated proteasome pathway is still elusive (Tofaris et al, 2001; Tofaris et al, 2003). A recent study indicates that ubiquitination by Nedd4 ligase promotes αS degradation by the endosomal–lysosomal pathway (Tofaris et al, 2011). Nitration is a potential mediator of PD and other neurodegenerative diseases (Souza et al, 2000). There are 4 tyrosine residues, Y39, Y125, Y133 and Y136, which can be nitrated in αS. The selectivity and specificity of different tyrosines is linked to the onset and progression of synucleinopathies (Giasson et al, 2000). N-terminal acetylation of αS has been less studied than other PTMs mentioned above and only recently has been focused on its effects on protein conformation, lipid-binding, aggregation propensity (Bartels et al, 2011; Fauvet et al, 2012a; Kang et al, 2012; Maltsev et al, 2012).

Phosphorylation is the dominant PTM and the phosphorylation sites at C-terminal are highly conserved through the different species [Figure 1.2] (Hejjaoui et al,

2012; Oueslati et al, 2010a). Of the Ser, Tyr and Thr phosphorylation, Ser phosphorylation has been extensively studied due to its prevalence in PD. Approximately 90% of αS has been identified as phosphorylated at Ser129 of αS. However, there are several key issues with respect to this phosphorylation which remain elusive: 1) which kinases are responsible for regulating this phosphorylation; 2) what is the consequence of this phosphorylation on αS structure *in vivo*; 3) whether this phosphorylation facilitates, inhibits or has no affect on αS aggregation; 4) dose phosphorylation occur before or after αS aggregation and LB formation; 5) how does this phosphorylation modulate the neuronal toxicity of αS. Several kinases are involved in the Ser129 phosphorylation. Polo-like kinase (PLKs), G protein-coupled receptor kinases (GRKs), LRRK2, and Casein kinase II (CKII) are reported to specifically phosphorylate αS at Ser129 (Oueslati et al, 2010a). CKI is a kinase that is able to phosphorylate αS at both Ser87 and Ser129. NMR studies point out that phosphorylation of Ser87 and Ser129 together or individually can extend the conformation of αS *in vitro* (Paleologou et al, 2010; Paleologou et al, 2008). The phosphorylation of Ser87 and its mutation mimics exclusively inhibit the fibril formation of αS (Paleologou et al, 2010). But at Ser129, the major phosphorylation site, the effect of phosphorylation at this residue on αS aggregation still needs to be determined. Recent studies indicating that αS fibrils are able to be phosphorylated at Ser129 *in vitro* and that this phosphorylation is likely independent of aggregation, suggesting that this modification can occur after aggregation (Mbefo et al, 2010; Waxman & Giasson, 2011). One central issue is to investigate the effects of phosphorylation on aggregation behavior and toxicity of αS *in vivo*. However, the related results obtained from different animal models present large diversity, which due to the model difference and partially due to the mimics can not completely reproduce the effects of real phosphorylation (Braithwaite et al, 2012; Oueslati et al, 2010a). Interestingly, in the SH-SY5Y cell model, it's suggested that Ser129 phosphorylation activates ER stress by inducing unfolded protein responses (UPRs) which is possibly caused by the disruption of ER-Golgi trafficking (Sugeno et al, 2008). On the other hand, Ser129 phosphorylation is suggested to suppress αS-induced vesicle trafficking deficit depending on genetic context in yeast model (Sancenon et al, 2012). These two

findings together suggest that Ser129 phosphorylation possesses a potential role in regulating vesicle trafficking.

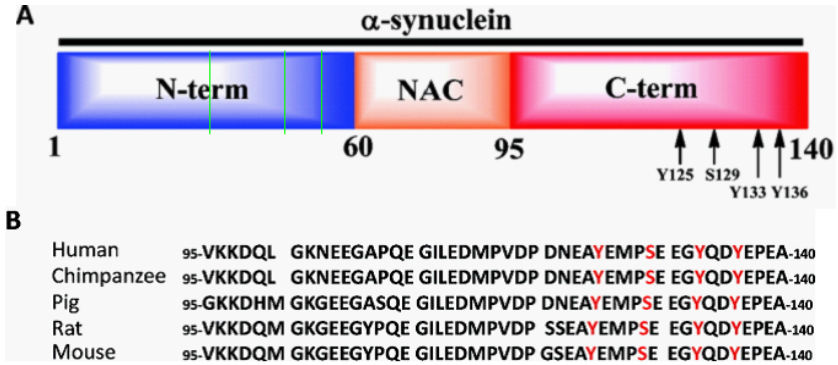

Figure 1.2 Primary structure of αS. (A) Schematic depiction of αS sequence with its 3 domains. The positions of 3 familial mutations at the N-terminal are indicated by green lines. Identified and putative phosphorylation sites at C-terminal are indicated by black arrows. (B) Sequence analysis for the C-terminal from 5 different species indicates that the phosphorylation sites are highly conserved. Figures are taken from (Hejjaoui et al, 2012).

Alpha-Synuclein affects vesicle trafficking and its interplay with Rab-GTPases

Several lines of evidence suggest that αS is involved in the vesicle trafficking in synaptic neurons. αS was reported to assist synaptic vesicle recycling and neurotransmitter release (Ben Gedalya et al, 2009; Liu et al, 2004). αS ameliorated the neurodegeneration caused by the depletion of cysteine-string protein-alpha (CSPalpha), which suggests it has a positive role in co-operation with CSPalpha and SNAREs (Chandra et al, 2005). Moreover, it has been suggest that αS has a role in the maintenance of synaptic vesicle pools (Cabin et al, 2002; Murphy et al, 2000), activity-dependent dopamine release (Abeliovich et al, 2000) and as a negative regulator of the vesicle priming (Larsen et al, 2006). However, more commonly, altering the expression levels and biophysical properties of αS and its familial mutants leads to the deficits of vesicle trafficking at multiple steps in animal models (Auluck et al, 2010).

Rab-GTPases play a key role in coordinating both vesicle formation and trafficking (Stenmark, 2009). Serveral Rab proteins have been implicated in directly or indirectly interactions with αS in PD models. Immunoprecipitation suggests Rab3a binding to αS aggregates in LBs (Dalfo et al, 2004a). At same time, Rab3a, Rab5 and

Rab8 were reported to coimmunoprecipitate with αS in A30P αS transgenic mice (Dalfo et al, 2004b). In PD models, αS overexpression disrupted vesicle trafficking between the ER and Golgi and overexpression of Rab1 attenuated αS toxicity (Cooper et al, 2006). Furthermore, Rab homeostasis was generally disturbed by αS in yeast and the overexpression of Rab1, Rab3a and Rab8a was protective against αS-induced toxicity in 3 different animal models (Gitler et al, 2008). αS was also reported to induce aggregation of many yeast Rab GTPases in the yeast model (Soper et al, 2011). In addition, Rab11a together with HSP90 displayed a regulatory role in the recycling of extracellular αS (Liu et al, 2009). Moreover, overexpression of Rab3b, an isoform of Rab3, protected dopaminergic neurons in the PD model by improving dopamine handling and storage capacity at presynaptic terminals (Chung et al, 2009). These findings suggest extensive interactions between Rab proteins and αS and Rab proteins generally protect against vesicle trafficking deficits in neuronal models of synucleinopahy.

Cellular toxicity

Gain of toxic functions through protein misfolding/aggregation is one unifying feature of neurodegenerative diseases i.e. Alzheimer's disease, PD etc. (Lansbury & Lashuel, 2006; Stefani & Dobson, 2003). But which is the major toxic species of αS – monomers, oligomers or fibrils? This is a central question to be addressed in the research into the the synucleinopathy in PD. In the last ten years, a significant amount of evidence has developed which suggests that the most toxic species of αS and Aβ is the pre-fibrillar species (oligomers) rather than the insoluble neuronal deposition i.e. mature fibrils, LBs; whereas the well-formed amyloid fibrils are less harmful or even protective (Caughey & Lansbury, 2003; Cookson, 2009; Cookson & van der Brug, 2008; Lashuel et al, 2002a; Lashuel et al, 2002b; Volles & Lansbury, 2003; Winklhofer et al, 2008). One prevalent hypothesis attributes the basis of the oligomeric toxicity to the high membrane affinity of the soluble species of oligomers with respect to the membrane distortion and membrane leakage caused by the pore-forming capacity of the oligomers (Auluck et al; Bodner et al, 2009; Bodner et al, 2010; Butterfield & Lashuel; Lashuel & Lansbury, 2006). In our lab, the pore-forming propensities have been well-characterized *in vitro* by generating the aggregation on-pathway oligomers from the cold-dissociation of

mature αS fibrils (Kim et al, 2009) and the oligomers of triple proline αS mutant designed on the basis of NMR structure (Karpinar et al, 2009). However, the oligomeric species normally presents continuum distribution in size and molecular weights, structural heterogeneity, instability and the mixture with αS monomers that make oligomers difficult to be separated. Therefore, we are still lacking the high resolution structural information of αS oligomers that determine its critical mechanism in the scenario of αS cellular toxicities.

A concomitant question is whether we can exclude the cellular toxicities of αS fibrils with the dominant assumption that the oligomeric species are most toxic. However, a consensus upon the role of αS fibrils has still not achieved. Recent studies have reported that exogenous fibrils of αS were transmitted into cells and thus seeded intra-cellular aggregation and prompted LB formation (Li et al, 2008; Luk et al, 2009). This mechanism of fibril transmission can then lead to synaptic dysfunction and neuron death (Volpicelli-Daley et al). Furthermore, this transmission was also observed between the affected neurons and the grafted neurons in both clinical trials and animal models (Hansen et al; Li et al, 2008). Thus, the mechanisms of αS cellular toxicity still need to exact and systematic determination. Meanwhile, two relatively novel conceptions have been emerging: 1) the prion-like transmission of the pathological aggregates propagate the synucleinopathy between cells, different brain regions and organs, where the transmissions are realized by exo/endocytosis, membrane leakage, passive membrane translocation or alternatively by exosomal release or transport along tunnelling nanotubes (Angot et al, 2010; Braak et al, 2002; Brundin et al; Brundin et al, 2010; Hawkes et al, 2007; Pan-Montojo et al, 2010; Steiner et al) [Figure 1.3]; 2) the aggregation process is toxic in comparison with the single species (monomers or oligomers, fibrils) (Taschenberger et al, 2012).

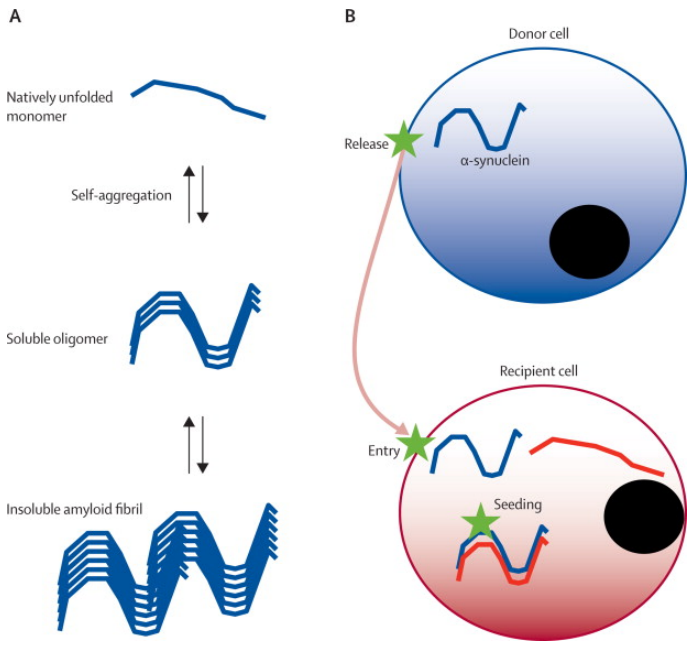

Figure 1.3 Putative mechanisms of α-synuclein prion-like propagation. (A) The different species of α-synuclein coexist in a highly dynamic equilibrium. (B) The prion-like transmission of αS follows an order that donor cell - the extracellular space -recipient cell. Figures are taken from (Angot et al, 2010)

1.2 Intrinsically disordered proteins and protein misfolding

Intrinsically disordered proteins (IDPs) are one category of proteins which are not folded in their functional form (Jensen et al, 2009). But differently from other unstructural proteins, IDPs possess the possibility of transient long-range and local order and the possibility of folding after binding to the partners (Jensen et al, 2009; Rezaei-Ghaleh et al, 2012). IDPs have been shown to participate in a broad range of cellular processes and the development of several human pathologies like neurodegenerative disease and cancer (Dyson & Wright, 2005).

IDPs present high structural flexibility and thus the traditional structural methods established on precise determination of well-defined protein structures are not suitable for IDPs (Jensen et al, 2009). In addition, X-ray crystallography is not applicable to IDPs due to their disordered nature. Rather than the determination of a single set of atomic coordinates, therefore, the conformational behaviors of protein backbone or an explicit ensemble description of interconverting structures are more appropriate for the structural description of IDPs. For this, NMR spectroscopy is an

excellent for defining the transient long-range interactions and local conformations at atomic resolution on a wide timescale window (Dyson & Wright, 2004). The solution NMR terms such as PRE, RDCs, relaxation parameters, and chemical shift perturbation are powerful in describing the conformational ensemble and protein-protein/ligand interaction for IDPs. αS as paradigm in the structural studies of IDPs has been well characterized by these solution NMR methods (Bertoncini et al, 2005b; Cho et al, 2007; Mukrasch et al, 2007; Salmon et al, 2010; Skora et al, 2006).

In one subcategory of IDPs which includes αS, Tau *et al.*, the proteins are able to fold and assemble into higher ultramolecular structures and are thus highly involved in the neurodegenerative diseases (Uversky, 2009; Uversky et al, 2008). According to the prevaling theory, the folding of the nascent polypeptide chain passes through the folding intermediates or partially folded states, to the native state that is located at the lower bottom positions in the funnel-shaped folding energy landscape [Figure 1.5] (Hartl et al, 2011; Hartl & Hayer-Hartl, 2009). Due to the ruggedness of the free-energy landscape, several kinetically trapped conformations during the folding need to overcome the energy barrier to reach an energy-favored downhill path. Protein chaperones play an important role in facilitating this energy conversion and controlling the conformational correctness of folding.

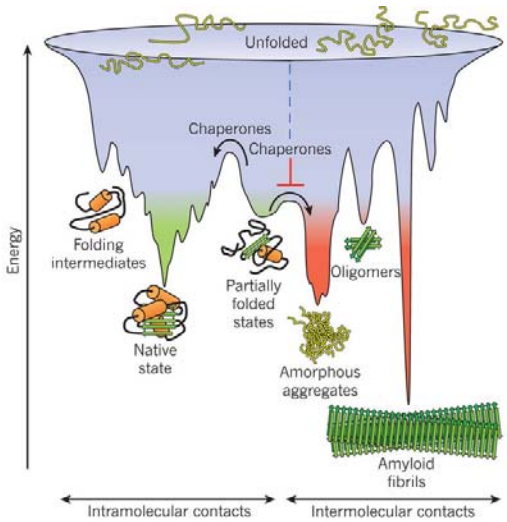

Figure 14. Schematic representation of funnel-shaped folding energy landscape. The kinetically trapped conformations as the folding intermediates present in the folding or aggregation pathway. The figure is adapted from (Hartl et al, 2011).

The aggregation normally occurs as a consequence of the energy surface of intramolecular folding overlaping with the surface of intermolecular aggregation in the energy funnel. As described in Figure 1.4, this is the reason that proteins might through partially folded states adopt the aggregation pathway to misfold to the amorphous or the ordered aggregates. For αS, Tau, and Aβ, due to their hydrophobic regions highly exposing to outer environment, they are readily able to achieve the intermolecular association with neigbouring proteins in cellular (Fink, 2006). Therefore, they preferentially fold though the downhill routine of intermolecular aggregation in the energy funnel to form well-ordered amyloid fibrils. This fibrillar aggregation typically occurs in a nucleation-dependent manner for the oligomerization. As protein chaperones are able to inhibit the misfolding, the study of interactions of the chaperones (i.e. HSPs) with αS and their role in modulating αS cellular toxicities is an active field in the research of Synucleinpathies (Dedmon et al, 2005a; Falsone et al, 2009; Huang et al, 2006; Liu et al, 2009; Lo Bianco et al, 2008; Putcha et al, 2010; Roodveldt et al, 2009). At the same time, the aggregation of αS has been developed as the promising therapeutic target for PD treatments (Brundin & Olsson, 2011; Madine & Middleton, 2009).

1.3 Major challenges

The major research interests and challenges are summarized in the following section.

(1) Assess structures of the αS oligomers at atomic resolution and characterize the interaction of proteins/ligands with αS intermediates.

(2) Clarify the toxic species in the scenario of αS aggregation, monomers, oligomers, fibrils or establish alternative hypothesis.

(3) Define the functional relevance of posttranslational modification, particularly the dominant phosphorylation at Ser129 of αS.

(4) Identify the protein-protein interactions involved in αS pathologies.

(5) Investigate the structural basis for the cell-to-cell prion-like transmission.

(6) Detect the origin and functional relevance of polymorphism of αS aggregates

(7) Search for the interplay between different PD genes.

The issue (1)-(4) will be discussed in this dissertation, as based on our experimental data.

2 Materials and Methods

2.1 Materials

2.1.1 Facility

Table 2.1 Facility used in sample reparation, NMR measurements and biophysical studies

Facility	Specifications
Atomic force microscope	Asylum Research MFP-3D™ Stand Alone Atomic Force Microscope
Balances	Sartorius B 3100 S & AC 210 S
Centrifuge	Eppendorf Centrifuge 5415D Eppendorf Centrifuge 5804 Beckman TL-100 with TLA-100.3 rotor
Concentrators	Amicon Microcon, Centricon, Centriplus/ Amicon Ultra, Ultracel
Dialysis	Thermo Scientific Slide-A-Lyzer Dialysis Cassettes
Dynamic light scattering	Wyatt DynaPro Titan
Electron microscope	Philips CM12
Fluorescence	Varian Cary Eclipse Spectrophotometer
Filter (syringe)	Millipore 0.2 μm syringe filter
Gel Electrophoresis	BioRad Power Pac 300
Incubator	Thermo Scientific, Heraeus, B6 and B20
Lyophilization	Braun Biotech Christ Alpha 2-4
NMR spectrometers	Bruker Avance 400 MHz, TXI probe, Bruker AvanceIII 600 MHz, QXI probe Bruker Avance 600 MHz, cryoprobe Oxford Avance 700 III MHz, TXI probe Bruker Avance 700 MHz, cryoprobe Bruker Avance III 800 MHz, 1.7mm and 5.0mmcryoprobe, Bruker Avance 900 MHz, cryoprobe
UV-Vis Photometer	Hewlett-Packard 8453

2.1.2 Chemicals

Table 2.2 Chemicals used in experiments.

Application	Chemicals
Bacterial phage for RDC	Pf1, Asla, Riga, Latvia
Fibril dissolving	GuSCN, Sigma-Aldrich, Deisenhofen, Germany
Phosphorylation	PLK1-3, Cell Signaling Technologies and Invitrogen, USA CKI, New England Biolabs, USA,
Other chemicals	Thioflavin T, Sigma, Steinheim, Germany DTT, Gerbu, Gaiberg, Germany Bench Mark protein ladder, Invitrogen, Karlsruhe, Germany SDS, Serva, Heidelberg, German Acetonitrile, APS, ATP, HEPES, TEMED, Roth, Karlsruhe, Germany Formic acid, Glycine, Hydrochloric acid, Manganese chloride

dihydrate, Sodium chloride, Sodium dihydrogen phosphate, Sodium hydroxide, TFA, Tris, Merck, Darmstadt, Germany

2.1.3 Software

Table 2.3 Software

Programe	Source
Topspin 2.1	Bruker Biospin, Karlsruhe, Germany
NMRPipe/NMRDraw	spin.niddk.nih.gov/NMRPipe (Delaglio et al. 1995)
Sparky 3	www.cgl.ucsf.edu/home/sparky (Goddard and Kneller)
MARS(graphic interface)	http://www3.mpibpc.mpg.de/groups/zweckstetter/_links/software_mars.htm (Jung 2004, Narayanan 2010)
PALES	http://www3.mpibpc.mpg.de/groups/zweckstetter/_links/software_pales.htm (Zweckstetter and Bax 2000, Zweckstetter 2008)
Pymol	DeLano Scientific LLC, Palo Alto, CA, USA
MATHEMATICA	Wolfram Research, Champaign, IL, USA
ORIGIN 7.5	OriginLab Corporation, Northampton, MA, USA
Excel:mac	Microsoft, USA

2.2 Sample preparation

2.2.1 Protein expression and purification

Sample expression and purification of *wt*-αS, ^{15}N *wt* -αS, ^{15}N-E46K αS, ^{15}N-A53T αS, P128E/S129E αS, M127E/P128E/S129E αS were performed by Dr. Stefan Becker, Karin Giller, Sebastian Wolff in Dept. NMR-based Structural Biology, Max Planck Institute for Biophysical Chemistry in Göttingen. Wild-type αS and its mutants were expressed in *E. coli* in M9 medium and purified as described (Bertoncini et al, 2005b; Hoyer et al, 2002). The samples of ^{15}N-A30P αS, ^{15}N-E46K αS, ^{15}N-A53T αS for real-time NMR assays were prepared by Prof. Dr. Hialal Lashuel's group.

Rab1b-GDP, Rab1b-GppNHp, Rab3a-GDP, Rab3a-GppNHp, Rab8a-GDP, Rab8a-GppNHp, Rab8a(6-176)-GDP, Rab8a(6-176)-GppNHp, ^{15}N-Rab1b-GDP, ^{15}N-Rab8a-GDP, ^{15}N-Rab1b(1-175)-GDP, ^{13}C,^{15}N-Rab1b(1-175)-GDP, ^{13}C, ^{15}N-Rab8a-GDP were prepared by the group of Dr. Amyelt Itzen, Dept. Physical Biochemistry, Max Planck Institute of Molecular Physiology in Dortmund.

2.2.2 Synthesis of Rab8a C-terminal peptide

The C-terminal Rab-peptide of Rab8a comprising residues Asp^{176}-Arg^{205} was synthesized by Kerstin Overkamp (Dept. NMR-based Structural Biology, Max Planck

Institute for Biophysical Chemistry in Göttingen) by using standard solid-phase fluorenylmethoxycarbonyl chemistry. The peptide was purified by semipreparative reverse-phase HPLC, and the purity (>95%) was analyzed by MS.

2.2.3 Preparation of the phosphorylated Ser129 α-Synuclein

α-Synuclein was dissolved in the phosphorylation buffer containing Mg^{2+}, ATP and the phosphorylation was stated by the addition of Polo-like Kinase 3 (PLK3). The solution was incubated at 30 °C for 2.5 hours to reach full phosphorylation at the Ser129. Trace amount of the phosphorylation product was loaded into MS to identify the single phosphorylation which was indicated by the mass change of 80 Da compared with *wt*-αS [Figure 2.1 (A) and (B)]. The phosphorylated αS was purified by semipreparative reverse-phase HPLC coupled with the online monitors of UV-Vis and MS. The purified protein was lyophilized and dissolved into the aggregation buffer. The single phosphorylation was further confirmed by 1D NMR spectrum [Figure 2.1 (C)]. The steps of HPLC/MS were implemented by Gerhard Wolf (Dept. NMR-based Structural Biology, Max Planck Institute for Biophysical Chemistry in Göttingen).

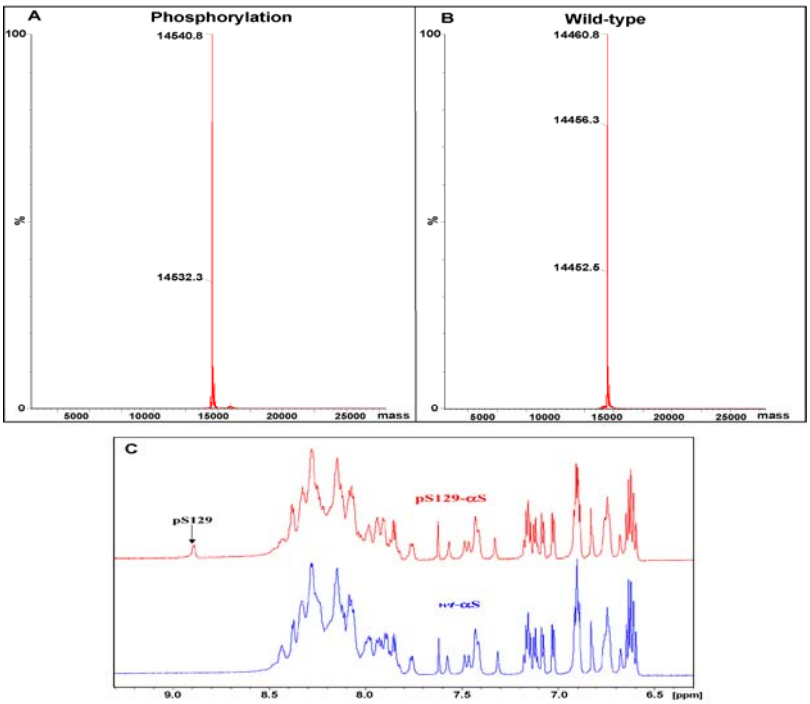

Figure 2.1 Characterization of Ser129-phosphorylation of αS. Mass spectrum of the phosphorylated αS (14540.8 kDa) (A) and *wt*-αS (B) as a reference (14460.8 kDa). (C) 1D ^{1}H NMR spectra comparison demonstrates the single peak of the phosphorylated Ser129 occured after PLK3 phosphorylation.

2.3 Methods

2.3.1 Phosphorylation assays

PLKs phosphorylation

For real-time NMR to measure the enzymatic kinetics, samples contained ~ 0.1 mm 15N-labeled αS in 20 mm HEPES, 10 mm MgCl2, 2 mm dithiothreitol, and 1.09 mm ATP, pH 6.9. The real-time assay was started by the addition of kinase into the sample, with a protein/kinase ratio of 100:0.5. The temperature was set to 303 K to allow for efficient phosphorylation. To reduce the impact of signal broadening due to amide proton exchange, the temperature was lowered to 288 K during the measurement of $^{1}H,^{15}N$ heteronuclear single quantum coherence (HSQC) spectra. In the case of PLK3, the phosphorylation reaction proceeded very rapidly at 303 K. Therefore, we also followed the kinetics of phosphorylation of αS by PLK3 at 293 and 288 K using ~ 0.075 mm αS (protein/kinase = 100:0.5 μg).

CKI

The kinase was incubated at 37°C for 5 minutes before mixing it with the protein (225 μM) in CK1 Reaction Buffer (New England Biolabs), pH 7.4. The reaction was carried out in the presence of 1.09 mm ATP and 1200 units of CK1/145 μg of αS. Afterwards, the phosphorylation was started and monitored by the real-time NMR method at 15 °C.

2.3.2 Aggregation assays

Aggregation assays for αS performed in this thesis follow the steps: 1) concentration calibration (UV-Vis, NMR); 2) solution processing: filtering with 0.22 μm membrane to remove of large particles and ultracentrifuge with 60K rpm to remove the oligomeric species; 3) aggregation with constant stirring at specified temperature. Thioflavin-T (ThT) as specific dye was used to monitor the fibril-formation kinetics. Dynamic light scattering (DLS) was used to monitor the oligomerization process. Electron microscopy (EM) and Atomic force microscopy (AFM) were selectively used to morphologically characterize the αS aggregates.

Three buffer systems are used in this thesis. (1) HEPES buffer: HEPES 50mM, NaCl 100mM, pH 7.4, used in the assays: aggregation in the presence of the Rab proteins, aggregation of the phosphorylated αS and the phosphorylation mimics. (2) Phosphate buffer: Phosphate 50mM, NaCl 100mM, pH 7.4, used in the generation of the compounds-stablized oligomers. (3) Tris buffer: Tris 20mM, NaCl 100mM, pH 7.4, used in the producing the fibrils of the pathological αS mutants. 0.1% $NaNa_3$ is normally included in the buffer for sterilization.

Standard temperature for αS aggregation is at 37°C. For the aggregation assays in the presence of Rab proteins, the temperature was set at 21°C taking into account the stability issue of Rab proteins. And the co-aggregating factors i.e. ligands, proteins should be added before the filtering step.

2.3.3 NMR spectroscopy

2.3.3.1 Backbone assignment

Backbone assignment methods

Backbone assignment, determing the nucleus that the resonance originates from, is the primary work to analyze the structure of macromolecules like proteins and nuclear acids by NMR spectroscopy (Wüthrich, 1986), particularly after the advent of multidimensional spectroscopy (Bax & Grzesiek, 1993; Oschkinat et al, 1988). Protein backbone assignment is achieved by transferring of coherence along the network of scalar coupled spins ^{1}HN, ^{15}N, $^{13}C_{\alpha}$ ($^{13}C_{\beta}$), and ^{13}CO of the ^{13}C, ^{15}N isotropic labeling protein in 3D NMR experiments [Figure 2.2] (Sattler et al, 1999). INEPT (Insensitive Nuclei Enhanced by Polarization Transfer) is a fundamental block responsible for the coherence transfer based on the scalar coupling (J) specific to the different coupled spins. INEPT is designated to transfer nuclear spin polarization from spins with large Boltzmann population differences to nuclear spins of interest with low Boltzmann population differences (Morris & Freeman, 1979). To obtain maximal sensitivity, the proton with largest gyromagnetic ratio (γ) is firstly polarized by the excitation of pulse in most of the cases and then the polarization was transferred by INEPT to the heteronuclei that this proton attaches to i.e. ^{15}NH, $^{13}C_{\alpha}$, $^{13}C_{\beta}$. The following phase is performing the mixing and evolution, by which the coherence is transferred along the

pathway targeting the specified sequential connectivity and chemical shifts of the indirection dimensions were labeled by encoding the modulation of Larmor frequencies of each nuclear in spin system to the magnetization strength. The final phase is transferring the magnetization back to the proton which would be detected by recording the FID.

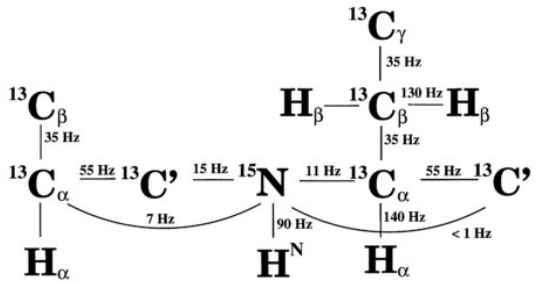

Figure 2.2 Network of the scalar coupling along protein backbone. Spin system of the peptide backbone and the size of the ^{1}J and ^{2}J coupling constants that are used for magnetization transfer in ^{13}C-, ^{15}N-labelled proteins. Figure is adapted from (Sattler et al, 1999).

There are two manners, “out and back” and “one way”, commonly used for the INEPT transfer pathway for constructing 3D experiments. The “out and back” experiments such as HNCO, HNCA, HNCACB are in one category experiments that magnetization transfer was started and ended at same protons. The “one way” is that the transfer is started from one proton and ended at another proton, for instance the CBCAcoNH is started from H_α/H_β and ended at amide HN. The time set for the INEPT delay is taken into account the compromise between sufficient coherence transfer based on J coupling and the diphase caused by transverse relaxation (R_2) during the longer delay time as described in the following formula:

$$\Delta_{opt} = \frac{1}{2\pi J} \bullet a \bullet \tan(\pi J T_2) ,$$

where J is the coupling constant and T_2 is the transverse relaxation time. Therefore, the relaxation features should be estimated prior to start recording of 3D experiments. One-one echo experiment designed based on the rotation frame is a straightforward and ready way to estimate the T_2, global rotational correlation time (τ_c) and thereby the molecular weight of the protein that assessing situation of the oligomerization (Sklenar & Bax, 1987). At the same time, 1D NMR spectrum can also

be used as an evidence to judge if protein is folded after sample preparation procedure. However, the proteins with larger molecular weights (≥20kDa) exhibit worse the spectra qualities with respect to the sensitivity and resolution, which are the results of strong nuclear relaxation and singal overlap because of the large number of residues. A major trend in the development of NMR spectroscopy applied in structural biology is extending the detection limits posed by the large molecular weight of proteins. Transverse relaxation optimized spectroscopy (TROSY) is one approach that improves the spectra qualities by select the component with the mutual cancellation of dipole-dipole couplings (DD) and chemical shift anisotropy (CSA), where the transverse relaxation of the large proteins are dominated by these two mechanisms (Pervushin et al, 1997). TROSY as the alternative to heteronuclear correlation spectroscopy (HSQC) can be incorporated into the well-established 3D or higher dimension experiments (Salzmann et al, 1998) and thus successfully enables NMR assignment and the following structural analysis for the large proteins.

Following the acquisition of 3D experiments required for establishing the sequential connectivity [Table 2.3.1], the backbone assignments will be implemented by the steps of spin system recognition and sequential connectivity searching. Herein, the assignments were performed by MARS, a robust automatic backbone assignment program (Jung & Zweckstetter, 2004a; Jung & Zweckstetter, 2004b). The manual peak-picking and prediction of secondary chemical shifts based on the primary sequence are required prior to running MARS. The specified assignments, the residual dipolar couplings (RDCs), dihedral angles and existed crystal structure can be optionally contained in the input data. The sequential connectivity of the local fragment and globular backbone is established by linking the inter- and intra-residue signals and mapped onto the protein sequence, which the secondary structure propensity is taken into account. The assignment is finally output by combining the local and globular assignment.

Table 2.3.1 3D experiments used for backbone assignments of the Rab proteins

Experiments	Bruker pulse code	Parameters [⊥]
HNCA	trhncagp3d2	50×24×1024 pts; ns=16; 600MHz [*]50×25×1024 pts; ns=24; 800MHz
HNCACB	trhncacbgp3d	68×21×1024 pts; ns=32; 700MHz [*]61×26×1024 pts; ns=48; 800MHz
CBCA(CO)NH	trcbcaconhgp3d	64×20×1024 pts; ns=36; 700MHz [*]64×23×1024 pts; ns=32; 800MHz
HNCO	trhncogp3d	50×33×1024 pts; ns=32; 700MHz
HN(CA)CO	trhncacogp3d	65×21×1024 pts; ns=32; 700MHz

[*]*Recorded for Rab8a-GDP with 1.7mm cryoprobe*

[⊥]*Specification for spectrometer parameters: number of complex points (pts) in t_1, t_2 and t_3 time domain; number of scanes (ns); field strength for ^1H*

Structural analysis based on chemical shifts

After the backbone assignment is obtained, we are able to perform the structural analysis for protein based on the chemical shifts. Firstly, the secondary chemical shifts of carbon (C_α, C_β, CO) are highly indicative of the structural propensity of secondary structure. The secondary chemical shifts were determined by the difference between the experimental chemical shifts (δ_{exp}) and the random coil chemical shifts (δ_{coil}) of the residue (Schwarzinger et al, 2001; Schwarzinger et al, 2000):

$$\Delta\delta = \delta_{\exp} - \delta_{coil}$$

To correct the referencing errors, the difference between the secondary chemical shifts of C_α and C_β has been applied (Wang et al, 2005):

$$\Delta\delta_\alpha - \Delta\delta_\beta$$

Secondly, residual dipolar couplings (RDCs) can be measured by adapting the protein into the weak alignment mediums i.e. the liquid crystal and bacterial phage where the dipolar coupling between two nuclear dipoles is partially retained due to the motion of molecule is restricted in the medium (Prestegard et al, 2004). For instance, the RDCs of NH vector can be measured by comparing the difference of scalar coupling of NH between the aligned sample and isotropic sample (in free solution). To this aim, the IPAP-HSQC (Ottiger et al, 1998) and interleaved TROSY/HSQC (Kontaxis et al, 2000) are two common approaches to measure the J-couplings.

Herein, the RDCs for ^{15}N-Rab1b-GDP were obtained from the interleaved TROSY/HSQC spectra:

$$^{1}D_{NH} = 2\bullet(\nu_N^{HSQC} - \nu_N^{TROSY})$$

At the same time, the RDC values were back-calculated from the crystal structure of Rab1b (PDB code: 3NKV) using singular value decomposition (SVD) by the program PALES (Zweckstetter, 2008). A comparison of the experimental and the calculated RDCs was used to evaluate the difference between solution conformation and crystal structure. The solution conformation matches the crystal structure well if the Q-factor of fitting is below 0.2.

2.3.3.2 HSQC-based study of protein-protein/ligand interactions

NMR signals of backbone amides provide excellent information to probe protein-protein/ligand interaction with the description of interaction interface and binding affinity according to perturbation of chemical shift and line-width analysis (Craik & Wilce, 1997; Gao et al, 2004). In practice, ^{1}H,^{15}N-HSQC spectra have been recorded for the ^{15}N-labeled protein in the absence and presence of the interaction partners that are normally unlabeled proteins or ligands. The chemical shifts perturbations are calculated as:

$$\Delta\delta_{HN} = \sqrt{(\Delta\delta_N / 5)^2 + (\Delta\delta_H)^2}$$

The HSQC spectra of ^{15}N-labeled sample are recorded in the presence of the binding partners at different molar ratios to the sample. In this case, the chemical shift perturbations are increased as a function of concentration of the binding partners, which the dissociation constant K_d can be estimated by fitting to a single-site binding model (Cavanagh et al, 2007):

$$\Delta\delta = \Delta\delta_{\max}\bullet\left([L]_T + [P]_T + K_d - \left\{([L]_T + [P]_T + K_d)^2 - 4[L]_T\bullet[P]_T\right\}^{1/2}\right) / (2[P]_T)$$

where the $\Delta\delta_{max}$ is the maximal chemical shift perturbation value at saturation, $[P]_T$ and $[L]_T$ are the total concentration of protein and ligand. This approach is particularly advantageous to determine the K_d for weak binding system (K_d >10^{-6}M). The

crystallization for such system is difficult or impossible (Cavanagh et al, 2007) and ITC used for measuring such weak binding might bear bigger uncertainty.

2.3.3.3 Real-time NMR method used in the investigation of phosphorylation kinetics

Real-time NMR methods used in studies of the enzymatic kinetics possess predominant advantages than other common methods like MS spectrometry and immunodetection (Landrieu et al, 2006). Firstly, 2D NMR HSQC spectrum is able to unambiguously identify the residues undergoing phosphorylations and the resonances of the phosphorylated residues are located at the downfield region of the spectrum which is well-resolved with the unphosphorylated resonance. Secondly, the enzymatic resolution can be monitored at atomic resolution, which the onset time and reaction rate can be assessed for different phosphorylation sites simultaneously.

For our phosphorylation kinetics studies, ^{15}N-labelled αS and the assignment for ^{1}H,^{15}N-HSQC of αS are required. The real-time assay was started immediately after the sample was mixed with the kinases and ATP. A series of HSQC spectra were recorded and quantitative analysis of the phosphorylation kinetics was implemented based on the measurement of resonance intensity. For better time resolution, the fast acquisition pulse SOFAST-HMQC was applied to investigate the fast kinetics instead of common HSQC (Schanda & Brutscher, 2005; Schanda et al, 2005). SOFAST, "band-Selective Optimized-Flip-Angle Short-Transient", is a technique to design the pulse sequence based on the Ernst-angle excitation:

$$\cos\alpha_{opt} = \exp(-t_{rec} / T_1)$$

where α_{opt} is the optimized flip angle of the excitation or so-called "Ernst angle", t_{rec} is the time of recover delay and T_1 is the longitudinal relaxation constant. Here, the SOFAST is combining this technique with the selective ^{1}H pulses which are aiming to optimize the longitudinal relaxation.

2.3.3.4 NMR approach to study H/D exchange rate of protein backbone

Hydrogen/Deuterium exchange method has been widely applied to characterize the structures of amyloid fibrils (Carulla et al, 2010). In this dissertation, this method based on solution NMR has been used for structural analysis of αS fibrils and Oligomers. For

αS fibrils, as demonstrated in Figure 2.3, the collected fibrils were adapted into 99.9% D_2O solution containing 200mM NaCl and 0.1% formic acid (pD 4.0) for two weeks. During this period, the hydrophobic core buried inside fibrils should be protected against the solvent but other fraction of protein not in the core would exposose to the solvent and thus was exchanged by deuterium. After this exchange period, the fibrils were collected again and dissolved by GuSCN into NMR observable monomers which encode the protection information. This dissolving solution contains 50% D_2O only and at pH 2.4. Thus the residue previously expososed to the solvent would experience a back-exchange from 99.9% deuteration to 50%. The sample was transferred into NMR spectrometer immediately after the dissolving in order to start the acquisition of the HSQC spectra with the average dead time of 15 minutes and acquisition time of 25 minutes. The HSQC spectra were recorded at 5^oC to restrict the proton exchange rate. The residue from protected or exposed regions could be distinguished by mapping the change of resonance intensity against the time course. The increasing pattern of intensity denotes this residue was in an exposure region before, whereas the previously protected region would have the flat or decreasing patterns.

The working principle of H/D exchange for αS oligomers is similar. However, the distinct nature of the oligomers requires the modifications for most of steps. Firstly, for the exchange, D_2O has been directly added to the solution containing the oligomers and the time for the exchange was within 10 minutes since the hydrophobic protection in oligomers is expected to be wearker than in the fibril core. Secondly, the GuSCN was then directly added into the solution and adjust the pH down to 2.4, which the solution volume was thus expanded.

In addition, to shorten the acquisition time for better time resolution, we used HSQC with band-selective excitation Short-Transient (BEST-HSQC) (Lescop et al, 2010). The BEST-HSQC replaces all proton hard pulses by band selective excitation pulses to only excite the amide protons of protein and remain the other type protons and water signals not to be directly excited. The spin-lattice relaxation of a ^1H spin depends on the initial spin-state of the surrounding ^1H spins. The excited amide protons can exchange polarization with surrounding non-excited aliphatic protons and water protons though NOE or spin diffusion effects, by which the T_1 relaxation of the amide protons

can be shortened. By this way, the recover delay can be shortened, which both repetition rate and sensitivity can be improved.

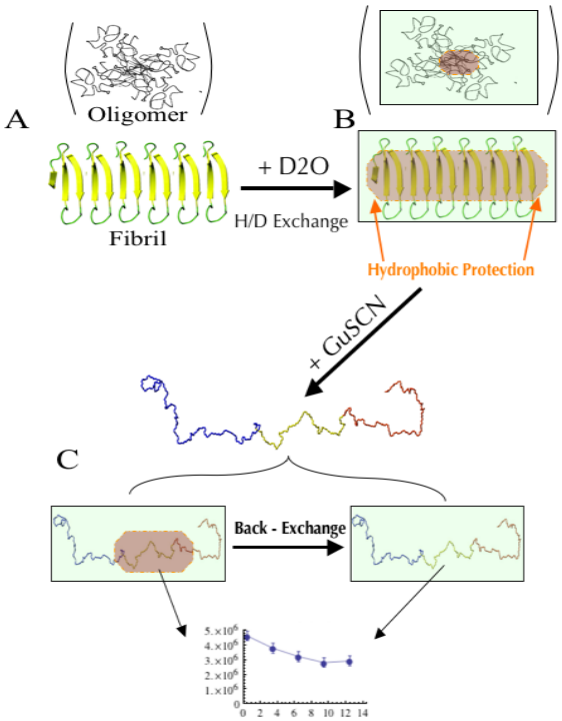

Figure 2.3 Schematic flowchart of H/D exchange. αS aggregates (fibrils/oligomers) (A) are adapted into the D_2O buffer (B) for a specified period. The hydrophobic core region of the aggregates should be protected against the solvent exchange. After the exchange period, the aggregates are dissolved by GuSCN into the monomers encoding the protection information (C) and quickly transferred to the NMR spectrometer to start recording a series of HSQC spectra. Finally, the change of residue-specific peak intensity reflects the extent of protection/exposure.

2.3.3.5 Diffusion coefficient

NMR diffusion experiments detect the translational diffusion of molecules in solution by using pulsed field gradients (Johnson, 1999). The spatial enconding for the molecules is firstly implemented by the pair of pulsed field gradients (bipolar gradients) coupled with one spin-echo pulse. Then there will be a diffusion period that allows the molecules to move away from the original encoding position.During this period, the motional rate of the molecules depends on the diffusion coefficient. After this diffusion time, the position of the molecule can be decoded by the second pair of pulsed field

gradients with same net strength but opposite direction. The gradient strength applied in the spectrum is normally varied from 25% to 95%. The diffusion coefficient of the molecule is estimated by fitting the signal intensities as the function of varying gradient strength according to:

$$I = I_0 e^{-D\gamma^2 g^2 \delta^2 (\Delta - \delta/3)}$$

where I is the observed intensity, I_0 the reference intensity, D the diffusion coefficient, γ the gyromagnetic ratio of the observed nucleus, g the gradient strength, δ the length of gradient and Δ the diffusion time. For αS, the peaks located with the range of 0.5-2.0 ppm were integrated for the fitting. The diffusion coefficient is defined by Stokes-Einstein equation:

$$D = \frac{kT}{6\pi\eta R_h}$$

where K is the Boltzman constant, T the temperature, η the viscosity of the solution and R_h hydrodynamic radius of the molecules. Thus, we can measure the hydrodynamic radius of the protein by referring to the internal reference molecule, dioxane, with known R_h (2.12 Å). In our measurements, we used the pulsed field gradient spin-echo (PGSE) sequence with the incorporation of WATERGATE (W5) element which significantly suppresses the water signal (Zheng et al, 2008).

2.3.4 Biophysical methods

2.3.4.1 Fluorescence spectroscopy

Fluorescence measurements with specified excitation and emission wavelength enable us to detect specific information. Thioflavin-T (ThT) is a dye specific to the structure of crossing β-sheets and thus widely used to characterize kinetics of the fibril formation process (LeVine, 1999). The excitation wavelength is 446nm and the emission wavelength is 460 to 600nm, where the maximum emission is at 482 nm for amyloid fibrils. For the fluorescence measurement, 5μL in-time aggregation solution is mixed into 5μM×2mL ThT solution.

2.3.4.2 UV-Vis Spectroscopy

UV absorption at 280 nm is used to determine protein concentration according to Beer-Lambert law:

$$A_{280} = \varepsilon_{280} \cdot c \cdot d$$

A_{280}: the absorption at 280 nm

ε_{280}: The molar extinction parameters at 280nm calculated by the TRP, TYR amino acid content in the protein sequence.

c: protein concentration (M)

d: path length of light (cm)

2.3.4.3 Dynamic light scattering

Dynamic light scattering (DLS) is an approach to measure the particle size, namely hydrodynamic radius, in solution based on the evaluation of their translational diffusion constants of Brownian motion, which is also known as Photon Correlation Spectroscopy. DLS was performed by Wyatt Dynamo Titan with temperature control. Sample that would be used for DLS measurement should be filtered by 0.22 μM membrane at beginning. If solution conains large fibrils, it should be centrifuged at 10k rpm for at least 15 mins and only supernatant can be used for DLS measurement. Then, the sample is transferred into DLS cuvette and 18 μL as a minimal volume are required. The DLS measurement was implemented at 25^{o}C. The laser power is set at 15% and can be adjusted according to the size of oligomeric species formed during aggregation. Acquisition time for each scan is 20 seconds and each measurement contains 20 scans. The measurement is normally repeated for 3~5 times.

The hydrodynamic radius calculated based on the light scattering data are containing the contribution of hydration. To keep control, the diffusion measurements (DOSY) performed by NMR spectroscopy are an alternation and the gyrations measured by small angle X-ray scattering are a complementary approach to further investigate the configuration of particles.

2.3.4.4 Electron microscopy

Transmission electron microscopy (TEM) for characterization of αS aggregates, the oligomers and fibrils, were performed by Dr. Dietmar Riedel and Gudrun Heim in Max Planck Institute for Biophysical Chemistry. Aggregated protein samples were deposited on Formvar-coated 200 mesh copper grids (Electron Microscopy Sciences) at a concentration of 25 μM. For more concentrated sample, the dilution by buffer is required for better resolution. Grids were washed with two drops of water and stained with two drops of freshly prepared 0.75 % (w/v) uranyl acetate (Electron microscopy sciences). Specimens were inspected on a Philip CIME 12 electron microscope, operated at 80 kV. Digitized photographs were recorded with a slow scan CCD camera.

2.3.4.5 Atomic force microscopy

Atomic force microscopy (AFM) is an alternation approach to TEM for characterizing the αS aggregates. The set-up is installed in Dept. NanoBiophotonics, Max Planck Institute for Biophysical Chemistry.

The aliquots of 3~5 μL from aggregation system were deposited on freshly cleaved mica. After drying in air for 1 hr, unbound sample and buffer were removed by 3 times washing with 30 μL distilled water. The samples were imaged using an Asylum MFP3D AFM machine, with a resonant frequency of about 100 kHz, a scan frequency of 1 Hz using silicone nitride tips.

3 Results

3.1 Phosphorylation of alpha-Synuclein

Phosphorylation at Ser129 of αS is one of major posttranslational modifications. Approximately 90% of αS is phosphorylated at this site in pathological inclusion-Lewy body, a hallmark of PD (Fujiwara et al, 2002). Ser87 at NAC region of αS can also be phosphorylated by kinases, inhibiting the fibrillization of αS (Paleologou et al). However, the functional role of αS phosphorylation has still not been defined. Therefore, based on atomic resolution provided by NMR spectroscopy, we investigated the residue-specific kinetics of phosphorylation at both Ser87 and Ser129 of αS as mediated by different kinases.

We first investigated the effects of 3 disease mutations of αS, A30P, E46K and A53T on phosphorylation kinetics of Ser87 and Ser129. Two kinases, CKI and PLK2 were respectively used in this assay to phosphorylate αS mutants. Furthermore, PLKs phosphorylate αS selectively at Ser129 but not Ser87 in CNS as well *in vitro* (Inglis et al, 2009; Mbefo et al). This offers us an opportunity to study the phosphorylation specifically at Ser129. Thus, the kinetics of αS phosphorylation mediated by PLK1, 2, and 3 were investigated. Finally, we studied whether phosphorylation at Ser129 of αS can affect its aggregation. We generated Ser129-phosphorylation (pS129) αS and two phosphorylation mimics, P128E/S129E αS and M127E/P128E/S129E αS. Aggregation assays for pS129 αS and its two mimics were implemented *in vitro*. These results extended our understanding the structural mechanism and aggregation behaviors involved in αS phosphorylation.

3.1.1 Phosphorylation of disease-associated α-Synuclein mutations

Three familial mutations in gene coding of αS (*SNCA*) were linked to the autosomal dominant inherited form of PD: A53T (Golbe et al, 1990; Polymeropoulos et al, 1997; Puschmann et al, 2009), A30P (Kruger et al, 1998) and E46K (Zarranz et al, 2004).

Increasing evidence suggests that these point mutations can alter the monomeric conformation, fibril formation, and membrane binding and thereby inducing differently physiological and pathological behaviors (Bisaglia et al, 2009; Bodner et al, 2010; Bussell & Eliezer, 2001). Therefore, our study of the effects of these three mutations on the phosphorylation enables us to depict the interplay between the familial mutations and the major posttranslational modifications.

3.1.1.1 Kinetics of α-Synuclein phosphorylation by PLK2

Heteronuclear NMR spectroscopy on ^{15}N-labeled protein modified by a kinase allows the identification of the phosphorylation sites, measures the level of integration, and yields kinetic data for the enzymatic modification of the individual sites (Landrieu et al, 2006). Although the reaction mixture contains enzyme, ATP and αS, filtering through the ^{15}N label allows monitoring of the kinase activity in the NMR tube without any further sample purification. To obtain single-residue resolution and identify all potential phosphorylation sites, the enzymatic reaction was followed by two-dimensional ^{1}H-^{15}N heteronuclear correlation spectra. For *wt*-αS and its 3 familial mutants, the resonances were sharp and showed a limited dispersion of chemical shifts, reflecting a high degree of backbone mobility [Fig. 3.1.1 A]. Phosphorylated serine residue was readily detected because phosphorylation shifts their amide proton resonance downfield of 8.8 ppm, to an empty region of the ^{1}H-^{15}N HSQC spectrum.

With increasing incubation time, the intensity of the NMR signal of phosphorylated Ser129 increased with the concomitant decrease of unphosphorylated Ser129. In agreement with data from cell assays (Mbefo et al, 2010), only Ser129 was phosphorylated, highlighting the specificity of PLK2 for Ser129 phosphorylation. Quantitative analysis of the phosphorylation kinetics of *wt*-αS and the 3 mutants was implemented based on the measurement of resonance intensity. After one day, 40-50% of the *wt* protein, and the three αS mutants were phosphorylated at Ser129, and the reaction reached saturation in the following 10 hours [Fig.3.1.1 B]. A comparison of the kinetics of phosphorylation revealed that *wt*-αS was phosphorylated faster than all three genetic variants under controlled *in vitro* conditions using the same kinase and protein concentrations. Although the saturation levels are only slightly different, after four

hours of incubation the degree of Ser129 phosphorylation of *wt* αS was larger by a factor of 1.5 when compared to the genetic mutants.

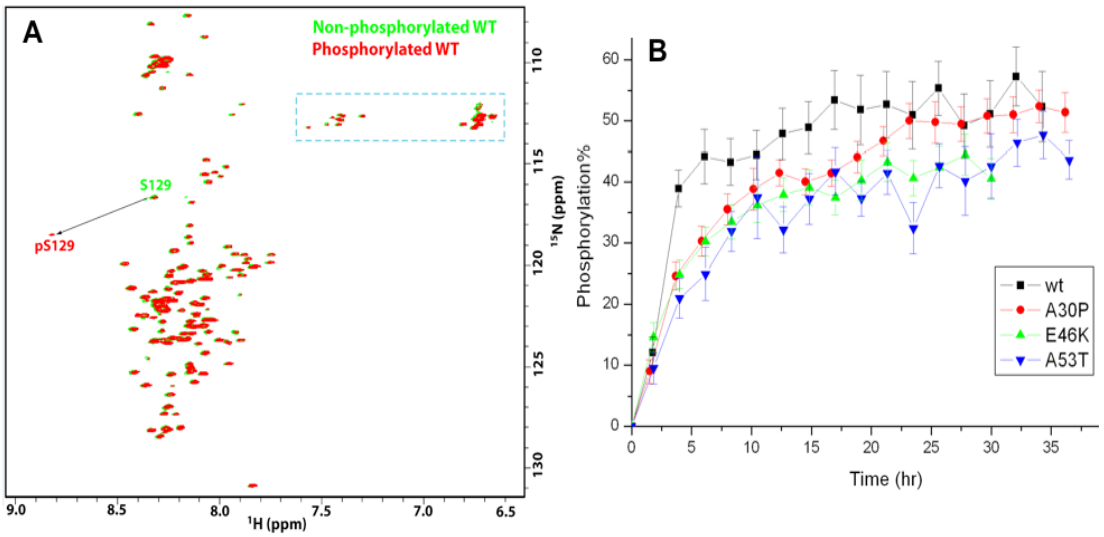

Figure 3.1.1. Kinetics of mutant αS phosphorylation by PLK2. (A) Comparison of two-dimensional ^{1}H-^{15}N HSQC spectra of unphosphorylated *wt* (green) and PLK2-phosphorylated WT αS (red). A dashed rectangle marks glutamine and asparagine side chain resonances. Note that PLK2 phosphorylates αS only at Ser129. (B) Kinetics of *in vitro* phosphorylation of Ser129 by PLK2 in *wt* (black), A30P (red), E46K (green) and A53T (blue) αS. The reactions were monitored by real-time NMR spectroscopy. Error bars are based on the signal/noise ratio observed in the NMR spectra.

3.1.1.2 Kinetics of α-Synuclein phosphorylation by CK1

Real-time NMR spectroscopy was also used to follow the kinetics of phosphorylation of *wt*-αS and its 3 familial mutants by CK1. The NMR signals appearing in the downfield region of the HSQC spectrum were assigned to phosphorylated Ser87 and phosphorylated Ser129. These two downfield signals were seen in the spectra of *wt*-αS and the 3 mutants, indicating that CK1 is capable of phosphorylating *wt*-αS as well as the three genetic variants at both sites.

During the phosphorylation reaction, the resonance intensities of phosphorylated Ser87 and Ser129 increased, and their unphosphorylated counterparts decreased [Fig.3.1.2 A]. The rate of phosphorylation at Ser87 was identical for all three genetic mutants and *wt* α-syn [Fig.3.1.2 B]. At the same time, a comparison of the kinetic profiles of phosphorylation at Ser129 α-syn revealed a slightly higher rate of

phosphorylation in the case of *wt*-αS [Fig.3.1.2 C]. It should be noted that the highly similar phosphorylation kinetics of all four proteins at Ser87 served as a ruler and proved that the conditions of the phosphorylation reaction were identical.

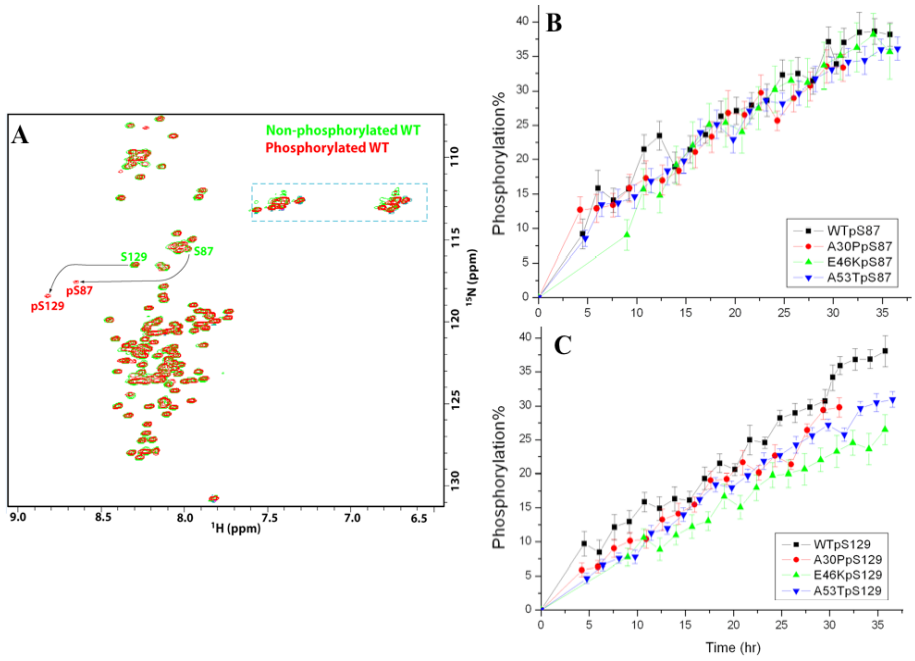

Fig. 3.1.2. Kinetics of phosphorylation of mutant αS by CK1. (A) Comparison of two-dimensional ^{1}H-^{15}N HSQC spectra of unphosphorylated *wt* (green) and CKI-phosphorylated αS (red). Both Ser129 and Ser87 are phosphorylated. Kinetics of *in vitro* phosphorylation of Ser87 (B) and Ser129 (C) by CKI in *wt* (black), A30P (red), E46K (green) and A53T (blue) αS. The reactions were monitored by real-time NMR spectroscopy.

3.1.2 Phosphorylation of α-Synuclein at Ser129

he study of the postmortem human brain shows that a significantly increased level of phosphorylation occurs at Ser129 of αS, from less than 5% of the population in healthy human brains to 89% in the brains of PD patients (Visanji et al; Waxman & Giasson, 2011). Recently, extensive research has been devoted to several issues regarding Ser129 phosphorylation, such as its impact on aggregation (Fujiwara et al, 2002), relevance to neuronal toxicity (Gorbatyuk et al, 2008; Sancenon et al, 2012), membrane binding (Kuwahara et al, 2012; Visanji et al, 2011) *et al*. In term of αS primary structure, Ser129 is located at the highly flexible and acidic C-terminal which plays an important role in ligand binding, enzymatic recognition, the maintainence of protein conformation and

modulating aggregation. Previous studies have indicated that the transient long range interactions existing between C-terminus and N-terminus were modified by the Ser129 phosphorylation and thereby the aggregation profile of αS was potentially affected (Paleologou et al, 2008).

As described in last section 3.1.1, PLK2 is suggested as a major kinase responsible for specific phosphorylation of Ser129 in neurons (Inglis et al, 2009). Together with the *in vivo* methods, we investigated three closely related members of the human Polo-like kinases (PLKs) family (PLK1, PLK2, and PLK3), to observe their enzymatic performances on phosphorylating αS in different cell cultures and catalysis kinetics *in vitro* (Mbefo et al, 2010). Furthermore, to assess impacts of the Ser129 phosphorylation on αS aggregation, we generated phosphorylated Ser129 of αS (pS129) for aggregation assay. Finally, two mimics of Ser129 phosphorylation of αS, P128E/S129E and M127E/P128E/S129E, were studied in terms of their aggregation propensities.

3.1.2.1 Kinetics comparison of different kinases (PLK1, PLK2, PLK3)

In collaboration with Dr. Hialal Lashuel, we identified that PLK1-3 phosphorylated both αS monomers and fibrils at Ser129 in the *in-vitro* assays, but PLK4 didn't phosphorylate both forms of αS (Mbefo et al, 2010). Lashuel's lab also observed that PLK2 and PLK3 phosphorylated αS efficiently in both HEK293T cells and HeLa cells and these two kinases partially co-localized with pS129 in primary hippocampal neurons and cortical brain areas of αS transgenic mice (Mbefo et al, 2010). These results suggest that PLKs play important role in the phosphorylation of αS Ser129. Therefore, we investigated the enzymatic performance of PLKs on the Ser129 phosphorylation of αS

The real-time NMR assay was applied to monitor the PLK1-3-catalyzed phosphorylation reaction by measuring yield kinetics and identifying all potential phosphorylation sites in the cases of PLK1 and PLK3. Taking advantages of the single-residue resolution realized by the real-time NMR method, amide proton resonance of pS129 was unambiguously shown in ^{15}N-αS HSQC spectrum in the case of PLK3-catalyzed reaction. Importantly, no additional NMR signals of phosphorylated residues appeared, indicating that PLK3 exclusively phosphorylated αS at Ser129.

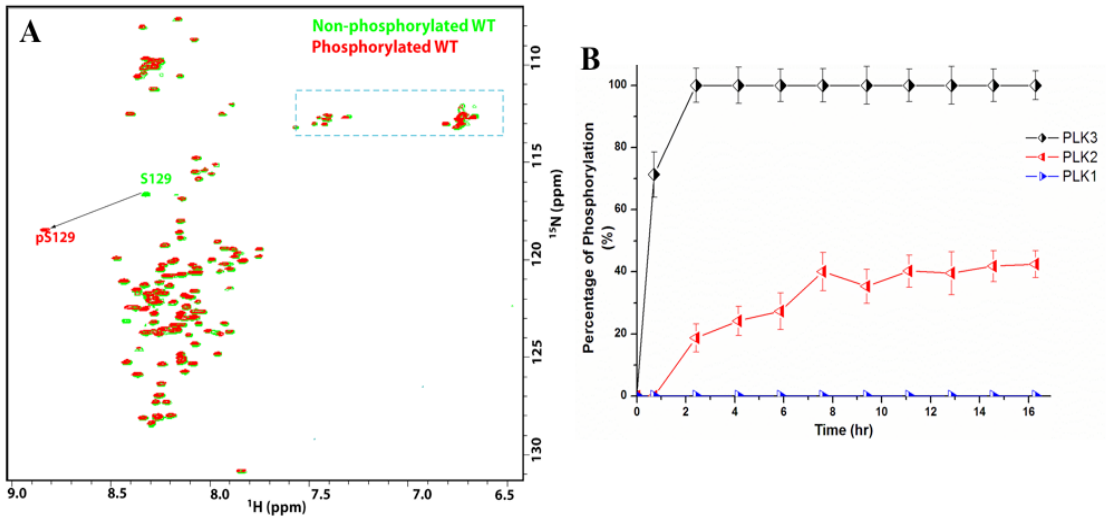

Figure 3.1.3. Phosphorylation of synucleins by PLK1-3. (A) Comparison of two-dimensional ^{1}H-^{15}N HSQC spectra of unphosphorylated WT (green) and αS phosphorylated by PLK3 (red). A dashed rectanglemarks glutamine and asparagine side chain resonances. (B) Kinetics of in vitro phosphorylation of Ser129 in αS by PLK3 (black), PLK2 (red), and PLK1 (blue) as monitored by real-time NMR spectroscopy. NMR samples contained ~0.1 mm ^{15}N-labeled αS in 200 mm HEPES, 10 mm MgCl2, 2 mm dithiothreitol, and 1.09 mm ATP, pH 6.9. The real-time assay was started by the addition of kinase into the NMR sample using a protein/kinase ratio of 100:0.5 mg. The error bars were determined based on the signal/noise ratio observed in the NMR spectra.

In the case of PLK3, the peak of phosphorylated Ser129 was already clearly observed already after 45 minutes [Figure 3.1.3 A]. With increasing incubation time, the intensity of the NMR signal of phosphorylated Ser129 increased. Quantitative analysis of the increase of the NMR signal of phosphorylated Ser-129 indicated that PLK3 fully phosphorylates αS within 2.5 hours under the conditions of the assay [Figure 3.1.3 B]. In the case of PLK1, no phosphorylation of αS could be detected during the time course of the experiment. The significantly reduced PLK1 phosphorylation of αS in the NMR experiments in comparison to the *in vitro* kinase assay, is most likely due to the fact that the NMR phosphorylation experiments were performed at a lower temperature (15 °C *versus* 30 °C for *in vitro* kinase assays) to reduce the impact of signal broadening due to amide proton exchange. As previously described, real-time spectroscopy of αS phosphorylation by PLK2 showed that PLK2 also showed phosphorylates αS at Ser129

only. However, the kinetics of the enzymatic reaction is significantly slower for PLK2 than for PLK3, and αS was not fully phosphorylated at the end of the assay.

In contrast to PLK1 and PLK2, our real-time assay showed that PLK3 possessed a remarkable efficiency in phosphorylating αS. However, the fast kinetics of PLK3-catalyzed phosphorylation largely limited the detailed information that can be accessed by a standard HSQC experiment at the initial stage. Consequently, we employed band-Selective Optimized-Flip-Angle Short-Transient (SOFAST) HMQC to circumvent this time restriction by shortening the time required for recording one spectrum.

The SOFAST-HMQC experiment generates the resonance signal of amide proton correlation with shorter time intervals of recovery delay between each scan than the standard HSQC spectrum. In particular, T_1 relaxation optimization and Ernst angle are collectively integrated into the pulse scheme of this experiment to achieve a markedly reduction in inter-scan delay. Sensitivity and resolution are key factors for practical considerations when handling NMR experiments. To reach maximal time-shortening whilst retaining the necessary sensitivity and resolution for measurement of phosphorylation kinetics, we further narrowed spectra width in indirect dimension to reduce the time spent on a large number of incrementing points. The recycle delay was finally set at 0.3 seconds. Extraordinarily, the peak of phosphorylated Ser129 is well-resolved in the spectrum [Figure 3.1.3.A], and thereby favored all the strategies adopted above. Moreover, according to theory of enzymatic reaction, temperature is an important factor that affects reaction kinetics. By lowering the experimental temperature, we were able to slow down the reaction rate and capture more kinetic information under the given spectroscopic conditions.

Finally, we measured the kinetics of PLK3-mediated Ser129 phosphorylation by optimized SOFAST-HMQC with time resolution of 17 mins at temperature of 288K and 293K. Kinetic profiles of Ser129 phosphorylation by PLK3 were mapped by measuring resonance intensity of pS129 within beginning 200 mins. Under both experimental temperatures, a distinguishable peak of the phosphorylated Ser129 already appeared after 20 min which contained the dead time and time for recording first spectrum. The peak intensity increased rapidly with increasing reaction time and approximately 90% phosphorylation was reached at 70 mins under both temperatures. After ~ 2 hours, the

kinetics under both temperatures had already achieved saturation, suggesting that the reaction finished and αS was fully phosphorylated at the Ser129 by PLK3.

Quantitative comparison between 288K and 293K shows that the kinetic difference is indistinguishable, indicating a temperature-independence for kinetics within this temperature range. Moreover, the kinetic curves measured by SOFAST-HMQC spectra under these two temperatures are highly similar to the kinetics measured by standard HSQC spectra under temperature of 303K [Figure 3.1.3 B], at which 70% αS has been phosphorylated at 50mins and a complete phosphorylation was reached within 2.5 hours.

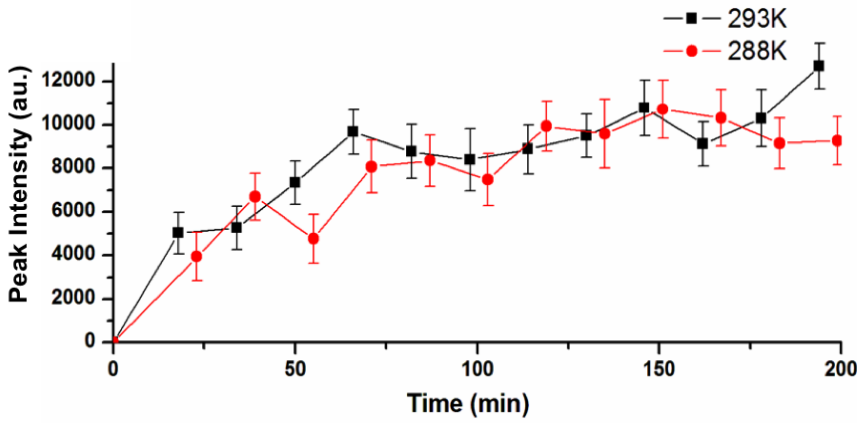

Figure 3.1.4. Phosphorylation of αS by PLK3 at the lower temperatures by SOFAST-HMQC. Kinetics of phosphorylation of Ser-129 of αS by PLK3 under temperature of 293K (black) and 288K (red) were monitored by real-time NMR spectroscopy. NMR samples contained ~0.1 mm ^{15}N-labeled αS in the phosphorylation buffer for PLKs described before. The real-time assays were started by the addition of kinase into the NMR sample using a protein/kinase ratio of 100:0.5 mg. The error bars were determined based on the signal/noise ratio observed in the NMR spectra.

In summary, real-time NMR spectroscopy revealed that PLK2 and PLK3 exclusively phosphorylated αS at Ser129, consistent with other *in-vitro* and *in-vivo* assays (Mbefo et al, 2010). Moreover, PLK3 phosphorylated αS with significant efficiency that full phosphorylation could be achieved within 2.5 hours under the assay condition. Based on the fast acquisition technique, we further demonstrated that PLK3 phosphorylated nearly 50% αS within 25 mins and its enzymatic kinetics were not strongly altered by changing reaction temperature.

3.1.2.2 Aggregations assays of phosphorylated Ser129 α-Synuclein

One major focus on αS phosphorylation is to address the relationship between phosphorylation and aggregation. Hitherto, the role of phosphorylation, particularly at Ser129, in modulating aggregation and the chronological order of these two events in pathological cascades of PD have still not been clearly defined. Fujiwara *et al*. firstly reported that αS was phosphorylated at Ser129 by their Mass Spectrometry assays and that this modification could promote αS aggregation *in vitro* (Fujiwara et al, 2002). However, by using phosphorylation-mimicking (Ser to Asp/Glu) and –retarding (Ser to Ala) mutants to simulate the effects of phosphorylation or to block other phosphorylation sites (i.e. Ser87), Paleologou *et al.* investigated the interplay between Ser129 phosphorylation of αS and its aggregation and suggested that the S129 phosphorylation blocked fibril formation (Paleologou et al, 2008). Similarly to *in vitro* studies, accumulating *in vivo* findings from different cell cultures and animal models presented diversified indications regarding the role of Ser129 phosphorylation in modulating αS aggregation and neuronal toxicity (Azeredo da Silveira et al, 2009; Chen & Feany, 2005; Chen et al, 2009; McFarland et al, 2009; Smith et al, 2005).

Most of studies mentioned above were performed by using the specified mutants to resemble the effects of phosphorylation. However, it should be noted that phosphorylation mimics by point mutation can not completely and accurately reproduce all aspects of native phosphorylation and the mutations at other sites are likely to introduce nonspecific side-effects. Thus, to produce accurate phosphorylation at an expected site without applying additional mutations is of critical importants in our experiment.

Our previous real-time NMR assay identified the exclusive selectivity and significant efficiency of PLK3 on phosphorylation of αS Ser129. Therefore, we chose PLK3 as the kinase to specifically phosphorylate Ser129 *in vitro*. To investigate whether the phosphorylation of Ser129 modulates its aggregation, the aggregation assay has been performed based on the PLK3-mediated phosphorylation is described in Figure 3.1.5.(A).

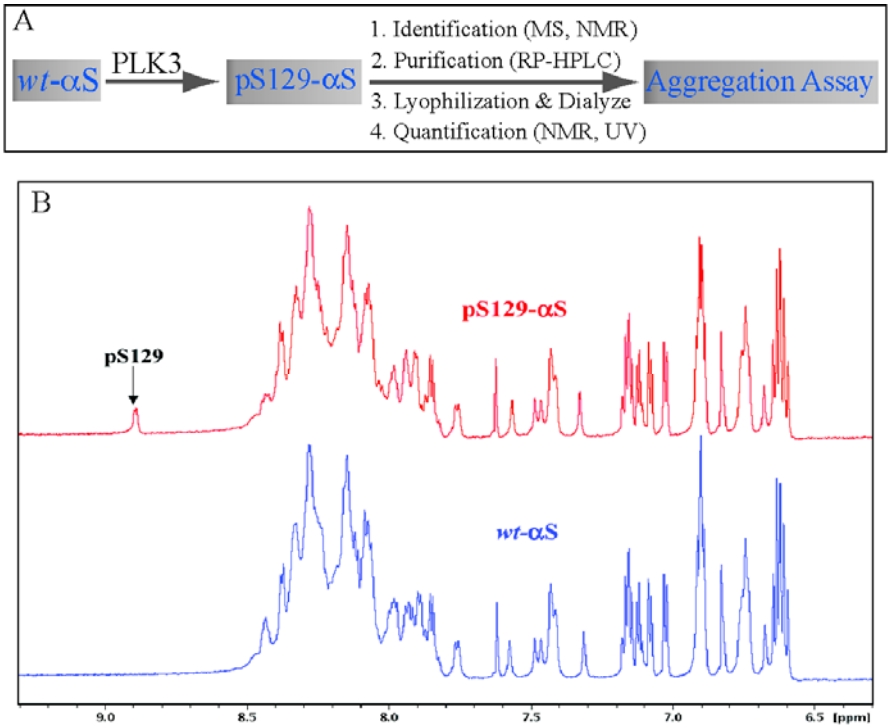

Figure3.1.5. Preparation for aggregation assay of phosphorylated-Ser129 αS. (A)Flow chart of the aggregation assay for pS129-αS. The consecutive steps include phosphorylation by PLK3, characterization and purification of phosphorylated sample. (B) Characterizing phosphorylation by 1D NMR spectrum. The spectrum of *wt*-αS (blue) and pS129-αS (red) are compared. In spectrum of pS129-αS, single peak at 8.8 ppm denotes the single phosphorylation at Ser129.

In the first stage, *wt*-αS was adapted into the phosphorylation buffer containing Mg^{2+} and ATP. Then phosphorylation was started by the addition of PLK3 and incubated under 30°C for 2.5 hours to achieve complete phosphorylation. Secondly, trace amount of the reaction product has been checked by Mass spectrometry to identify whether there was a mass difference of 80-Dolton in comparison to the *wt*-αS sample. At the same time, the purity of the phosphorylation product was examined. Accordingly, the confirmed sample was loaded into RP-HPLC coupled with UV and MS detection to collect pS129-αS. The purified material of pS129-αS was lyophilized to remove the solvent used in HPLC and further dialyzed against the aggregation buffer together with *wt*-αS to assure that both samples dissolved in identical solution for the aggregation assay. At the end, PULCON method (Wider & Dreier, 2006) based on NMR spectroscopy was employed to calibrate the protein concentration of pS129 αS and *wt*-αS aiming to produce identical concentrations for both proteins in the aggregation assay

for both proteins. A comparison between 1D NMR spectrum of pS129 αS and *wt*-αS clearly shows one single peak at 8.8 ppm [Fig. 3.1.5(B)] which was identified as the phosphorylation of Ser129 by HSQC spectrum in the previous real-time assay.

Following the purification and concentration-calibration, the samples of pS129-αS and *wt*-αS were further processed by getting rid of small particles and small oligomeric species and were consequently adapted to start the aggregation assay with a monomeric concentration of 50μM. Kinetics of the fibril formation were monitored by Thioflavin T (ThT) fluorescence. Unexpectedly, within the time course of 150 hours, general kinetic trend and fibril yield reflected by ThT did not show a significant difference between pS129-αS and *wt*-αS under the assay condition [Figure 3.1.6 A]. After 40 hours of the time course, the growth rates of fibrils for both samples became much slower and no distinguishable difference between two samples was observed. This revealed that the aggregation kinetics were close to saturation and the fibril yields for these two samples were similar. In line with kinetic data, EM images revealed that fibrils of pS129-αS [Figure3.1.6 D] and *wt*-αS [Figure3.1.6 E] presented similar morphology.

Interestingly, a significant difference was observed at 24hours. Including the consideration of experimental uncertainty, the sample of pS129 αS shows relatively stronger ThT intensity than that of *wt* αS at 24 hours. This observation agrees with the structural findings that phosphorylation at Ser129 of αS potentially modifies protein conformation by partially releasing the long-range interactions within the polypeptide chain (Paleologou et al, 2008). As an intrinsically disordered protein (IDP), the transient long range interactions between N-terminal and C-terminal of αS importantly contributes to maintaining the protein conformation and inhibiting aggregation propensity(Bertoncini et al, 2005b; Dedmon et al, 2005c). Furthermore, this phenomenon was reproduced in the aggregation assay at a lower αS concentration (10μM) shown in Figure3.1.6 (B).

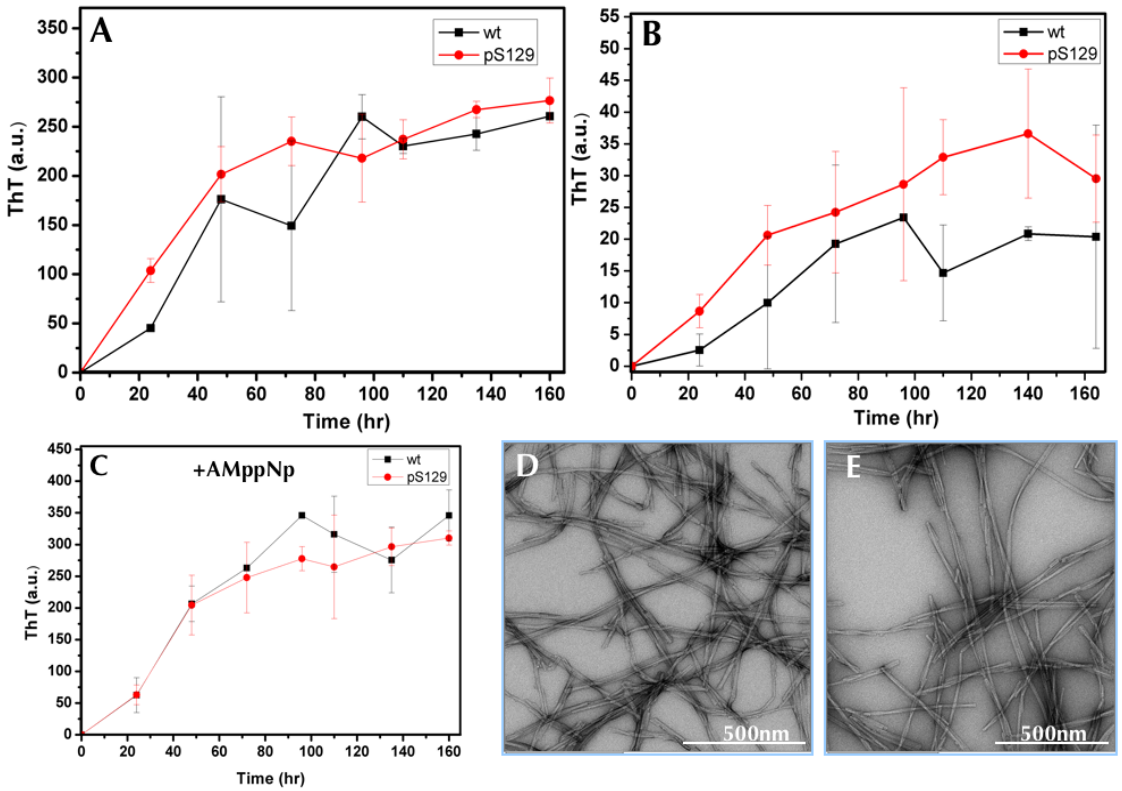

Figure 3.1.6. Aggregation assay of pS-129 αS and *wt*-αS. Fibril formation of pS129 (red) and wt-αS (black) were followed by ThT fluorescence under the different aggregation conditions. (A) pS129-αS and wt-αS started aggregation at a monomeric concentration of 50μM. EM images of the final aggregation products of pS129 and *wt*-αS are shown in (D) and (E) respectively. (B) Reproducing aggregation for both proteins at the lower concentration (10μM). (C) Agregation assay was performed with the presence of AMppNp(500μM), a hydrolysis-resistant analogue of ATP. All error bars were estimated based on statistics of triplicate trials for each sample.

In addition, we checked whether ATP can have impact on αS aggregation. ATP is the necessary compound for phosphorylation and is likely present during the aggregation of phosphorylation *in vivo*. Therefore, AMppNp, one hydrolysis-resistant analogue of ATP, has been included in the aggregation system with the amount of 10-fold in excess of the proteins (AMppNp: 500μM and proteins: 50μM). The aggregation profile in the presence of AMppNp is similar to the aggregation profile counterpart observed in the case of its absence. A slight increase of fibril amount during the saturation phase compared to the assay without the addition of the compound was observed in Figure 3.1.6 (C). Also, ThT intensities for the two samples at 24 hours were also similar. Hence, modifications of aggregation kinetics and fibril yield induced by

AMppNp were not drastic, suggesting that these minute effects were non-specifically caused by this ATP analogue, but were not critical.

3.1.2.3 Aggregation assays of Ser129 phosphorylation mimics of α-Synuclein

Although the effects of phosphorylation can not be completely reproduced by the mimics, genetic mutation of Ser to Glu or Asp still provides us opportunity and freedom to artificially modify the side-chain of the residue and simulate the steric and electrostatic properties of phosphorylation not only *in vitro* but also *in vivo* (Figure3.1.7).

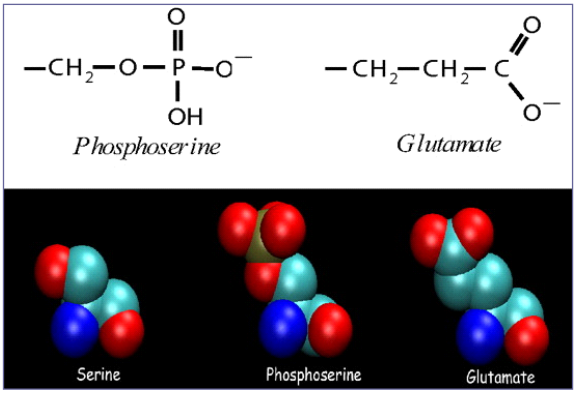

Figure3.1.7 The atomic structures of the side chains of Glu and phospho-Ser demonstrate the structural and electrostatic similarities between the two moieties. The figure is taken from the publication (Paleologou et al, 2008).

To further determine the potential roles of Ser129 phosphorylation on protein aggregation, we produced two Glutamine mutants to mimic the phosphorylation. Double mutant P128E/S129E αS and triple mutant M127E/P128E/S129E αS were designed aiming at multiplying the effects of phosphorylation at the neighboring region of Ser129 and hence further clarifying the issues regarding how these mutations impact on αS aggregation.

The aggregation assay for the two mutants and *wt*-αS indicated that these two mutations did not affect aggregation kinetics [Figure3.1.8]. Three samples displayed similar scales of lag phase and fibril growth rate. The final yields of fibrils were also very similar. This was also consistent with corresponding EM images, which the fibrils of the three proteins were in similar size and morphology.

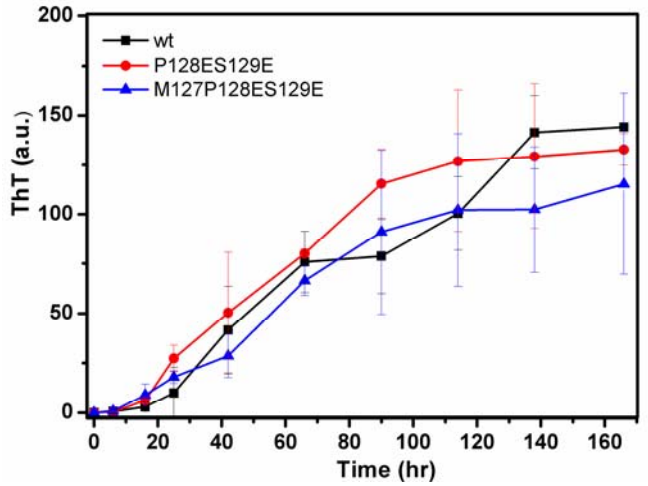

Figure3.1.8 Aggregation assay for the αS phosphorylation mimics. The aggregation kinetics of *wt* αS (black), double mutant P128E/S129E (red) and triple mutant M127E/P128E/S129E (blue) are shown.

In conclusion, we examined the aggregation propensity of αS with Ser129 phosphorylation. Both αS with phosphorylation at the Ser129 by kinase PLK3 *in vitro* and the phosphorylation mimics displayed similar aggregation kinetics of fibril formation and morphology of fibril products, suggesting that phosphorylation at this site does not significantly change the aggregation. This finding agrees with the observations that phosphorylation of Ser129 of αS is independent of αS aggregates formation, where the kinase (CKs and PLKs) was co-expressed with αS *in vivo* (Waxman & Giasson, 2011).

3.2 Interplay between alpha-Synuclein and Rab proteins

The family of Rab GTPases belongs to Ras superfamily of small G proteins. The human Rab family consists of 70 members and most of them exert important functions in regulating vesicular trafficking and the exocytosis of living cells (Hutagalung & Novick, 2011). In neurons, vesicle trafficking is a pivotal process responsible for neurotransmitter transport and release. The specified Rab proteins are involved in all steps of the trafficking process from the vesicle budding to final diffusion to plasmid membrane. Meanwhile, the deficit of vesicle trafficking is characterized as one phenotype of αS neuronal toxicity (Auluck et al, 2010). In well-established yeast assay for αS (Outeiro & Lindquist, 2003) , the overexpression of Rab1, Rab3a, and Rab8a respectively were found to rescue the αS-induced deficits occurring at multiple stages of vesicle trafficking (Cooper et al, 2006; Gitler et al, 2008).

What are the structural mechanisms underlying this rescuing effect of the Rabs? To answer this question, we performed NMR based structural analysis and correlated biophysical assays to study the interactions between αS and Rabs. Analysis of amino acid sequences of Rab1b, Rab3a and Rab8a revealed diversity at their C-termini. Following this, we used NMR titration to study potential interactions that might exist between αS and these Rabs at atomic resolution and found that Rab8a was capable of binding to αS. Using the peptide synthesis technique and the expression of the truncated protein, this interaction has been dissected with respect to different parts of Rab8a. To further characterize the interaction in details, we implemented the NMR assignment for Rab1b and Rab8a. Accordingly, we were able to map interaction sites on Rab8a exactly. Moreover, we also found that the binding affinity of Rab8a to αS depending upon the different nucleotide-bound states of Rab8a.

In parallel to the studies of the interactions based on NMR structures, we also performed an aggregation assay for αS in the presence of different Rabs. Our scope was thus extended to search for potential interactions between the Rabs and αS aggregates and to evaluated the influence of Rab proteins on the oligomerization and fibrillization of αS. Taken together, the studies reveal the interplay between the different Rab proteins andαS of different states.

3.2.1 Sequence alignment of Rab1b, Rab3a and Rab8a

The *in vivo* investigation demonstrates that the overexpression of Rab1, Rab3a and Rab8a can suppress dopaminergic neuron loss caused by overexpression of human αS in *C. elegans* and primary rat midbrain cultures (Gitler et al, 2008). Interestingly, in the model of *C. elegans*, Rab8a reduced the neurodegeneration of affected worms from 85% to 60%, whereas Rab1 reduced the neurodegeneration to 80% and Rab3a reduced to 75%. Thus, this suggests that 3 Rab proteins might differentiate mechanistically in their interactions with αS.

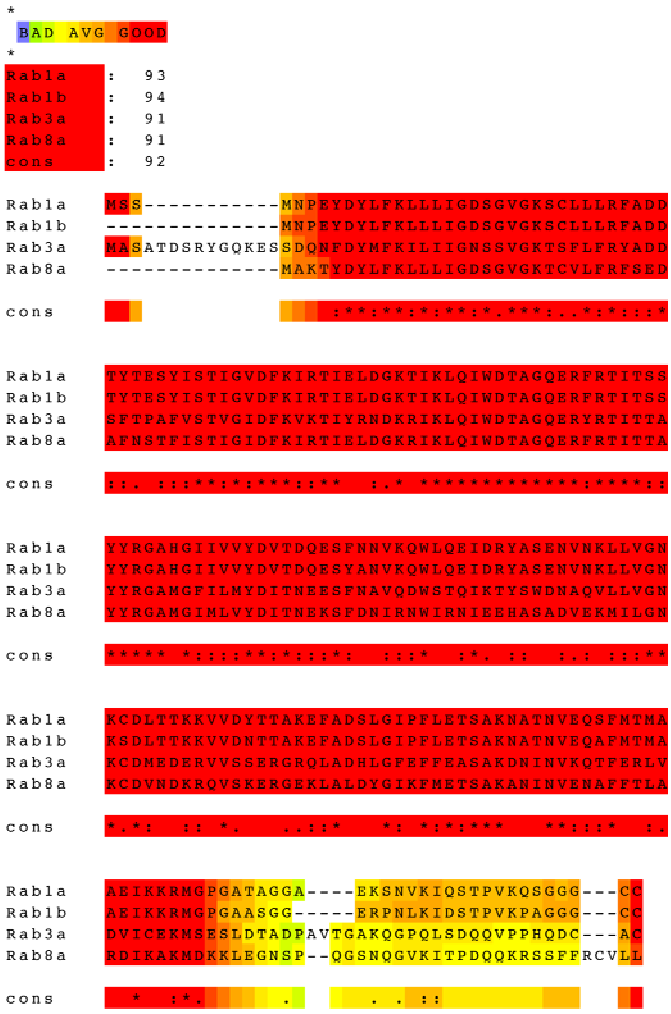

Figure 3.2.1 Sequence alignment for Rab1a, Rab1b Rab3a and Rab8a. Multiple sequence alignment has been implemented for the four protein sequences (homo sapiens) by T-coffee method on the server (Notredame et al, 2000; Poirot et al, 2003). "*": Identical, ":":conserved substitution, ".": semi-conserved substitution. The color scale indicates the scoring of alignment from blue (score=0) to red (score=100), where the intermediate score is indicated by range of yellow.

Sequence alignment provides us a preliminary insight into the difference between the primary structures of 3 Rab proteins. As shown in Figure 3.2.1, Rab1a and Rab1b share very high degrees of similarity and identity of sequence in which only 14 residues differ, most of them are restricted to the range 180-199 (Touchot et al, 1989). Rab8a as the closet paralog to Rab1, also displays a high degree of similarity to Rab1a (75% similarity and 55% identity) and it mainly differs from Rab1 at at its C-terminal tail regarding its distinct physiological function on post-Golgi vesicles. Of these four Rab proteins, Rab3a shows the least similarity to the other three, particularly that its N-terminal possesses additional 11 residues that are not present in the other three proteins, accounting for the neuron-specific expression of Rab3a (Hutagalung & Novick, 2011). Apart from the amino and carbonyl termini of these four proteins, the majority of the sequences corresponding to the folded parts of Rab proteins are highly similar. This is a common feature conserved in members of the Ras-GTPases family as this part is responsible for GTP hydrolysis (Itzen & Goody, 2011).

3.2.2 Unique binding of Rab8a to α-Synuclein

NMR signals of backbone amides provide excellent information to probe protein-protein/ligand interactions with description of the interaction interface and binding affinity according to perturbation of chemical shift and line-width analysis (Craik & Wilce, 1997; Gao et al, 2004). Thus, based on NMR spectroscopy, we studied interactions of αS with different Rabs and identified the corresponding binding sites at αS.

3.2.2.1 Rab8a, but not Rab1b and Rab3a binds α-Synuclein

The $^{1}H–^{15}N$ HSQC spectra of αS in the presence of Rab1b, Rab3a, and Rab8a respectively for molar ratios up to 1:10 of αS to the Rab were recorded at 15°C and pH 7.4. The resonances of the spectra for αS were well resolved and sharp. Both GDP- and GppNHp-(a hydrolysis-resistant structural analogue to GTP) bound Rabs were titrated into αS.

As reflected in Figure 3.2.2(A), titration of unlabeled Rab8a (GDP- and GppNHp-) into isotropic ^{15}N-labeling αS resulted in the shifting of the C-terminal resonances of αS. However, there were no significant bindings found in the cases of

Rab1b and Rab3a. In the presence of Rab1b and Rab3a, the C-terminal and rest parts of αS did not show a clear trend of chemical shift perturbation. In the presence of Rab8a, the affected residues of αS with chemical shift perturbation beyond 0.06ppm were mainly located at the acidic C-terminal region from G111 to A140. The rest parts of the N-terminus and NAC region of αS remain unperturbed by the presence of Rab8a. Displacement of αS peak positions was demonstrated as the function of stepwise addition of Rab8a(GDP) and Rab8a(GppNHp) [Figure3.2.2 (B), (C)]. Neighboring regions of residue Y125 and D134 of αS were mostly influenced by an increasing molar ratio of Rab8a to αS. Both GDP- and GppNHp-bound Rab8a displayed similar binding pattern to αS but different affinities.

Based on the chemical shift perturbation of αS at different amounts of Rab8a, the K_d values for Rab8a(GDP) and Rab8a(GppNHp) binding to αS were estimated as 0.186902 ± 0.008463mM and 0.45089 ± 0.045431mM respectively. Indeed, quantitative comparison represented by K_d demonstrated that GDP-bound Rab8a possessed stronger binding affinity to αS than the GppNHp-bound Rab8a, consistent with the observation of titration [Figure3.2.2 (B), (C)]. The K_d difference in these two states would have importantly functional implication regarding to the interplay between αS and Rab8a. Hence, in the following analysis, we mechanistically dissected this interaction to identify the binding sites at both proteins in detail.

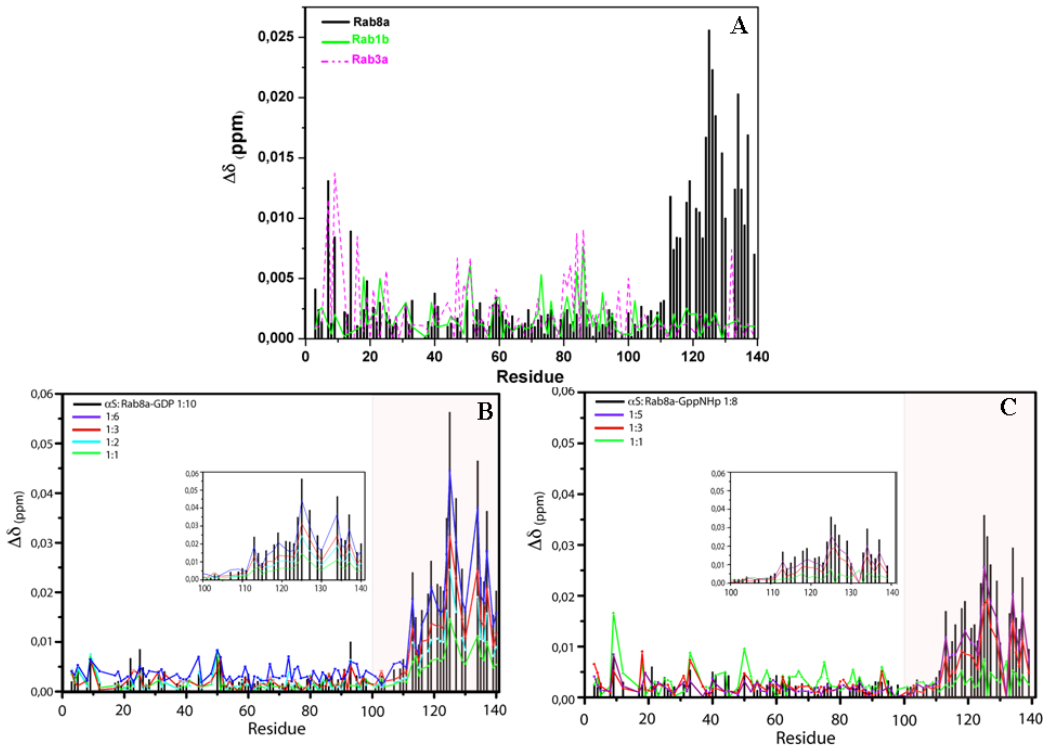

Figure 3.2.2 NMR titration of Rab1b, Rab3a and Rab8a into ^{15}N-αS. (A)Chemical shift perturbation for studying protein interaction was shown by defining resonance shifting in NMR HSQC spectra of αS, which were in the presence of Rab GTPases at the concentration ratio 1 to 5 (black bar: Rab8a, green line: Rab1b and purple dash line: Rab3a). Replacement of the affected peaks of αS was increased as the function of added concentrations of Rab8a at GDP-bound state (B) and GppNHp-bound state (C). (The HSQC spectra were recorded by María L. Orcellet.)

3.2.2.2 Anatomy of the interaction between α-Synuclein and Rab8a

αS consists of three functional domains, namely the N-terminus, the NAC region and the C-terminus. Each of these three domains has been well-characterized with distinct features with respect to monomeric structure, fibril formation, molecular modification, membrane affinity, ligand binding etc (Bisaglia et al, 2009). It's therefore necessary to determine the structural reason why Rab8a specifically binds to C-terminal part of αS (residue110-140).

Compared with other two domains, negatively charged residues (Glu and Asp) are enriched in the C-terminal part of αS. Such significant number of negative charges contributes to the long-range interactions and stabilizes the tertiary conformation of αS (Bertoncini et al, 2005b; Dedmon et al, 2005c). Meanwhile, the abundant negative

charges offer the opportunity for positively charged binding partners to interact with the C-terminal of αS, which was found in the case of polyamines binding (Fernandez et al, 2004). It's has also been noticed that the members of the Rab family differs mainly at their C-termini. Based on this fact, we firstly analyzed the sequence of αS and the 3 Rab proteins [Figure 3.2.3]. Unsurprisingly, a significant number of negative charges "-13" are distributed at C-terminal part (100-140) of αS and Rab8a is the only one possessing positive net-charge "+3" at its C-terminus. However, Rab1b and Rab3a possess rather neutral or even negative charges at their C-termini respectively. Therefore, the observed binding of Rab8a to αS by NMR titration occurs probably as a result of charge-driven electrostatic interaction between C-termini of the two proteins.

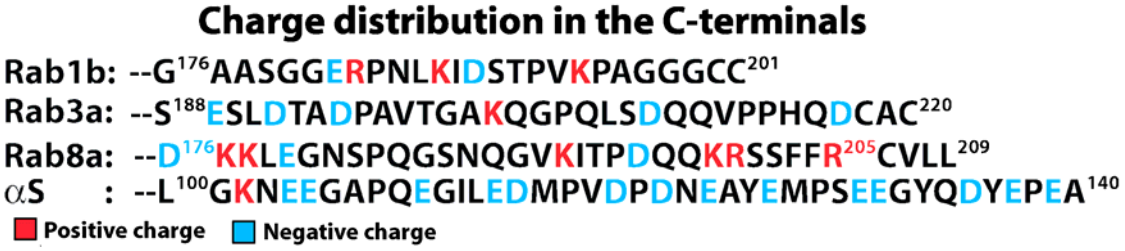

Figure3.2.3. Charge distribution of C-terminal residues of Rab1b, Rab3a, Rab8a and αS. The charge distribution has been demonstrated by labeling the charged residue by specified color (red: positive charge, cyan: negative charge). The significant positive net-charge of Rab8a and negative net-charge of αS were unambiguously indicated.

According to the analysis of the charge distribution, we synthesized the C-terminal peptide of Rab8a comprising of 30 residues (Asp176-Arg205) and titrated it into αS. The six positively charged residues Lys177, Lys178, Lys192, Lys199, Arg200, Arg205 and three negatively charged residues Asp176, Glu180, Asp196 were included in this peptide and together were characterized as "+3" net charges. The peptide-induced perturbations of chemical shifts to αS resembled well the effect of full-length Rab8a on the C-terminal of αS [Figure3.2.4]. The black bars in the figure represent the chemical perturbation at the molar ratio of Rab8a-GDP to αS as 5:1, shown as a reference in this figure. The red line indicates the chemical perturbation of αS at 10:1 ratio of peptide:αS. The pattern and the magnitude of perturbation of the peptide is similar to full-length Rab8a. But, the amount of peptide used is twice the amount of the

full-length protein, suggesting that full-length protein maintain a stronger affinity to αS than its C-terminal fraction.

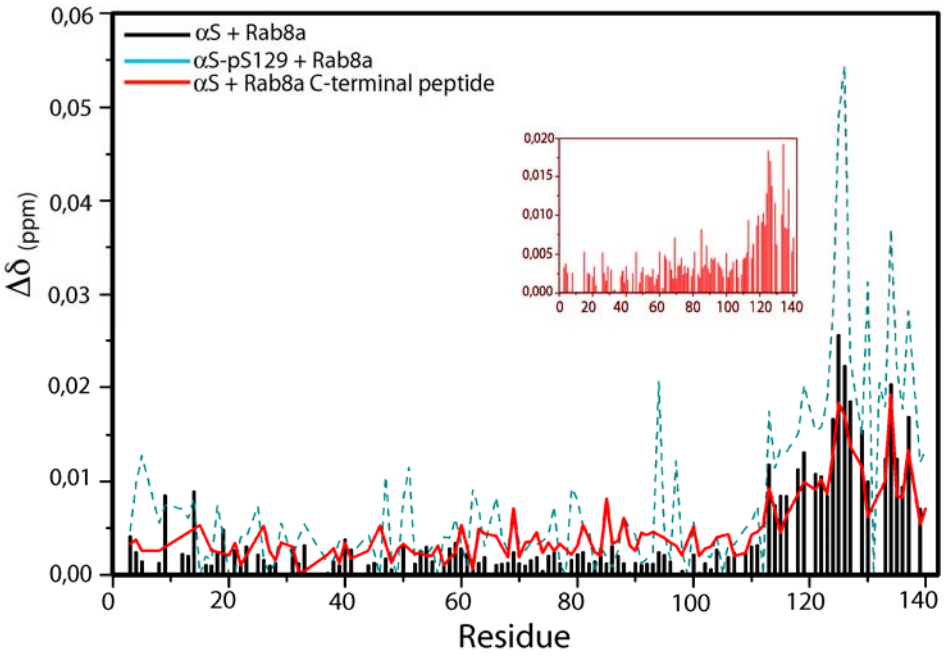

Figure 3.2.4. Interaction between C-termini of αS and Rab8a. Chemical shift perturbations show the binding between the C-termini of Rab8a and αS. αS (Black bar) and phosphorylated-Ser129 αS (cyan dash line) were titrated by Rab8a at αS:Rab8a ratio of 1:5. Meanwhile, αS was titrated by Rab8a C-terminal peptide at αS to peptide ratio of 1:10 (red line) and the inlet represents the corresponding chemical shift perturbation plot of the peptide titration.

Phosphorylated Ser129 αS was generated by using Polo-Like Kinase 3 (PLK3) and the interaction between phosphorylated αS and Rab8a was then assessed. Phosphorylated-Ser129 αS displayed a similar binding model to *wt*-αS but the degree of perturbation was enhanced by approximately a factor of approximately 2 due to the phosphorylation [Figure 3.2.4]. The phosphorylation at Ser129 introduced one more negative charge to C-terminus of αS, which can be reflected by the increased perturbation around pSer129. Therefore, the opposite charges existing at the carboxyl termini of αS and Rab8a play an important role in adjusting their interaction.

Table 3.1 Statistics of charged residues for C-terminally truncated Rab1b, Rab3a and Rab8a

	Positively charged residues (K+R)	Negatively charged residues (D+E)	Sum of charges (Net-charge)
Rab1b(1-175)	21	24	-3
Rab3a(1-187)	23	27	-4
Rab8a(1-173)	27	24	+3

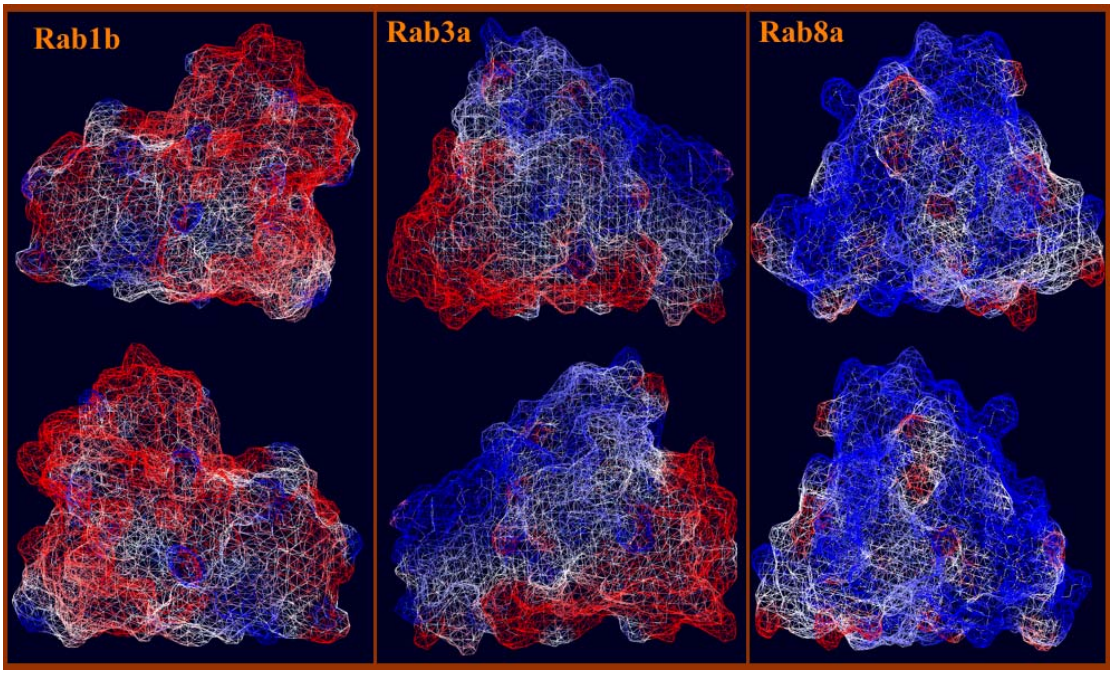

Figure 3.2.5. Surface mapping of electrostatic potential for C-terminally truncated Rab1b, Rab3a and Rab8a. Electrostatic potential based on the coulomb interactions was calculated by Swiss-PdbViewer (Guex & Peitsch, 1997). The structures of Rab1b (PDB code: 3NKV), Rab3a (PDB code:3RAB) and Rab8a (PDB code: 3QBT) were chosen for the surface mapping (Dumas et al, 1999; Hou et al, 2011; Muller et al, 2010). Each structure with the surface mapping was displayed with the view of both facing and back. The blue color stands for positive potential, whereas red color and white color stand for negative potential and neutral potential.

The positively charged C-terminal peptide can resemble the effect of full-length Rab8a binding to αS, but has a relatively weaker affinity of this peptide to αS than the full-length protein has been recognized. This suggests that except for the C-terminal tail, other parts of Rab8a are capable of binding to C-terminus of αS as well. Therefore, we investigated the charge states of the folded parts of these 3 Rab proteins. The statistic of charge states for the C-terminally truncated parts of 3 Rabs has been performed by the ExPASy Protparam Tool (Artimo et al, 2012) [Table 3.1]. By counting the number of

positively and negatively charged residues in the N-terminal folded part, the total charge of Rab8a is positive 3, contrary to the -3 for Rab1b and the -4 for Rab3a. This suggests that the folded part of Rab8a also has potential to bind to the C-terminal of αS. Furthermore, surface mapping by electrostatic potential was performed for the published crystal structures of these three Rab proteins [Figure 3.2.5]. In line with the charge statistics described in Table3.1, the surface of Rab8a largely presents positively electrostatic potential which indicates that the outer surface of Rab8a is dominantly occupied by positively charged residues. Whereas, Rab3a shows relatively neutral surface and Rab1b presents more negative potential on its surface. In conclusions, charge statistics and surface potential mapping suggests that N-terminally folded part of Rab8a possesses a strong propensity to bind to the highly negative C-terminus of αS.

3.2.2.3 C-terminally truncated Rab8a binds to α-Synuclein

Rab8a(6-176) with the truncation of the C-terminal tail (Rab8a-δC) has been used to study its potential to interacting with αS. Both Rab8a-δC(GDP) and Rab8a-δC(GppNHp) were titrated into ^{15}N-αS and changes of αS were reflected by cross-peaks of backbone ^{1}H-^{15}N resonance of αS in two dimensional HSQC spectra [Figure3.2.6]. Both Rab8a-δC(GDP) and Rab8a-δC(GppNHp) reproduced the binding effects to the acidic C-terminus(G111-A140) of αS similarly to the full-length protein and the C-terminal peptide described before. Interestingly, the change of resonance positions illustrates that the Rab8a-δC(GDP) binds to αS with a stronger affinity than Rab8a-δC(GppNHp) at the same molar ratio to αS.

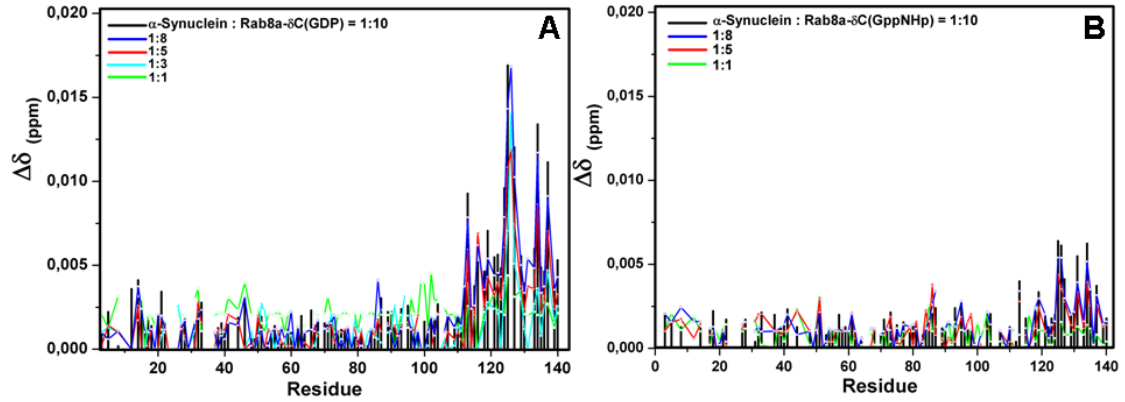

Figure 3.2.6. Analysis of Rab8a(6-176) binding to αS by NMR spectroscopy. Changes in individual cross-peak positions of backbone ^{1}H-^{15}N resonance of αS in two dimensional HSQC spectra in the presence of Rab8a(6-176)-GDP(A) and Rab8a(6-176)-GppNHp(B) for the molar ratios up to 1:10 of αS/Rab.

To clearly represent the different affinities, the changes of the peak positions in HSQC spectra of αS in presence of molar ratio 1:1, 1:5, 1:10 αS/ Rab8a-δC(GDP) and Rab8a-δC(GppNHp) have been selectively displayed and compared in Figure3.2.7. At molar ratio 1:1, the presence of both Rab8a-δC(GDP) [Figure3.2.7(A)] and the Rab8a-δC(GppNHp) [Figure3.2.7(B)] did not induce obvious changes in αS. At the ratio of 1:5, both samples shows the binding to the C-terminal of αS. But, the GDP-bound form [Figure3.2.7(C)] already shows ~3-fold larger magnitidue of resonance shifts as the GppNHp-bound form [Figure3.2.7(D)] and this trend remains until the molar ratio of Rab8a-δC to αS reached 10:1 for the GDP-bound form [Figure3.2.7(E)] and GppNHp-bound form [Figure3.2.7(F)]. The higher affinity of Rab8a-δC(GDP) than Rab8a-δC(GppNHp) for binding to αS was also demonstrated by the intensity plot at the Rab8a-δC to αS molar ration of 10:1 [Figure3.2.7 (G) and (H)].

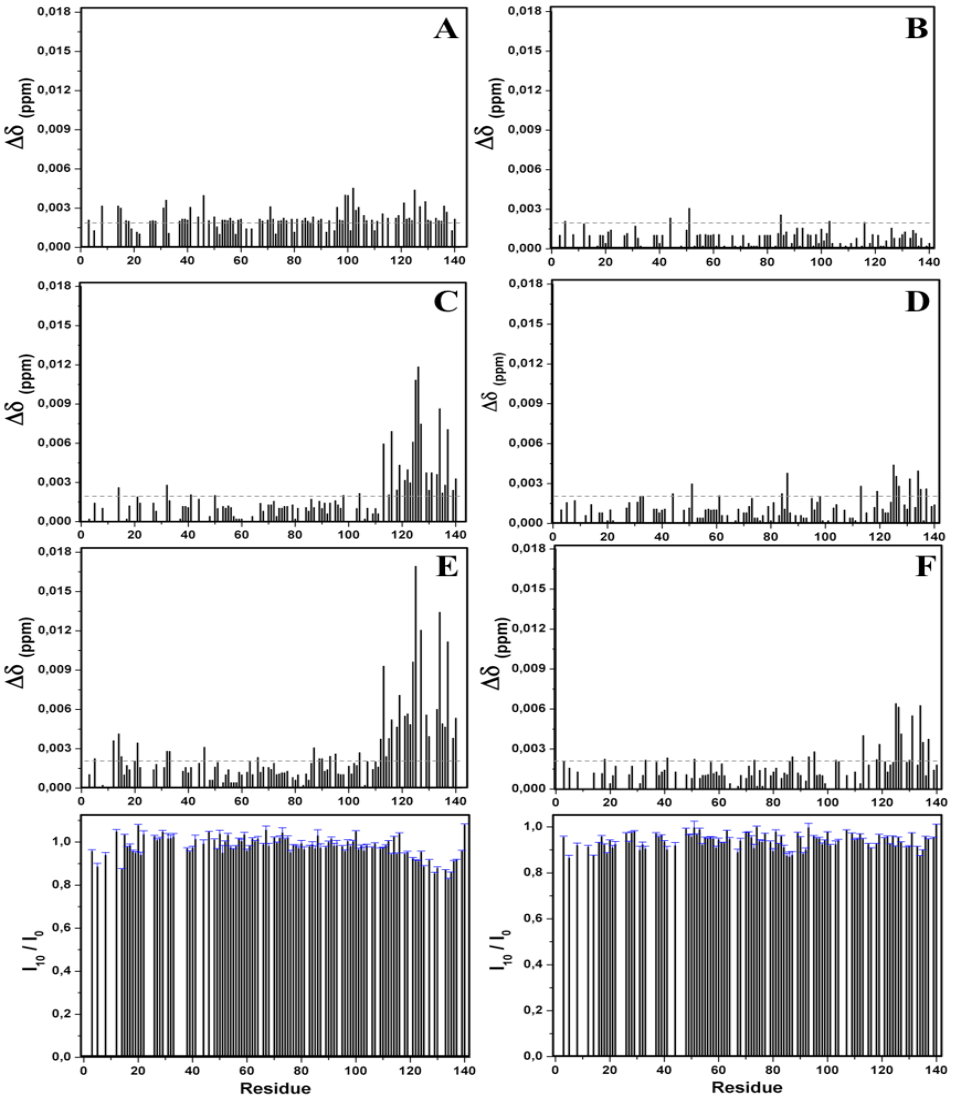

Figure3.2.7 Analytic comparison for Rab8a(6-176)-GDP and Rab8a(6-176)-GppNHp binding to αS. Change in chemical shifts of individual HSQC peaks of αS in the presence of Rab8a(6-176)-GDP (A, C, E) and Rab8a(6-176)-GppNHp(B, D, F) at molar ratio of 1:1, 1:5, 1:10 of αS to Rab8a(6-176). The dashline in chemical shift perturbation plots indicates average noise level as estimated by comparing repeating experiments. The intensities of cross peaks of αS at 1:10 molar ratio to Rab8a(6-176) have been shown in (G) and (H) for GDP and GppNHp bound Rab8a(6-176). Error bars were calculated based on signal to noise.

In summary, we found that the electrostatic interactions existing between αS and Rab8a were important for the binding of Rab8a to αS. This was further confirmed by the fact that Ser129 phosphorylation of αS enhances the binding remarkably and that the C-terminus peptide of Rab8a can reproduce the binding to αS. Furthermore, not only the C-terminus but also the N-terminally folded part of Rab8a possesses capacity

to bind to αS, indicated by surface mapping of its crystal structure. NMR titration of Rab8a-δC into αS proved that this truncated Rab8a could bind to αS. We also observed a different affinity of GDP- and GppNHp- bound Rab8a-δC to αS, consistent with the results of full-length Rab8a.

3.2.3 Aggregation assays of α-Synuclein with Rab8a and it's C-terminus

Following the identification of Rab8a/αS interaction by NMR, we investigated the role of Rab8a in mediating αS aggregation by ThT fluorescence. Linking with the NMR interaction assays, αS was incubated with full-length Rab8a(GDP) and the C-terminus peptide of Rab8a respectively under the aggregation conditions. Firstly, Rab8a displayed a distinctive efficiency in modulating αS aggregation [Figure 3.2.9. (A)]. For the applied molar ratio of Rab8a to αS, all 1:0.3, 1:1, 1:3 ratios revealed that substantial enhancement of fibril formation was achieved by shortening the lag phase time and reaching the saturated stage more rapidly than in the absence of Rab8a. Interestingly, however, when the molar ratio was raised up to 5:1 of Rab8a to αS, the profile of aggregation kinetics was different to the cases with lower amount of Rab8a. At this ratio, no kinetic improvement was observed and the fibril growth displayed similar trend to the αS control without the addition of Rab8a.

Following the aggregation, EM was used to distinguish between the different fibrillar species generated under the different molar ratios of Rab8a to αS [Figure 3.2.9. (B)-(D)]. Referring to the characteristic morphology displayed by the fibrils of αS control, EM images addressed the increased protein backgrounds accumulated on the surface of fibrils as a consequence of increased amounts of Rab8a. With the increased amount of Rab8a, morphological diversity and the content of fibril association were also enlarged, particularly for the circumstances where the amount of Rab8a exceeded αS. This protein background is likely as a result of the Rab8a attaching to the fibril surface by binding to the αS C-terminus. The C-terminus of αS retains its disordered conformation outside the fibril core and thus is readily recognized by binding partners, i.e. Rab8a. We also observed the precipitates in all trials in the presence of Rab8a. The amount of precipitates was well correlated with the amount of Rab8a added at the starting of aggregation as depicted in Figure 3.2.9 (B) – (D). This observation indicates

that the observed precipitates were from the amorphous aggregates formed by Rab8a during the time course of αS aggregation. Rab8a was reported to possess low stability and solubility under some expression conditions (Bleimling et al, 2009; Lim et al, 2011). Additionally, recent study shows that αS can cause the aggregation of many different Rab GTPases in yeast and additionally the aggregation of αS can also be enhanced (Lim et al, 2011).

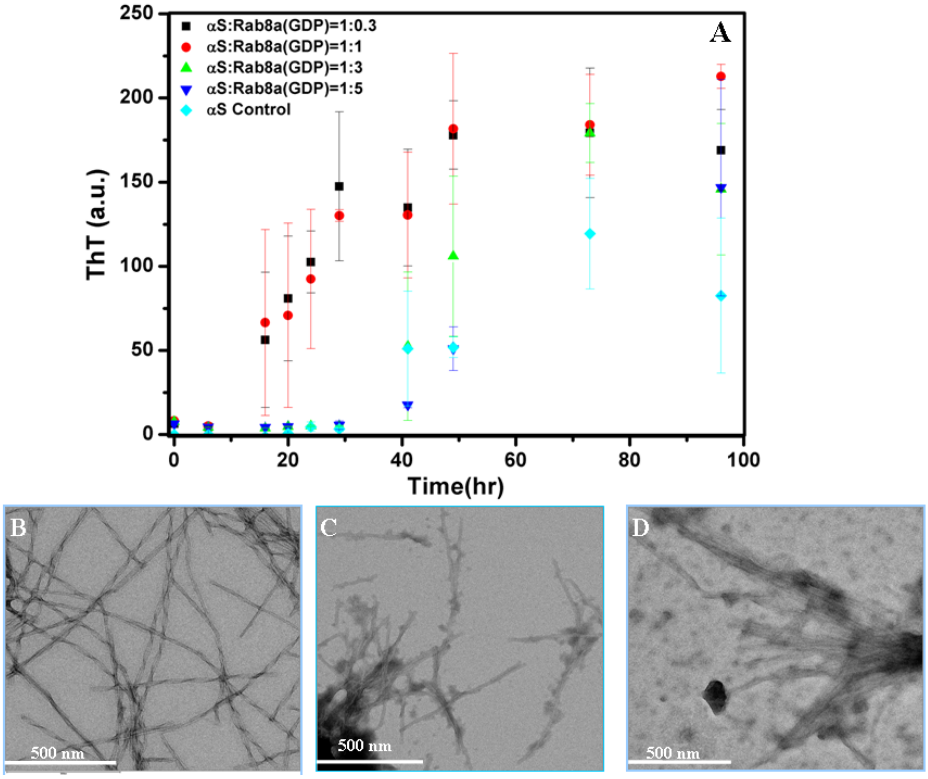

Figure 3.2.9. Aggregation assays of αS in the presence of Rab8a. (A) αS aggregations were influenced by Rab8a reflected by ThT fluorescence at αS:Rab8a ratio of 1:0.3, 1:1, 1:3, 1:5. The corresponding EM images for the αS control, 1:1 and 1:3 molar ratios are shown in figure (B) - (D), which illustrate both the amorphous background associated with Rab8a aggregates increased and the αS fibrils with distinct morphology decreased as the function of present amounts of Rab8a.

In line with the observation that the C-terminus of Rab8a simulated the binding of full-length Rab8a to αS, this segment can also contribute to the mediating effects of Rab8a on αS aggregation. The synthesized peptide containing 30 residues (174-205) of Rab8a C-terminal used in binding study was adapted in the aggregation assay by using 3 different molar ratios to αS (1:1, 3:1, 6:1). This peptide showed a does-independent

manner of enhancement to αS aggregation [Figure 3.2.10]. The comparison of kinetics of αS aggregations in the presence of Rab8a and its C-terminal fraction reflects that the peptide shortened lag phase to a similar extent to the whole protein, but prompted the fibril elongation by a relatively weaker efficiency than the full-length protein. Threfore, we found that the carboxyl terminus participates in the functions played by intact Rab8a on binding to αS and improving αS aggregation.

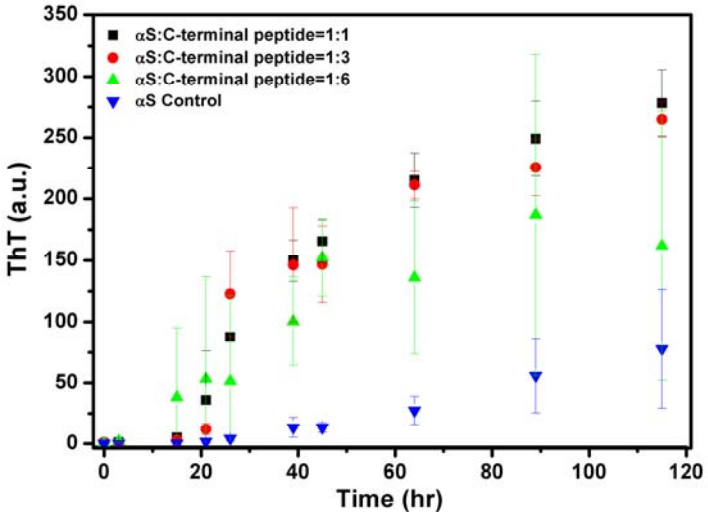

Figure 3.2.10. The C-terminal peptide of Rab8a simulated the effects of full-length protein on αS aggregation by enhancing the kinetics. The molar ratios of αS:peptide were set as 1:1, 1:3 and 1:6.

In conclusions, both Rab8a and its C-terminal peptide improve the aggregation of αS by significantly shortening the lag phase and enhancing the elongation rate. In concert with the interaction studies by NMR, Rab8a adjusts αS aggregation by binding to its C-terminus.

3.2.4 Aggregation assays of α-Synuclein with Rab1b and Rab3a

Rab1 and Rab3a were suggested to suppress the neuronal toxicity induced by αS in animal models (Gitler et al, 2008). However, we did not observe the interactions of Rab1b or Rab3a with monomeric αS in our NMR titrations. It's likely that these two Rab proteins selectively interact with αS aggregates, i.e. oligomers and fibrils, rather than monomers. To address this question, we implemented aggregation assays for αS in

the presence of Rab1b and Rab3a to identify effects of these two Rabs on αS aggregation.

3.2.4.1 Aggregation with Rab1b

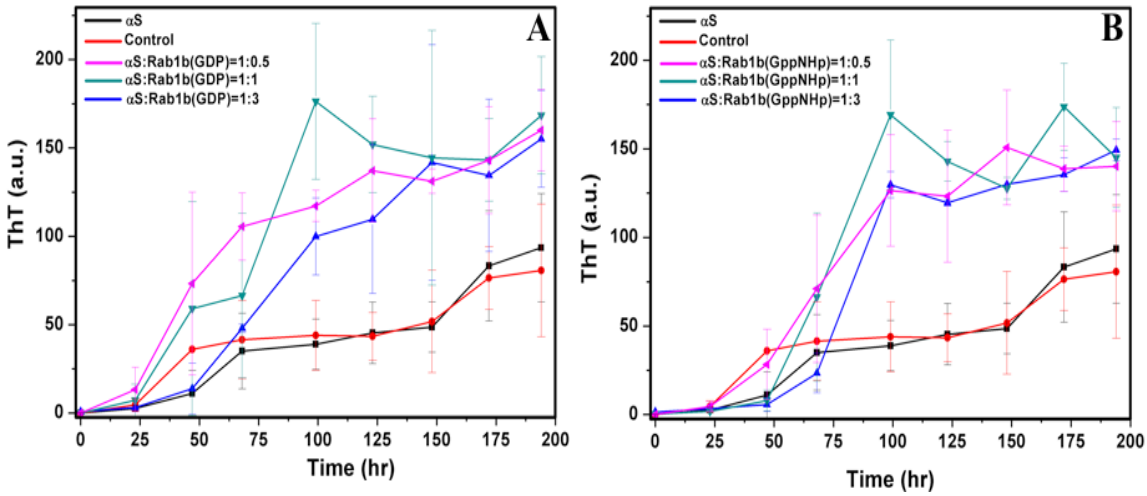

Figure 3.2.11. Aggregation assay of αS in the presence of Rab 1b. Aggregation kinetics of αS was catalyzed by the presence of Rab1b. αS was incubated with Rab1b(GDP) and Rab1b(GppNHp) at molar ratio of 0.5:1, 1:1, 3:1 to αS under aggregation conditions. The control here is including Rab buffer to examine its effects on αS aggregation. Fibril formation of αS followed by Thioflavin T fluorescence. The starting concentration of αS is 50μM, and the temperature for aggregation was 21°C.

As shown in Figure 3.2.11, the characteristic lag time of αS aggregation was slightly reduced due to the addition of Rab1b. Moreover, the elongation rate as an index highly correlated with the fibril growth rate was increased remarkably and thereby the time spanning for reaching saturation of fibril assembly was reduced by one half compared with αS alone. Interestingly, not only the modification of kinetics was observed, but the yields of fibril product mirrored by ThT intensity during the saturation stage were also amplified by a factor of 2 in the presence of Rab1b, which illustrated that the fibrillization was substantially improved by Rab1b. Additionally, EM images showed the fibrils generated with additions of Rab1b(GDP) and Rab1b(GppNHp) represent more twisted or bundled assemblies of protofilaments, which is different from the canonical morphology of αS fibrils as more single and extended forms.

Furthermore, the kinetic data highlighted that the fact that the presence of varied molar ratios of Rab1b to αS however did not lead to pronounced kinetic variance,

indicating that Rab1b mediated the aggregation by a dose-independent manner. The potential physiologically relevant differences between the active and inactive state of Rab is of major interests in our research. To this end, both Rab1b(GDP) and Rab1b(GppNHp) were adapted in the aggregation assays. However, there was no discrepancy in aggregation behaviors between the samples that modulated by the two forms of Rab1b. For Rab proteins, as members of GTPase family, the buffer used to dissolve Rabs contains nucleotide (GDP, GTP or its analogue) and ion Mg^{2+}. The aggregation of αS with only Rab1b buffer but without the protein was exerted as a control to examine the effects of these co-existing small molecules on aggregation. The kinetic of the Rab-buffer control kept same pattern as the αS alone, suggesting that the nucleotides and Mg^{2+} at the concentration used this assay did not interfere with αS aggregation.

3.2.4.2 Co-aggregation control with BSA

Besides Rab1b, globular proteins, such as protein chaperon HSP70 and HSP90, have been reported to effect on αS aggregation (Dedmon et al, 2005b; Falsone et al, 2009; Roodveldt et al, 2009). For the case of HSP70 in particular there were no direct interactions observed between this chaperon and monomeric αS either, but it did modify αS aggregation in an ATP-dependent manner. Therefore, does coexistence of globular proteins have generic impact on αS aggregation? To clarify this point, we placed protein BSA (Bovine Serum Albumin) as a globular protein control into αS aggregation.

Under the aggregation conditions, only the presence of Rab1b-GDP distinctively improves aggregation of αS [Figure3.2.12]. The presence of BSA slightly shortened the lag phase but it did not simulate the function of Rab1b in promoting fibril growth. Pure BSA and Rab1b did not generate the ThT-active fluorescence throughout 90 hours of aggregation time. Thus, in comparing with BSA, Rab1b significantly enhances αS aggregation with respect to fibril growth. We can thereby conclude that the aggregation improvement we observed in the previous assays was specifically as the result of Rab1b.

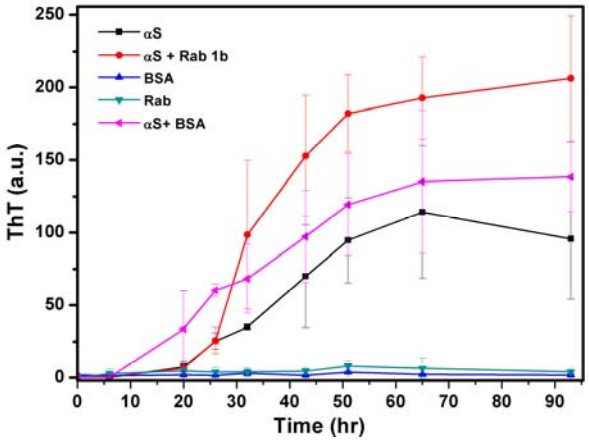

Figure 3.2.12. Co-aggregation control of αS with Bovine serum albumin (BSA). αS was aggregated with BSA and Rab1b(GDP) respectively at equal molar ratio. BSA and Rab1b-GDP were also incubated alone under the aggregation condition. The starting concentration of αS was 40μM, the concentrations of BSA and Rab1b(GDP) were 4μM. The temperature for aggregation was 21°C.

3.2.4.3 Aggregation with Rab3a

Rab3a has highly neuron-specific expression and it can suppress the neuronal toxicity of αS in the animal models (Gitler et al, 2008). At the same time, similar to Rab3a, Rab1b doesn't bind to monomeric αS but it does significantly enhance αS aggregation. Therefore, we investigated whether Rab3a has a similar effects on αS aggregation.

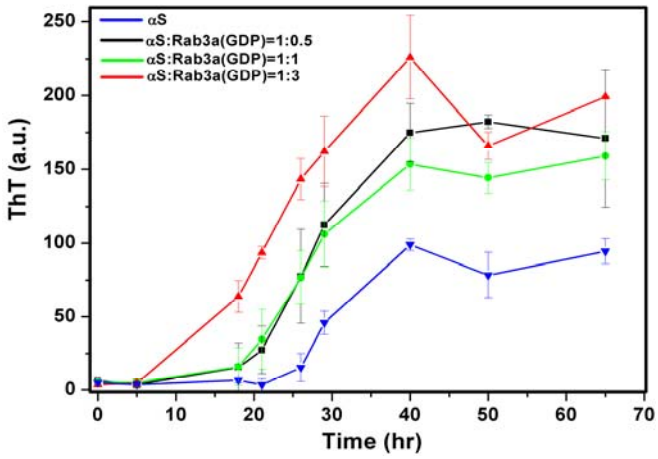

Figure 3.2.13. αS aggregation in the presence of Rab3a. αS: Rab3a ratios of 1:0.5, 1:1, 1:3 were adopted and compared to the control of αS alone. As Rab1b and Rab8a, Rab3a could effectively enhance αS aggregation at all 3 ratios and when it reached the ratio of 3:1 of Rab8a to αS, the aggregation kinetics was significantly modified.

Under the aggregation condition, the αS control displayed a typical lag phase more than 20 hours and reached the saturation phase at 40 hours of experimental time. In contrast, the aggregation kinetics was significantly accelerated by the presence of Rab3a-GDP at all 3 molar ratios. At the time point of 18 hours, all the trials with Rab3a already ended the lag phase and started the elongation. Similar to the control, the kinetics of αS aggregation with Rab3a achieved saturation around 40 hours, but the fibril yields of the all 3 ratios characterized by ThT fluorescence were shown as twice as great as the control. Moreover, there is no dose-dependence observed between the molar ratio αS to Rab of 1:0.5 and 1:1. For the molar ratio of 1:3, the lage phase was significantly shortened. And the elongation rate of αS showed an even faster rate than the other ratios, but finally remains at a similar level of fibril yield as the other two molar ratios. Therefore, Rab3a enhances αS aggregation in a manner similarly to Rab1b. Furthermore, unlike Rab8a, both Rab1b and Rab3a don't bind to monomeric αS but they rather modulate aggregation of αS, suggesting that these two Rabs interact with αS aggregates.

3.2.5 NMR assignment of Rab1b and Rab8a

In our studies described above, Rab1b, Rab3a and Rab8a have been shown to modulate αS aggregation in a similar manner. However, according to the NMR titrations, only Rab8a binds to monomeric αS whilst Rab1b and Rab3a do not. Hence, there two questions that arise following these observations: 1) How dose αS bind to Rab8a and are there additional binding sites on Rab8a other than its C-terminal tail?; 2) Even if no bindings are observed, Rab1b and Rab3a still impacts on αS aggregation. Does this implicate that they selectively interact with αS aggregates.

Bearing these two questions, we performed NMR assignment for Rab1b and Rab8a. Rab1b(1-175)-GDP (Rab1b-δC) and full-length Rab8a-GDP with uniformly ^{13}C and ^{15}N labeling were prepared based on the optimized conditions achieved by Dr. Amyelt Itzen's group. Based on the assignment we obtained, the solution structures of these two proteins have been analyzed and the interaction studies related to αS have been further implemented for these two Rab proteins.

3.2.5.1 Assignment and structural analysis of Rab1b

Uniformly ^{13}C, ^{15}N-enriched Rab1b-GDP was prepared with a concentration of 1.5mM and used in the backbone NMR assignment of Rab1b. The assignment was achieved by defining protein backbone sequential connectivity through the Cα/Cβ moiety and CO moiety based on corresponding NMR spectra (Sattler et al, 1999). For assignment, triple resonance NMR experiments were applied based on transferring of coherence along the network of scalar coupled spins^{1}H, ^{13}C and ^{15}N. 3D HNCACB and HNCA spectrums generated the resonances of both intra-residue and inter-residue Cα/Cβ. With aid of 3D CBCAcoNH that selectively presents the inter-residue resonance, the intra- and inter-peaks were distinguished in the spectra and their chemical shifts were labeled for construction of sequential connectivity through Cα/Cβ. Similarly, NHCO and HNcaCO together provided the distinguished peaks of both intra- and inter- CO. Thereby, the sequential connectivity through CO was further established. For better resolution, all 3D spectra were recorded with TROSY-based fashions (Salzmann et al, 1998). The chemical shifts of distinguished Cα/Cβ and CO were input into the automatic assignment program MARS (Jung & Zweckstetter, 2004a; Jung & Zweckstetter, 2004b). MARS achieved assignment by establishing sequential connectivity and propensity of secondary structure which was reflected by carbon chemical shifts. Finally, 80% backbone assignment for Rab1b-δC(GDP) was reliably obtained.

As shown in Figure 3.2.14(A), the resonances are well dispersed and characteristic of folded proteins in ^{1}H-^{15}N TROSY. Most of the resonances that appeared in the spectrum have been unambiguously assigned apart from the signals introduced by side chains. Meanwhile, the selected strips representing the resonances in the HNCACB spectrum are shown in Figure 3.2.14(B), where the sequential connectivity has been demonstrated by linking the intra and inter Cα and Cβ resonances of the fraction R49 to K56 of Rab1b-δC. All the chemical shifts of assigned residues were shown in the appendix I.

Interestingly, one part of protein consisting of residue Thr65-Thr75 could not be assigned. Inspecting into the spectra, these residues were likely disappearing. Mapping this sequence onto published crystal structure, we found this part corresponding to the Switch II region. This region is highly dynamical and strongly affected by the

nucleotides binding as a common feature of Ras-GTPases family (Lee et al, 2009). The Switch II region consists of one short α-helix (α2) and one long disordered loop (G3). The crystal structure with B-factor mapping [Figure 3.2.15(D)] indicates that this region possesses the highest B-factors in the whole protein (Muller et al, 2010). Therefore, the failure of assignment for this part might be as a result of the strong chemical exchange caused by its highly dynamic nature. To circumvent this, a series of ^{1}H-^{15}N HSQC spectra were recorded at different temperatures (283 K, 293 K, 298 K, 303 K and 308 K) to test the potential temperature dependence of chemical exchange.

We also employed the sensitivity-improved HSQC sequence that uses a CPMG pulse train during the INEPT stage to reduce the loss of dephasing of spin coherence due to chemical exchange (Mulder et al, 1996). However, despite applying both two approaches above, the state of the spectra was not improved and few newly appeared peaks were found.

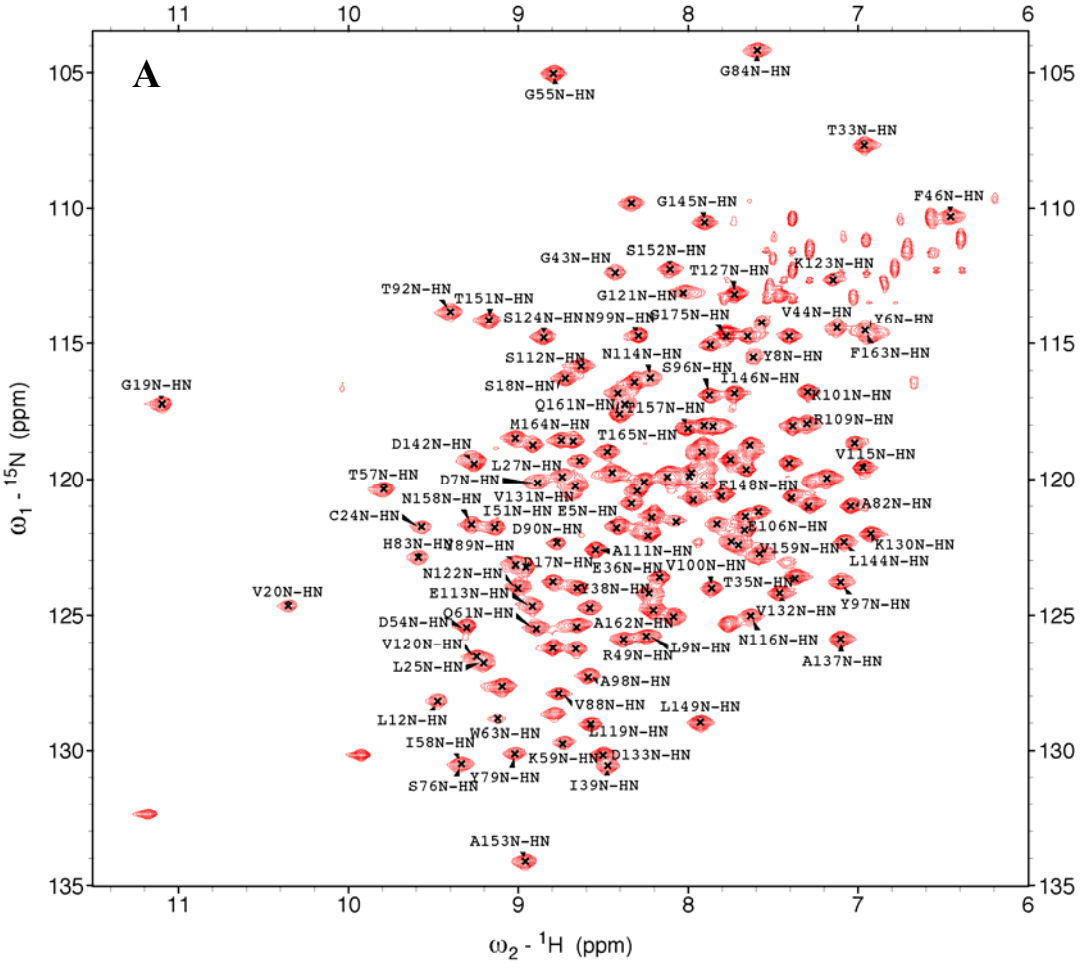

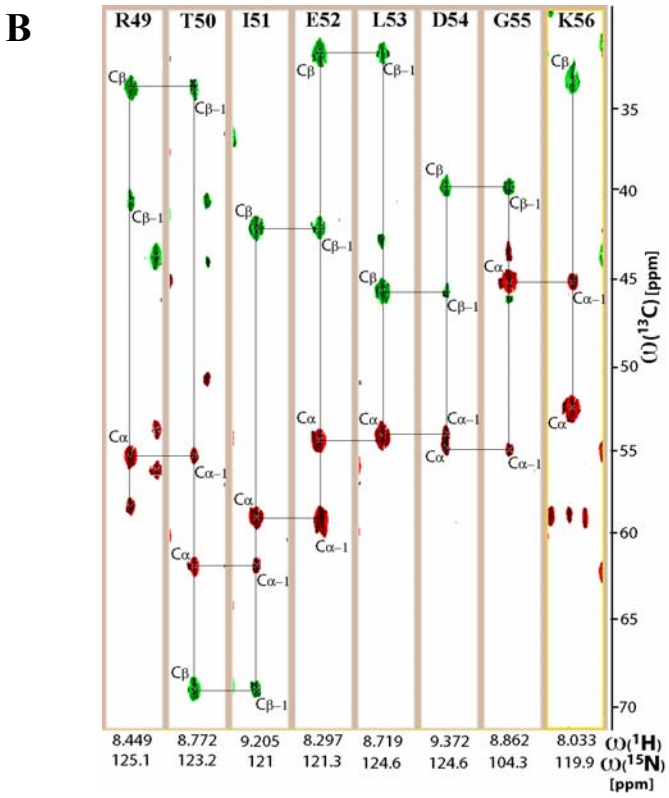

Figure 3.2.14. NMR assignments for Rab1b (1-175). (A) Resonance assignments are indicated with amino acid types and residue numbers in ^{1}H-^{15}N TROSY. (B) Strips of the HNCACB spectrum demonstrate the sequential connectivity represented by Cα/Cβ within the fraction of R49-K56.

To correlate the solution conformation and crystal structure, structural analysis for Rab1b was implemented based on the assignment we obtained. Secondary chemical shifts of Cα [Figure 3.2.15(A)] agree with the elements of secondary structure (on the top of the figure) determined by X-ray crystallography (Muller et al, 2010). This indicates that solution conformation measured by NMR is highly consistent with the crystal structure. Furthermore, residual dipolar couplings (RDCs) measured in pf1 bacterial phage shows basic agreement between the crystal structure and secondary chemical shifts [Figure 3.2.15(B), (C)]. However some parts, particularly the conjunction areas between structured and disordered regions, show inconsistence with the other types of structural data, suggesting that these locations adopt different orientations in solution than in crystals. Moreover, the crystal structure of Rab1b-δC(GppNHp) (PDB: 3NKV) is represented with b-factor mapping [Figure 3.2.15(D)].

As the core part of the Switch II region, helix α2 displayed in the X-ray structure is relatively short, looser and more distorted than other structured regions. B-factor mapping also points out that this region experiences more intensive thermal fluctuation than other parts, especially when compared with the core region of the fold denoted by the color blue. Hence, the Switch II region is highly dynamic in the protein. This region also provides the structural motif for tight binding of the regulator and effector proteins, i.e. GEF, GAP, GDI, and its conformation is highly sensitive to nucleotides binding (Lee et al, 2009). These features can largely contribute to chemical exchange that induced peak broadening and loss of sensitivity in the NMR spectroscopy. Hence, as described above, this feature accounts for the fact that corresponding resonances of α2 and G3 disappeared in the NMR spectra.

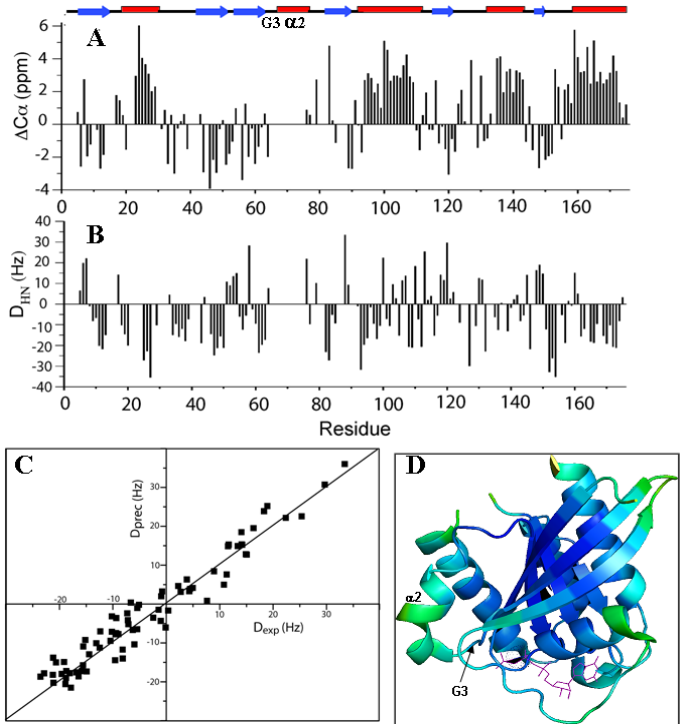

Figure 3.2.15 Structural characterization of Rab1b-δC. The secondary chemical shift of Cα (A) and residual dipolar couplings (RDCs) of NH of Rab1b(1-175) (B) are compared with the secondary structural elements determined by X-ray crystallography(The bar on the top: blue arrows indicate β-strand, red rectangles indicate α-Helix and black solid lines indicate the loop). (C) Correlation of experimental RDCs and SVD back-calculated RDCs based on crystal structure. (D) Crystal structure of Rab1b-δC(GppNHp) (PDB code: 3NKV, resolution 1.7 A) is represented with B-factor mapping (green: high, blue: low). The typical Switch II region consisting of α2 helix and G3 loop is denoted.

Previously, the interaction between monomeric αS and Rab1b was not observed by NMR titration. The titration experiments were implemented by titrating Rab1b material into ^{15}N-αS and observing changes in ^{1}H-^{15}N resonances of αS. To further confirm this finding, we repeated the titration assay by adding isotopically natural abundance αS into ^{15}N- Rab1b-δC and monitoring possible resonance-changes of the Rab1b. Moreover, we also titrated the fibrillar αS into ^{15}N Rab1b-δC to detect potential interactions between RAb1b and αS aggregates since Rab1b can modulate the aggregation of αS.

Figure 3.2.16 shows that there are no significant bindings of Rab1b to αS monomers and fibrils. For the case of monomeric αS, the region of Rab1b from residue 40 to 60 displays the trend that the chemical shifts were slightly affected by the addition of αS. But in comparison to the rest of the protein, the αS-induced perturbation is not pronounced. This might be due to some nonspecific interactions that partially perturbed this region. Both chemical shift perturbation and intensity plot indicated that no significant interaction took place between Rab1b and αS fibrils.

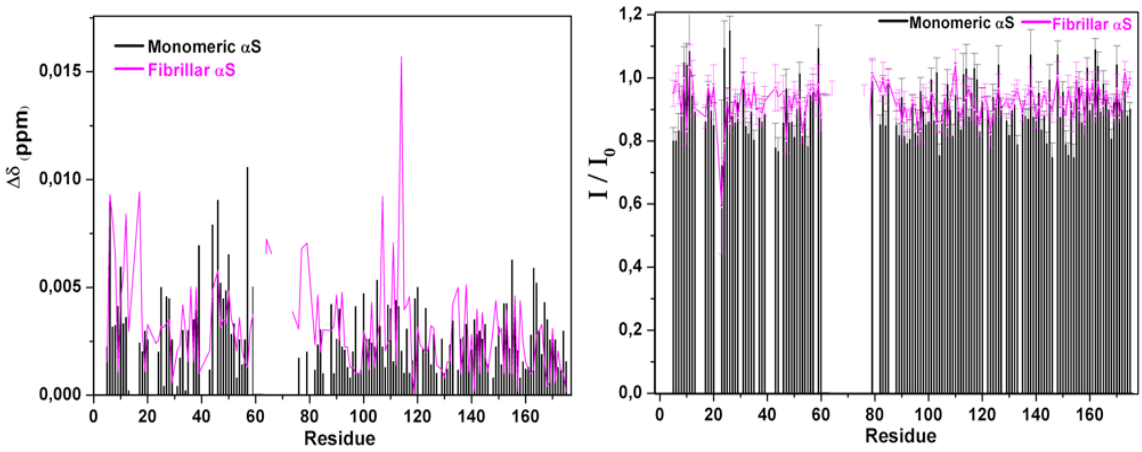

Figure 3.2.16. NMR binding assay for Rab1b and αS. Monomeric and fibrillar αS were titrated into ^{15}N-enriched Rab1b (1-175) by monitoring the variation of chemical shift (A) and signal intensity (B) of the peaks in the ^{1}H-^{15}N HSQC spectrum of Rab1b. The applied Rab1b: αS ratios were 1:7 for monomeric αS to Rab1b and 1:5 for fibrillar αS (molar equivalents of monomeric protein).

Additionally, the ^{15}N- Rab1b-δC used for the titration is C-terminally truncated. Thus, the titration did not reflect whether αS could interact with the C-terminus of Rab1b. Howevert, the Rab1b previously used for titrating into ^{15}N-αS is the full-length protein

and no binding was reflected by the resonances of αS [Figure 3.2.2 (A)]. Analyzing the sequence of amino acids for 3 Rab proteins also suggests that except Rab8a, the termini of Rab1b and Rab3a do not strongly bind to αS according to the charge distribution [Figure 3.2.3].

In conclusions, the solution conformation of Rab1b-δC(GDP) is consistent with the crystal structure. Moreover, we did not observe significant interactions between Rab1b-δC(GDP) and αS monomers and fibrils. However, based on our aggregation assay, Rab1b modulated the aggregation of αS. This suggests that Rab1b likely interacts with aggregation intermediates.

3.2.5.2 Assignment and structural analysis of Rab8a

Rab8a shares highly sequential similarity and identity with Rab1. In parallel to this, the folded parts of these two Rabs also possess high similarity, except their C-terminal loops, which is a conserved feature in Ras GTPases superfamily. Therefore, these factors enable us to apply NMR assignment to Rab8a based on the assignment of Rab1b. However, in comparison to Rab1b, Rab8a is more difficult for sample preparation. First of all, it requires protein chaperones to assist its folding, which is not common in the Rab family. Secondly, Rab8a is insoluble in *E. coli* expression system and its purification is restricted to C-terminally truncated Rab8a(1-183) due to the structural flexibility of the C-terminus. Through codon-optimization and co-expression with protein the chaperone GroEL/GroES in *E. coli,* Dr. Amyelt Itzen's lab produced full-length Rab8a with an improved yield as well as the a reduced insolubility and heterogeneity (Bleimling et al, 2009). However, the expression of the isotopic labeling sample suffered even more difficulties and thereby substantially hampered NMR assignment and assessment for Rab8a. Finally, 100μM ^{15}N-Rab8a-GDP in volume of 200μL and 300μM ^{13}C,^{15}N-Rab8a-GDP in volume of 70μL were prepared. The paucity of the sample largely restricted our NMR studies. However, it still provided us with the opportunity to approach the structural analysis of Rab8a and the mechanistic study on the binding of αS to Rab8a.

Not surprisingly, in reference to Rab1b-δC(GDP), ^{1}H-^{15}N HSQC of Rab8a(GDP) exhibits certain similarity in resonance distribution compared with Rab1b due to their

structural similarity [Figure 3.2.17]. Superposition of the spectra of the two Rabs indicates a few peaks of Rab8a were highly overlapped to the peaks of Rab1b.. Based on the sequence alignment of these two Rab proteins and the assignment of Rab1b, these paired peaks should correspond to the conserved residues between the 2 proteins, such as G56 and A154 of Rab8a. These specific residues were helpful for the assignment of Rab8a.

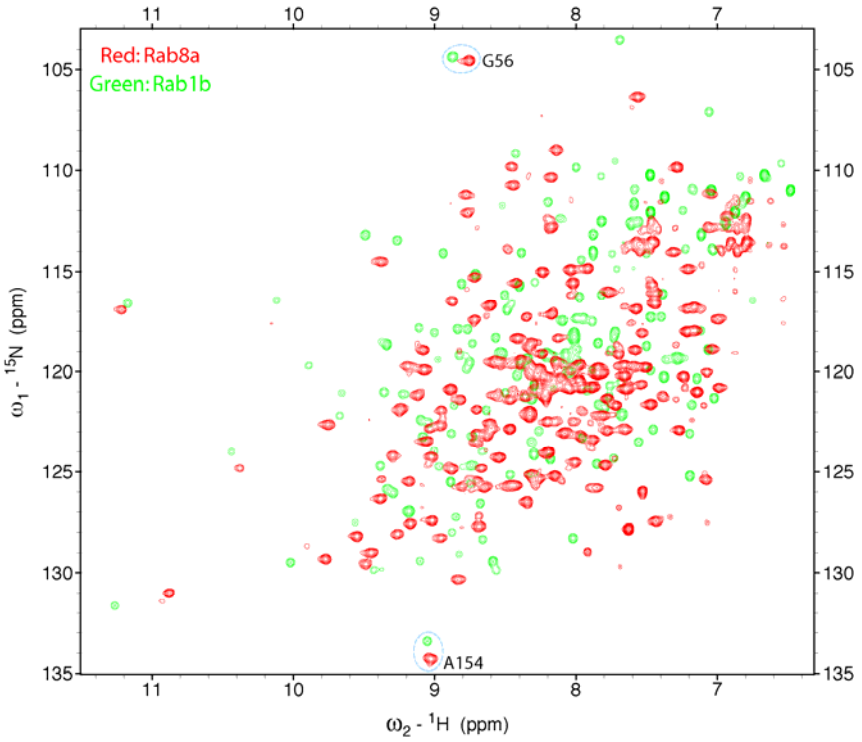

Figure 3.2.17. ^{1}H-^{15}N HSQC spectrum of Rab8a. HSQC of Rab8a (red) was shown with Rab1b(1-175) (green) as a reference. Both spectra were acquired at 298K. The conserved residues based on sequence alignment of Rab1b and Rab8a i.e. G56, A154 were labeled.

To correlate with full-length Rab8a, we also acquired natural abundance ^{1}H-^{15}N HSQC for the C-terminal peptide of Rab8a which previously identified that it could bind to αS C-terminus and affect the aggregation of αS. The HSQC of peptide was overlaid with the spectrum of full-length Rab8a, which showed that part of the resonances of the peptide were well overlaid with full-length protein, i.e. I193 and T194, but the rest of resonance were not. This is probably due to peptide adopts different conformation when it remains alone. It is necessary to obtain the assignment of Rab8a

and implement structural analysis of both the folded part and the C-terminal loop within Rab8a.

Since the sample amount of $^{13}C,^{15}N$-Rab8a was fairly limited, to record the NMR spectra required for assignment of Rab8a, a 1.7 mm cryogenical probehead was installed on the Bruker 800M spectrometer. 3D TROSY-based HNCA, HNCACB and CBCAcoNH were recorded for assignment. Sample instability caused substantial loss of the sample as the precipitation appeared after long time acquisition and this disabled further spectra aquistion.

Spectra overlaying and sequence alignment identified 3 peaks that belonged to 3 conserved residues between Rab8a and Rab1b, which are Gly20, Gly56, Ala154. The resonance positions of these 3 residues were well-resolved in the HSQC spectrum of Rab8a and were specified in MARS program to enhance the assignment. The cutoffs were optimized as 0.15ppm for C_α and 0.5ppm for C_β in order to maximally and reliably establish sequential connectivity by MARS.

Finally, 112 out of 209 residues of Rab8a were assigned reliably (appendix II). Secondary chemical shifts of Cα for assigned residues of Rab8a were consistent with secondary structural elements determined by X-ray crystallography for Rab8a-δC [Figure 3.2.19]. The missed assignments were mainly at the Switch II region, C-terminal tail and the short turn between β2 and β3. The Switch II region comprised of G3 loop and α2 helix (Asp65-Thr77) was also unassigned in Rab1b(1-175) due to its dynamics. Major fragments of the C-terminal loop starting from Asn182 to Lue209 were also largely unassigned. This is because the long loop region of 28 residues leads to the substantial degeneracy of the resonances due to it disordered state. The two proline residues Pro184 and Pro195 also interrupted the establishment of sequential connectivity for this loop region. A few repeats such as Gln197Gln198, Ser201Ser202, Phe203Phe204 and Leu208Leu209 were not readily distinguished very well under the conditions of spectra. Furthermore, the general limitations of the sample such as lower concentration, small amount and high instability also largely retarded the sensitivity and resolution of the NMR spectra. However, based on the half of Rab8a assignment, we still have an opportunity to examine potential bindings of Rab8a to αS.

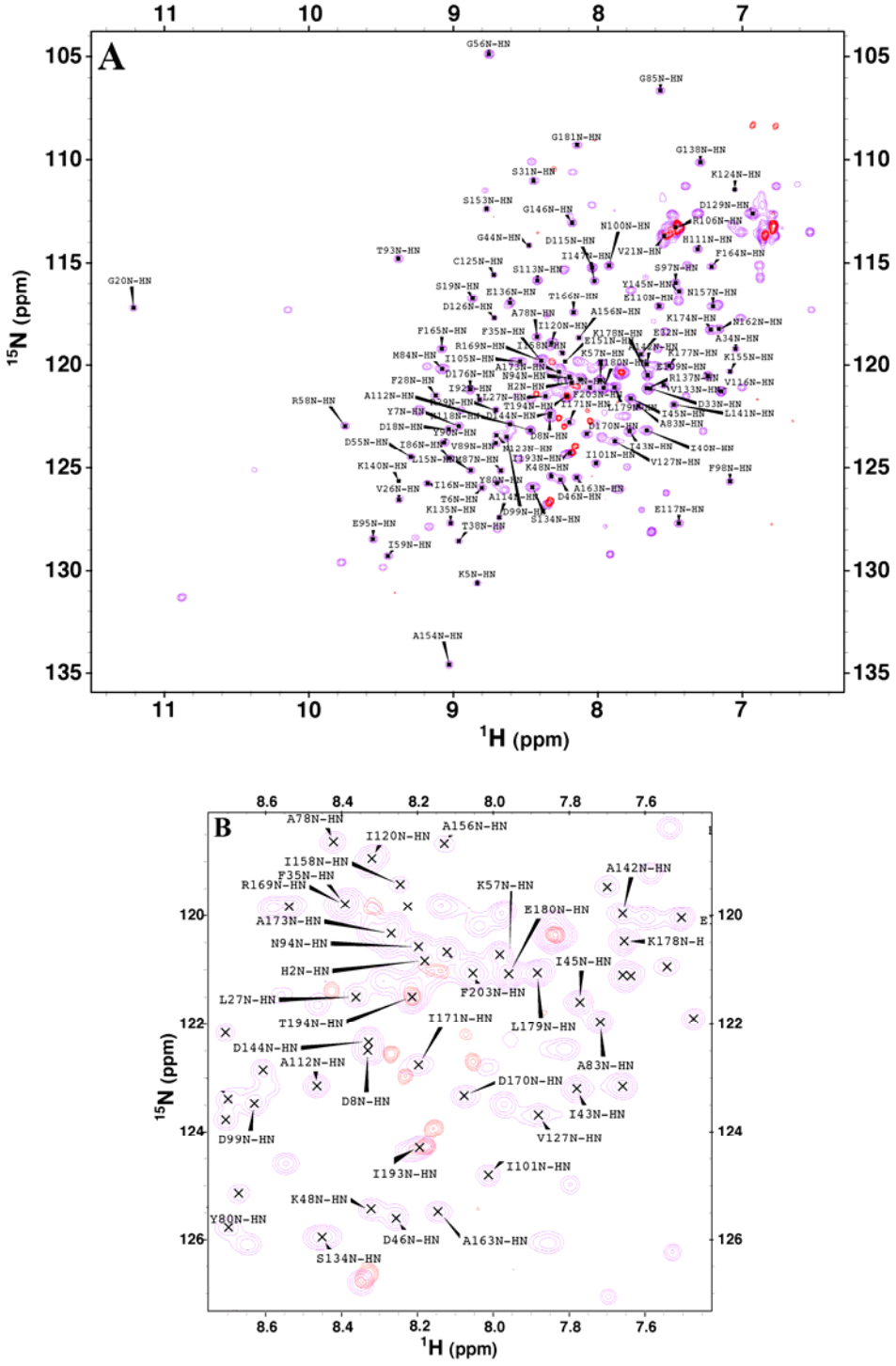

Figure3.2.18. ^{1}H-^{15}NHSQC spectrum of the C-terminus peptide of Rab8a. (A) ^{1}H-^{15}N HSQC for the C-terminus peptide was recorded at natural abundance (red) at 298K and the HSQC for full-length Rab8a recorded at same temperature was shown using the color blue as reference. The region containing most of the peptide resonances is enlarged and displayed in (B) indicating that the fingerprint of two spectrums is partially overlaying.

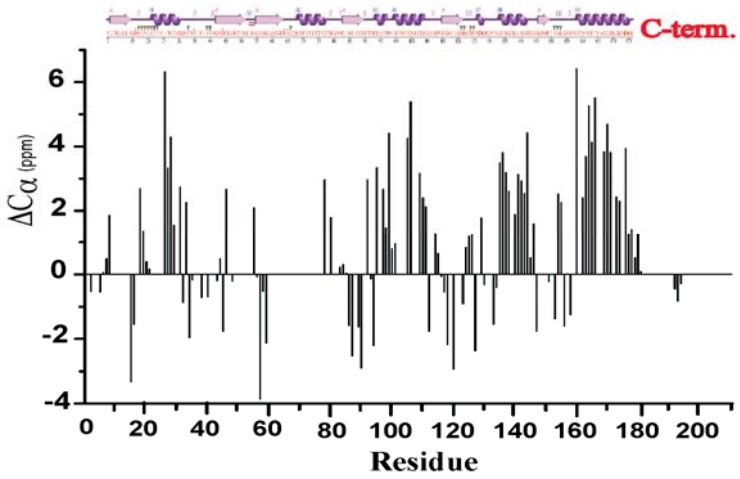

Figure 3.2.19 Secondary chemical shift mapping for Rab8a-GDP. Secondary chemical shifts of Cα were mapped aginst residue. The secondary structural elements of Rab8a determined by X-ray crystallography(PDB code: 3QBT) were described on the top of figure (Hou et al, 2011).

3.2.6 Mapping interaction sites on Rab8a

As described in the previous sections, both Rab8a-δC and the C-terminal tail of Rab8a can bind to the C-terminus of αS. Therefore, in order to map the interfaces of Rab8a that enable Rab8a to bind to αS, a series of HSQC spectra of ^{15}N-Rab8a(GDP) were recorded with the addition of different amounts of αS and analyzed based on the attained assignment.

In Figure 3.2.20, three segments of Rab8a(GDP) are distinguished by increasing the added concentration of αS. The first motif is $I^{43}G^{44}I^{45}D^{46}$ identified by the change of both resonance positions and intensities. The changes of chemical shift were increased as a result of the increased concentration of αS. Interestingly, the resonance intensities of these 4 residues also increased with the continuous addition of αS and this effect was significantly shown at the molar ratio Rab8a/αS of 1:8 referencing to the neighbor regions. This suggests that chemical exchange in this region was restricted due to the binding of αS and thereby the previous broadening of the resonances of these residues was alleviated. Mapping this motif onto the crystal structure of Rab8a(1-178) (Hou et al, 2011), we found that it corresponds to the end of the G2 loop [Figure3.2.20], typically defined as the Switch I region that experiencing drastically structural change during the process of GTP hydrolysis. Switch I region consists of the G2 loop and the beginning of

the following β2 strand, where there are positively charged residues such as K48, R50 that might provide binding potential.

According to the intensity plot [Figure3.2.20. B], the region D55-I59 displayed propensity for increased intensities upon the addition of αS. This fraction is located at the β3 strand which is encompassed in the Interswitch region that typically represents the region between the Switch I and Switch II. This Interswitch region normally undergoes allosteric effects caused by the structural regulations of the two Switch regions. Another region from residues A112 to I120 also shows changes in the chemical shifts but not in resonance intensities. This part contains one loop region between the α3 helix and β5 strand and the starting fraction of β5, which is labeled in pink color in Figure 3.2.21. The composition of amino acids in this region contains D115, E117 and K118 which does not display strongly positive potential and suggests the changes of chemical shifts are likely to be secondary effects of αS binding.

The C-terminus of Rab8a as a loop region enriched by positively charged residues displayed strong propensity for binding to αS reflected by both chemical shifts and resonance intensity in Figure 3.2.20 as expected. Missed assignment for the majority of the C-terminus led to substantial loss of binding details at this region. However, M119I120 in the C-terminal loop shows significant chemical shift perturbation since at the ratio of 1:3. These two residues are directly after K117K118 that very likely acts as a binding motif for αS. Moreover, the intensity plot indicates a clear trend of intensity increase starting from A173 until Gly181. In addition, the short fraction K192I193T194 showed intensity increase as well. The increase of intensities observed for these assigned C-terminal residues also indicates that the backbone dynamics were affected by the binding of αS. Thus, in agreement with our previous result from the Rab8a C-terminal peptide, the C-terminus of Rab8a provides a another binding motif for αS.

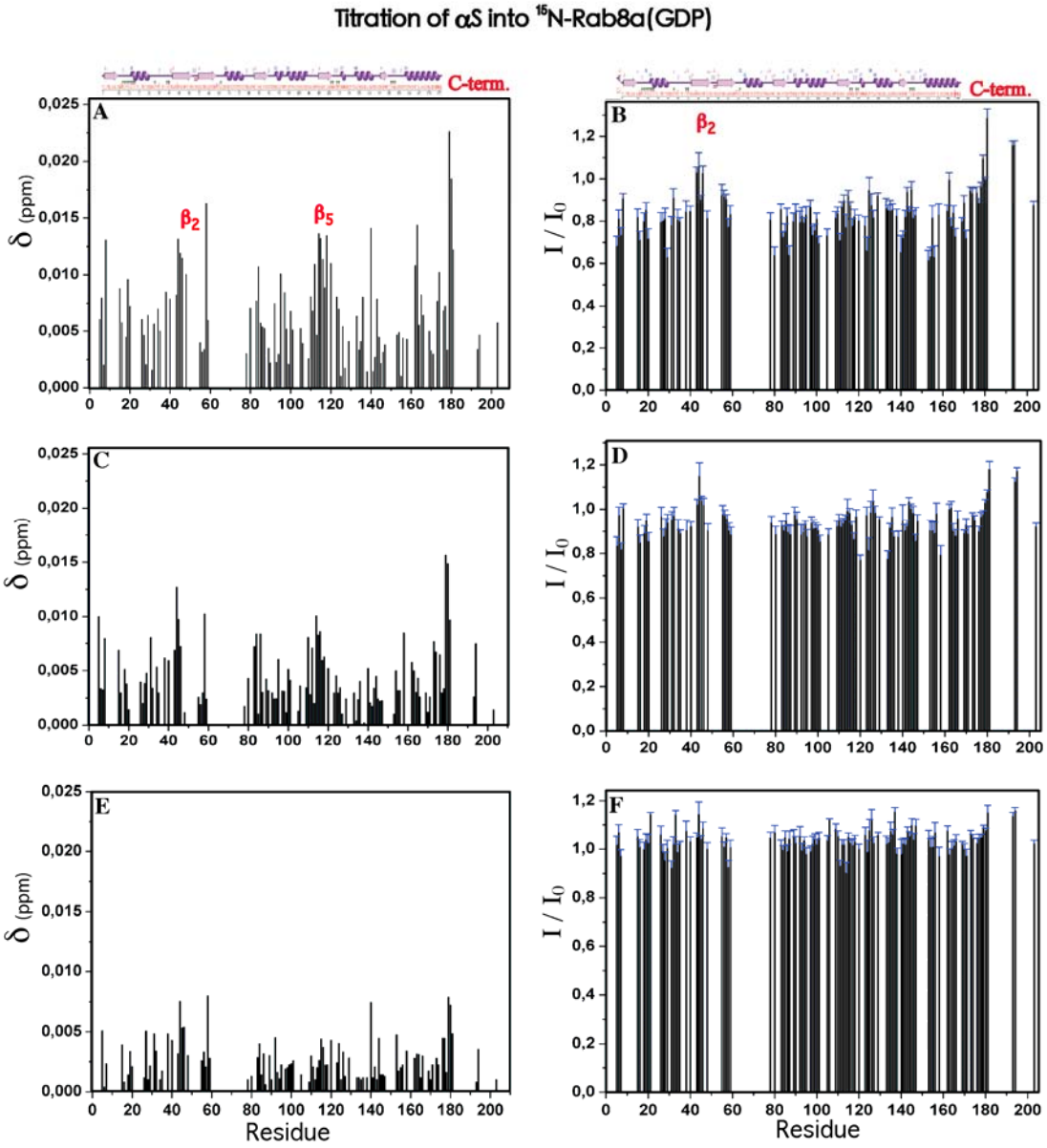

Figure3.2.20 αS binds to Rab8a-GDP revealed by NMR titration. Changes in chemical shift and intensity of resonances of ^{1}H-^{15}N HSQC spectra of Rab8a-GDP were resulted from the addition of αS with 1:1, 1:3 and 1:8 molar ratio of Rab8a:αS. The changes of chemical shifts and intensity are reflected in (A) and (B) for the ratio of 1:8, (C) and (D) for the ratio of 1:3, (E) and (F) for 1:1. Error bars for intensity plots were estimated based on signal to noise.

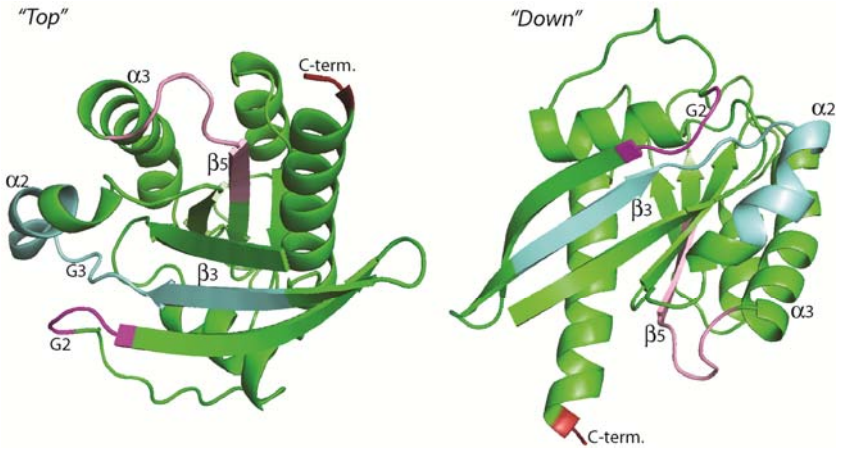

Figure 3.2.21. Mapping interactions between Rab8a-GDP and αS. The binding of αS to Rab8a was recognized by the NMR titration assay and mappedonto the crystal structure of Rab8a (9-178)-GppNHp (PDB: 3QBT). Both "top" (left) and "down" (right) views are displayed. The binding motif of $I^{43}G^{44}I^{45}D^{46}$ which is part of G2 loop is labeled in magenta. Another motif of residues A112 to I120 is labeled in pink color. The unassigned Switch II region is labeled in light blue and the starting of C-terminal loop is labeled in red. According the nomenclature for secondary structure elements of Ras-GTPases, loops (G2, G3), helixes (α2, α3), β-strands (β3, β5) are selectively noticed.

In conclusion, by using NMR titrations assays, we defined the interactions between Rab8a and monomeric αS. The binding is reflected in the NMR spectra of both Rab8a and αS. For αS, the binding of Rab8a occurs at its highly negatively charged C-terminus. Rab8a is a protein that is enriched by positively charged residues at its C-terminus and N-terminally folded parts as well. This feature of charge distribution enables Rab8a to offer multiple sites for αS binding.

Both GDP- and GppNHp-bound Rab8a can bind to αS but Rab8a(GDP) displays stronger binding affinity to αS than Rab8a(GppNHp). Moreover, the structural data of αS binding to Rab8a indicates that the binding likely reduces the chemical exchange around the major binding sites of Rab8a, i.e. the Switch I region and the C-terminal loop. Unlike Rab8a, Rab1b and Rab3a do not bind to monomeric αS, but they enhance the aggregation of αS in a very similar manner, indicating that they potentially interact with αS aggregates and facilitate fibrillization.

3.3 Structural characterization of alpha-Synuclein aggregates

The structural study of αS aggregates is important to understand the pathological consequences of αS. Fibrils of αS are recognized as a major component of Lewy bodies, the neuronal inclusion viewed as the hallmark of Parkinson's disease(PD) (Spillantini et al, 1997). And αS oligomers, the aggregation intermediates, were proposed as major toxic species responsible for neuronal degeneration of PD. Until now, fibril structure of *wt*-αS has been well-characterized by EPR (Chen et al, 2007), mass spectrometry (Del Mar et al, 2005), solid-state NMR (ssNMR) (Comellas et al, 2011; Heise et al, 2008), and combination of solution NMR and ssNMR (Vilar et al, 2008). On the other hand, oligomeric species as the intermediates of αS aggregation are rarely characterized by structural methods at atomic resolution due to their instability and heterogeneity.

As described in sections 1.2, αS fibrils still play an important role in PD pathology; and three disease-related mutants present different cellular physiologies and structural features. However, previous structural studies on fibrils of E46K and A53T αS by ssNMR still didn't achieve consensus regarding structural perturbation of the mutations to β-sheets enriched fibril core, particularly for E46K (Comellas et al, 2011; Heise et al, 2008). Moreover, a conserved solvent-protected core in amyloid fibrils of *wt* and A30P aS has been observed (Cho et al, 2011). It is also unknown whether a conserved core also exists in amyloid fibrils of E46K and A53T αS? To address these questions, we performed H/D exchange by solution NMR on the fibrils of these two mutants.

Most of low resolution data suggest that oligomers of αS mainly adopt β-sheet conformation similar to the fibrils. Thus, with the aid of the compounds that specifically maintain αS at oligomeric stage with certain size, we performed the optimized NMR H/D exchange method to tentatively detect the potential hydrophobic protections inside the oligomers.

3.3.1 H/D exchange for fibrils of E46K and A53T α-Synuclein mutants

Mutations of A30P, E46K and A53T are associated with familial forms of PD. Structurally, these 3 mutants were reported to perturb intra-molecular long-range

interactions between N- and C termini of αS and thereby alter its aggregation behavior (Bertoncini et al, 2005a). The A30P mutation slows αS fibrillization and produces more soluble oligomeric intermediates. However, it does not change the arrangement of β-sheets in core region of the fibrils (Lemkau et al, 2012). Compared with A30P, the E46K and A53T mutations are closer to the NAC region centrally for fibril formation. Both E46K and A53T promote the fibril formation and display faster kinetics than *wt*-αS (Fredenburg et al, 2007; Greenbaum et al, 2005). Moreover, by morphological comparison, ultrastructural diversity of amyloid fibrils was observed amongst the mature fibrils of *wt*-αS and its 3 mutants (van Raaij et al, 2006). These findings together suggest that the familial mutations of αS modify both fibrillization kinetics and assembly of protofilaments. It's thus intriguing to investigate whether the fibrils of E46K and A53T adopt a similar conformation at their fibril core region respecting to the fibrils of *wt* and A30P αS. Furthermore, it is interesting to assess how modifications of micro-environment of amino acids impact on fibrillization kinetics and ultrastructural assembling of fibrils.

The monomers of E46K and A53T αS were incubated respectively under the aggregation condition at 37^{o}C with constant stirring. Fibrils were harvested after 2 weeks. The formation of fibrils was characterized by ThT fluorescence and electron microscopy. ThT fluorescence of E46K αS aggregation after 2 weeks was 3 fold higher than A53T αS. Comparison of EM images illustrated that the fibrils of A53T αS adopted a typical morphology of αS fibrils, but the fibrils of E46K αS were relatively shorter, more branched and heterogeneous [Figure 3.3.1]. Therefore, the aggregation kinetics and morphological analysis indicates that these two αS mutants differ in manner of fibrillization and particularly in assembly of the protofilaments.

After two weeks of aggregation, the fibrils of E46K and A53T αS were collected by ultracentrifugation with 60k rmp for 2 hours at 4^{o}C. The pellet of fibrils was then re-suspend into distilled H_2O and ultracentrifuged again for removal of soluble components attached to the fibrils. At the end, the pellets of fibrils were suspended into the exchange buffer containing 99.9% D_2O, 200mM NaCl and 0.1% formic acid (pD 4.0). The system was set on a rotator for 1 week in the cold room where the temperature was maintained at 4^{o}C.

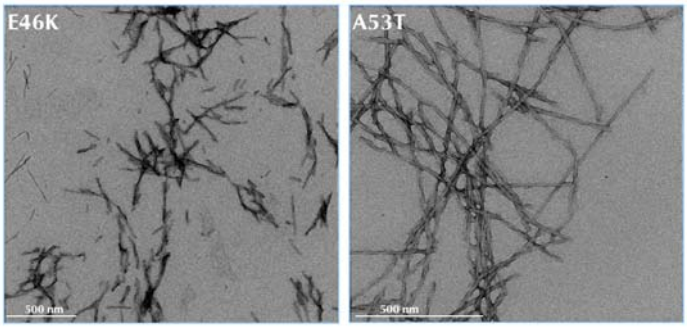

Figure 3.3.1. Electronic microscopy for fibrils of E46K and A53T αS. The fibrils were collected after 2 weeks under the aggregation condition and used for the following H/D exchange.

The fibrils after 1 week of H/D exchange were collected and washed 2 times by ultracentrifugation. The prepared fibrils were dissolved to monomers in 50% D_2O solution with 2M GuSCN, 0.4% formic acid (pD 2.4). Since the fibril pellets were dissolved, the monomers encoding the structural information of fibrils in solution were quickly transferred into the NMR spectrometer to start recording spectra. All the NMR parameters of acquisition were calibrated prior to fibril dissolution using a reference sample prepared in identical solution conditions. After a 12 minutes deadtime for sample tuning in spectrometer, a series of ^{1}H-^{15}N HSQC spectra with band-selective excitation (BEST-HSQC) were recorded with interval of 25 minutes for each spectrum.

Comparing with the solution used for forward-exchange described previously, the concentration of D_2O was reduced from 100% to 50% in the dissolving solution of GuSCN. This possesses the advantages that the region previously protected or exposed in the 100% D_2O environment can be distinguished by observing the decreasing or increasing trends of intensity in 50% D_2O, as a process of back-exchange. In addition, the pH was set at 2.4 and the spectra were acquired under 5^{o}C, which maintained the proton/deuterium exchange rate at a minimum level and enabled us to follow the kinetics of back-exchange with a better time resolution under given spectroscopic conditions.

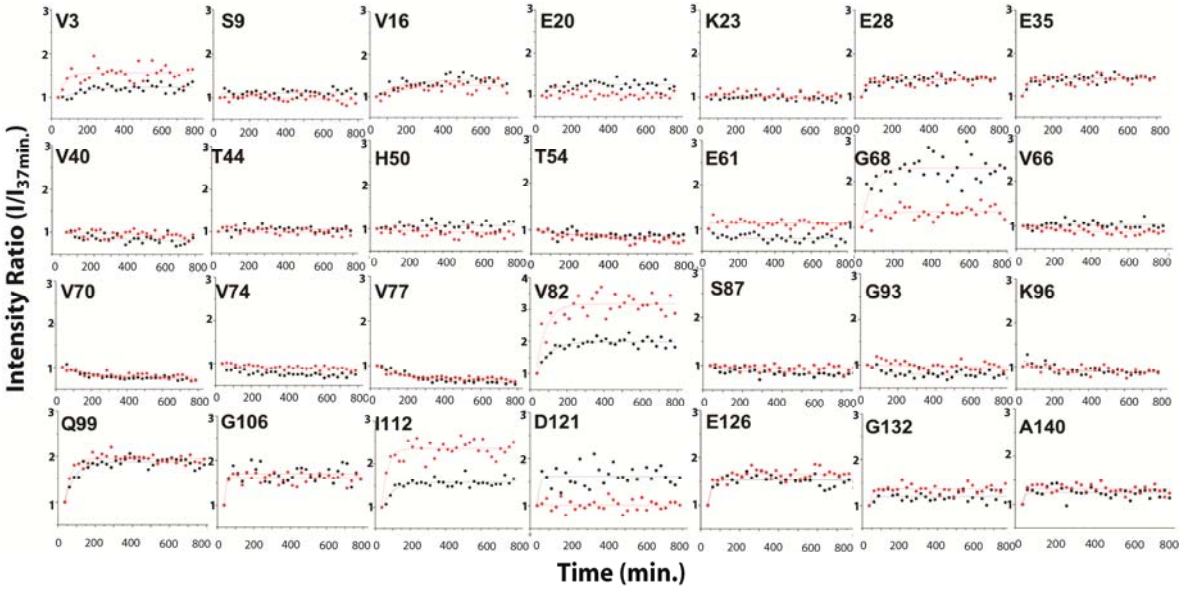

Figure 3.3.2. Intensity plots of HSQC spectra for back-exchange. The residue-specific resonance intensities were mapped as a function of dissolution time starteing from the time that fibrils were suspended into the GuSCN/D_2O solution (black:E46K, red:A53T). Each back-exchange profile was fit with a single exponential function curve.

In Figure 3.3.2, residues from different regions of αS respond differently during the back-exchange process and a few residues of the two mutants experience different kinetics. Most of the selected residues at the N-terminus display an exponential increase, such as V3, V16, E20, E28, E35, suggesting that these residues are exposed to D_2O during the forward exchange. Distinctively, residues from 37 to 97 majorly adopt a relatively flat or decreasing pattern in the intensity plot, denoting that the residues from this segment were buried inside the structured elements of mature fibrils and the amide protons were protected against exogenous deuterium by forming hydrogen bonds inside the fibrils. A few exceptions, like G68 and E82, implicates they might locate at the loop region between β-sheets. For the C-terminal residues starting from 98, both mutants showed an obvious increasing pattern in their intensity due to the less protection of the C-terminus than that of fibril core during forward exchange.

To quantitatively map the extent of protection and depict structure of fibril core, according to the back-exchange curve, we back-calculated the initial hydrogen content and the corresponding level of deuterium incorporation as two alternative representations for residue-specific protection extent of the fibrils against H/D exchange during forward-exchange [Figure3.3.3 (A) and (B)]. The patterns of both figures

consistently and clearly define the boundaries of fibril core at residue 37/38 and 97/98. According to the protection pattern, this core region is conserved in fibrils of both E46K, A53T αS. Out of the core region, C-terminal residues 98-140 were most strongly affected by the exchange and obtained averagely highest extent of deuterium incorporation. N-terminal domain also possessed significantly less protection than fibril core but relatively less pronounced than the C-terminus, indicating that there were likely residual structures presenting in N-terminal (Gath et al, 2012).

Based on the protection patterns inside fibril core, the putative β-sheets 1, 2, 3, 4, 5a and 5b were depicted on the top of the figures by identifying the putative loops between two consecutive β-sheets by recognizing the residues with less protection. This structural arrangement is in agreement with the previously defined fibril structures of *wt*-αS and A30P αS by H/D exchange coupled with HR-MARS (Cho et al, 2011), where the loop residues could be recognized by HR-MARS due to their flexibility.

Interestingly, the basic arrangement of fibril core remains conserved in both mutants. Slight difference is shown that the boundary residues were shifted from V37/K97 for E46K αS to L38/K96 for A53T αS. Accordingly, the first and last two putative β-sheets were shifted by one residue for the fibrils of A53T αS compared with the fibrils of E46K αS. But, generally, the structural patterns of the fibrils of these two αS mutants demonstrate that the mutations didn't drastically alter the conformation of fibrils core. The difference shown in EM pictures for these two mutants might account for that polymorphism of amyloid fibrils and association fashion of protofilaments was modified by mutation. At position 46, the mutation from Glu to Lys can reverse the charge state of side chain and potently affect the local structure and ambient regions. However, by protection pattern we notice that this position locates likely at the loop region between first and second β-sheets of fibril core and thus this mutation should not strongly change the arrangement of core. Moreover, no significant changes appeared at neighboring region of T53 by comparing with E46K fibrils.

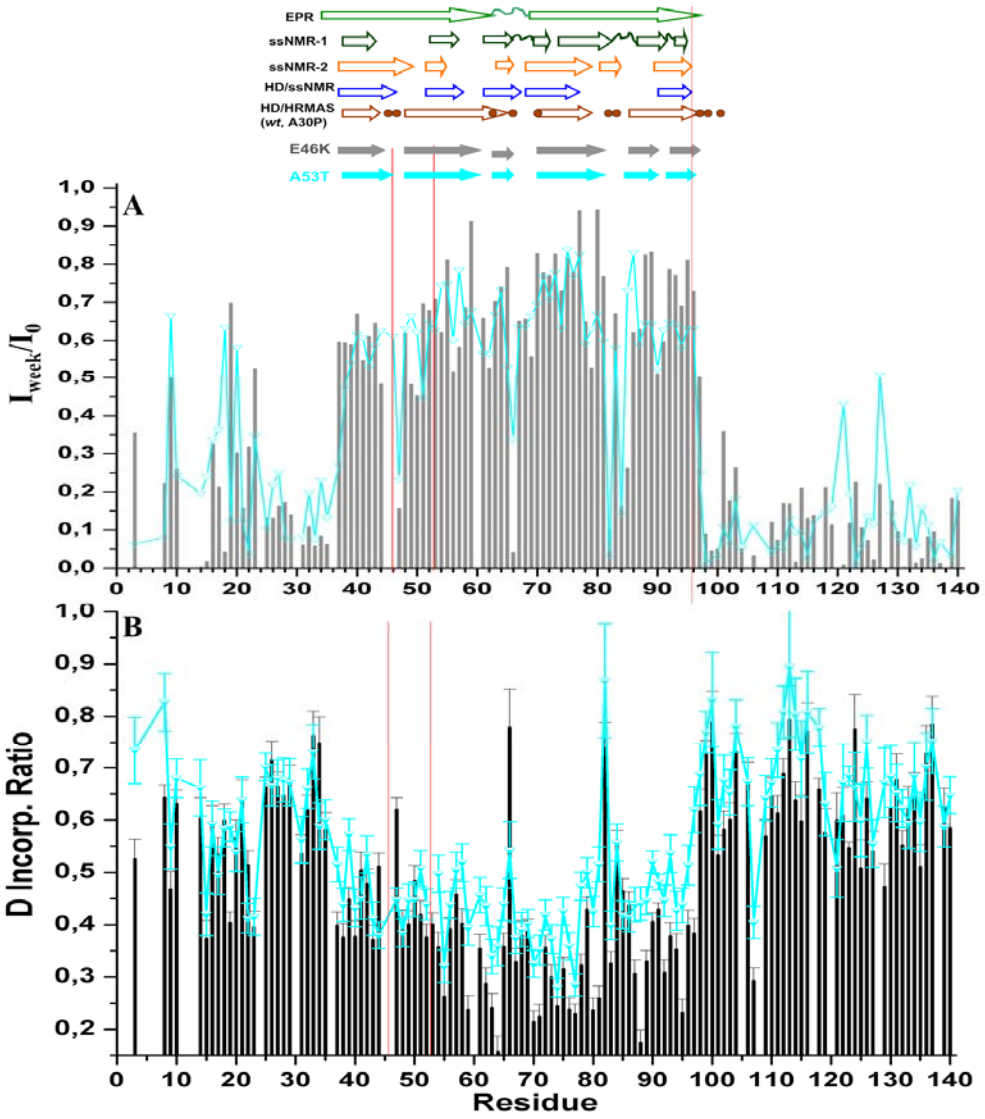

Figure 3.3.3. Characterization of protection extent against H/D exchange for fibrils of E46K, A53T αS. The mutation positions in protein sequence were labeled by red lines. The back-exchange profile was fit with single exponential function and extrapolated the initial intensity representing the hydrogen content at the starting point of back-exchange (A). Correspondingly, in (B), the original level that deuterium incorporated into fibrils after 2 weeks H/D exchange was back-calculated from back-exchange profile and taken into account that after completion of the back-exchange the protonation level was 47% (with calibration due to extra protons introduced by GuSCN). Error bars were calculated on the basis of the signal-to-noise ratio in the last and first HSQC spectrum. At the top of figure, the secondary structural elements of αS fibrils determined previously are described as arrows for β-sheets and as a curve for linker. (EPR(Chen et al, 2007); solid state NMR (ssNMR-1) (Heise et al, 2005); solid state NMR (ssNMR-2) (Comellas et al, 2011); H/D exchange and solid state NMR(Vilar et al, 2008); H/D exchange and HR-MAS (Cho et al, 2011), filled circle represents the flexible regions observed by HR-MAS.)

.

In summary, the mutations of E46K and A53T don't induce dramatical change of the solvent protection pattern of fibril core, suggesting a conserved core region in fibrils of these two mutants. And this conserved core is highly similar to fibrils of *wt*-αS and A30P αS. Therefore, our results suggest that a highly conserved structure embedding in fibril core of *wt*-αS and its 3 familial mutants.

3.3.2 Probing conformation of the compounds-stabilized oligomers of α-Synuclein

Several lines of evidences attribute neuron toxicity of αS to its oligomeric states (Caughey & Lansbury, 2003; Cookson, 2009; Cookson & van der Brug, 2008; Lashuel et al, 2002a; Lashuel et al, 2002b; Volles & Lansbury, 2003; Winklhofer et al, 2008). Thus it's of central interests to study physiological and biophysical features of αS oligomers. However, as aggregation intermediates, continuum distribution of molecular weight, highly structural heterogeneity and weak stability of the oligomers pose hindrances for us to acquire structural information of αS oligomers with high resolution and accuracy, which largely hampers us to understand in-depth mechanism of its neuronal toxicity.

A series of organic compounds have been successfully screened for developing potential therapeutic agents of PD by Sergey Ryazanov and Andrei Leonov in our department. These compounds can block fibrillization of αS by stabilizing the oligomers within a certain size range (hydrodynamic radii of ~100 nm) and significantly reduce cellular toxicity of αS in serveral animal models. Biophysical characterizations demonstrate that these compounds effectively convert the αS oligomers from on-pathway to off-pathway, from larger size to the smaller size with pronounced stability. Solution NMR investigation points out that these compounds do not bind to αS monomers, but preferentially interact with αS oligomers. Furthermore, recent research defined that there was one conversion from smaller oligomers of αS to the larger oligomers, which the αS oligomers with larger size were putatively more toxical than the smaller ones in cell tests (Cremades et al, 2012).

Therefore, the better stability and promising clinical application stimulates us to access high resolution structural information for these compounds-stabilized αS

oligomers. The H/D exchange method was adopted. Based on experience applied for αS fibrils, we specifically optimized the method for studying conformation of the compounds-stabilized oligomers.

The oligomer sample for H/D exchange was prepared by the standard aggregation procedures with the addition of compounds before aggregation started with ratio that 100μM αS/100 μM sery166a or 70μM αS/100 μM anle138c. Both sery166a and anle138c are names of the compounds that stabilize αS oligomers [Patent No.: WO 2010/000372 A2]. The aggregation of αS was maintained 3~4 days that maximal amount of oligomers was expected. At the end, sample was monitored by Atomic force microscopy (AFM), Dynamic light scattering (DLS) and Thiol-flavinT fluorescence (ThT) [Figure 3.3.4]. Fluorescence shows that no ThT-positive fibrils were formed under the aggregation condition up to 3 days. DLS measurement identified that the sizes of these oliomgers mainly distributed around 100 nm (hydrodynamic radii) and AFM characterized the oligomers with annular shapes distinct to the classical morphology of αS fibrils. To remove filaments probably existing in the solution, the samples were centrifuged with 5K rpm for 15 minutes prior to H/D exchange.

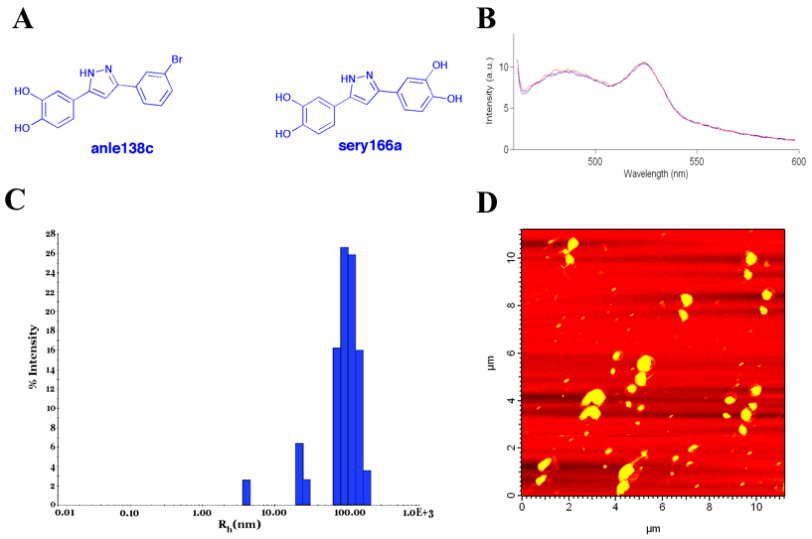

Figure 3.3.4. Biophysical characterization for the compounds-stabilized αS oligomers. Molecular structures of anle138c and sery166a are shown (A). ThT fluorescence (triplicate measurements) indicates that no fibrils formation after 3 days aggregation with anle138c (A). The oligomers were characterized by DLS with hydrodynamic radii around 100nm (B) and Atomic force microscopy with annular shape (C).

A primary consideration differing to the case of αS fibrils is that the oligomeric species of αS are soluble and hard to be separated from mostly populated αS monomers by the means like ultracentrifuge. Thus, for the process of forward H/D exchange, we directly added D_2O into the oligomer solution to reach the D_2O ratio not less than 50%. Then the whole system was kept in cold room of 4°C for forward exchange of 10 minutes. The following procedure including oligomer dissociation by GuSCN, quick transfer and tuning of spectrometer was mostly same as the H/D exchange for fibrils.

Two factors we took into account were: 1) unlike fibril sample, the deuterated oligomers were difficult to be further isolated from monomers; 2) the central part of oligomers was assumed to be solvent exchange-resistant due to hydrogen bonds and hydrophobicity. Therefore, after the forward exchange GuSCN was directly added into the oligomer solution to dissociate oligomers. After the dissociation by GuSCN, there should be different responses for the fraction inside central part of the oligomers and for the fraction that is out of hydrophobic center and highly exposural to solvent. Moreover, the original αS concentration used for aggregation was 100 μM and reduced to less than 50μM after the addition of D_2O and GuSCN. Thus longer experimental time for each HSQC spectrum was used to compensate signal to noise.

Under the condition described above, the H/D exchange profile after the addition of GuSCN is shown in Figure 3.3.5. Unlike profile of the fibril exchange, 6 selected residues from different parts of αS didn't display region-specific kinetics. In the case of fibril samples, the residues like A53, I88 were highly associated with the hydrophobic core of αS fibrils. But their H/D exchange profile of the oligomer sample reflected by peak intensities didn't tend to drop as expected. Moreover, most of residues showed a relatively plateau profile, suggesting that they have been saturated by solvents during the exchange process before starting dissociation. Only a few residues like Y133 tended to decrease, but this might be a result of bulkily side chain of residue which retarded solvent accessibility. Additionally, we observed strong average uncertainty represented by error bars. This was due to low concentration of αS as the solution was diluted by the addition of large extra amount of D_2O.

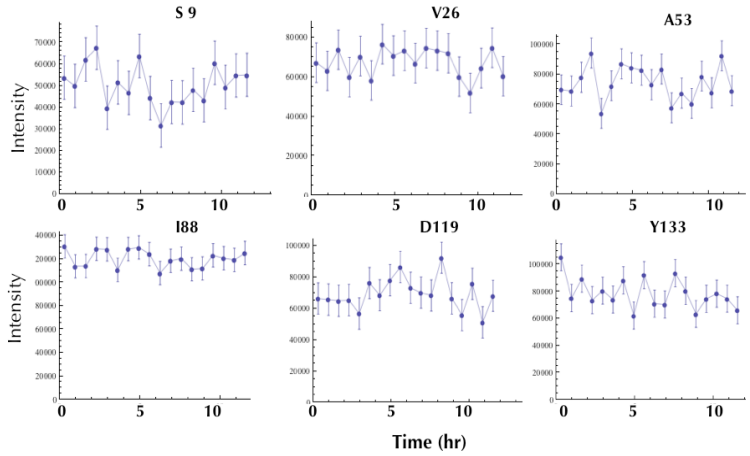

Figure 3.3.5. H/D exchange profile of the compound-stabilized (anle138c) αS oligomers. The curves represent the residue-specific change of peak intensities after the GusSCN dissociation. 6 residues from N-terminal, NAC and C-terminal are shown. The unit of Y axis is arbitrary.

Since exchange profiles of most residues were nearly plateau, it implicated that probably both the fractions outside and inside of the presumably hydrophobic center of oligomers already was saturated by solvent during the first exchange period. We considered that hydrophobic interactions and compactness of the oligomers should not be as strong as inside fibril core and the possibility to form hydrogen bonds should also be less than the fibrils. Therefore, it's necessary to improve the exchange conditions to circumvent these drawbacks. \

Firstly, we raised the D_2O ratio from 50% to 70% gradually for amplifying the potential difference of exchange behaviors between the central part and the outer part of the oligomers during the first period of the exchange. Secondly, considering that the oligomers might adopt a relatively loose conformation and thus the solvent could approach the assumed core region more easily than the case of fibrils, the exchange time was shorten from 10 minutes to 5 minutes. Under such condition, more solvent-exposed residues were expected to finish the deuterium to proton exchange within 5 minutes but the central part was not. Furthermoe, to improve sensitivity of NMR spectra, we used the membrane with specific molecular weight cut-off filter (i.e. 10 kDa) to concentrate the sample prior to the exchange condition.

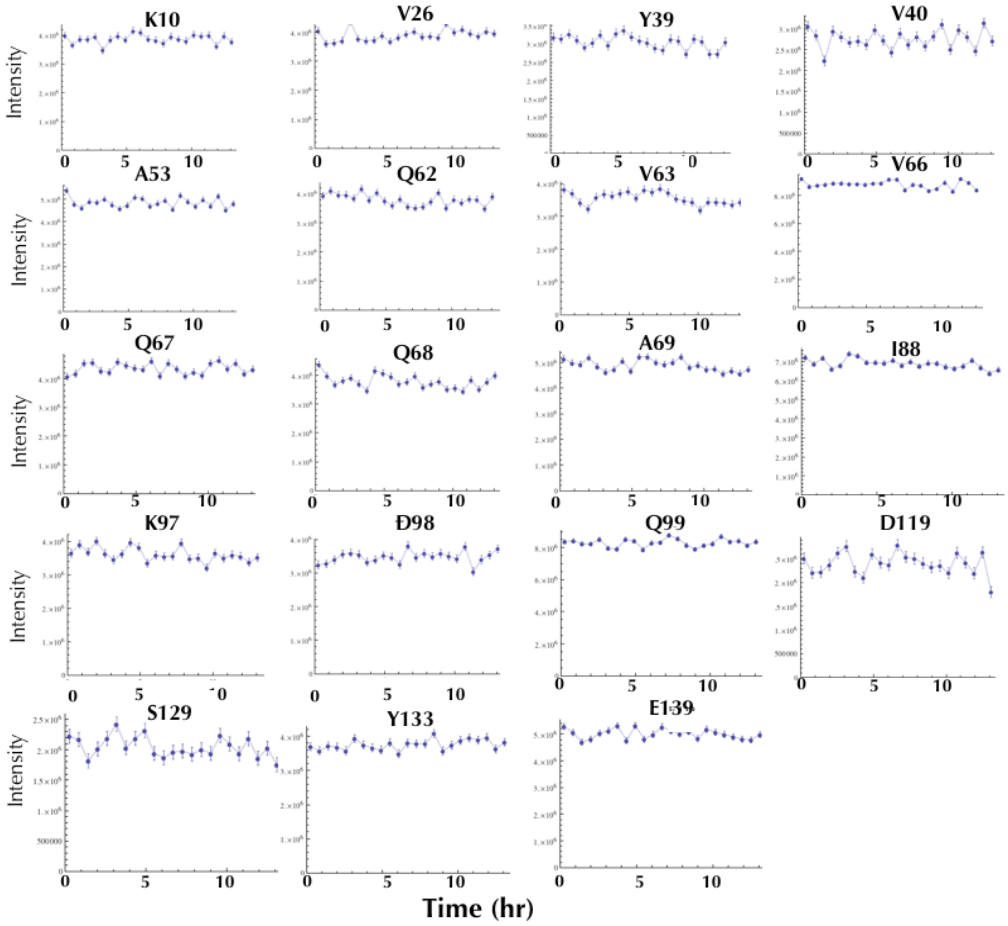

Figure 3.3.6. Optimized H/D exchange for the compound(anle138c)-stabilized oligomers. The peak residue-specific intensities were drawn as the function of exchange time after adding GuSCN. The unit of Y-axis is arbitrary.

Compared with the previous trials, under this improved condition, overall sensitivity reflected by the error bars was enhanced and the exchange curves of residues display slightly distinguishable patterns [Figure3.3.6]. Most of residues from N-terminal part like K10 and V26 tended to adopt plateau trend during 13 hours exchange time. Residue Y39, at the boundary region of αS fibrils defined by previous fibril exchange, showed slightly decreasing trend in the αS oligomeric sample. The residues like A53, V63, Q68, A69, I88 also exhibited the decreasing trend during the exchange. These residues were previously identified in β-sheets inside of fibril core. Other residues previously in the fibril core region like Q62, V66, Q67 showed fairly weak decrease or even slight increase. Interestingly, these residues located in the loops between two β-sheets of fibril core found by previous fibril exchange experiment. K97 should be the

residue at another boundary of the fibril core. The oligomeric sample showed that this residue display slight decrease pattern contrary to its following residues D98 and Q99 which were experiencing increase and plateau respectively but no decrease. Thus, these observations implicate that potential correlation of protection pattern against the solvents between the compound(anle138c)-stabilized αS oligomers and αS fibrils, suggesting that potential structural homology might be shared by these two types of αS aggregates.

We also found that some residues like D119 and E139 at C-terminus showed the decreasing pattern. Ser129 also experienced a clear decrease of peak intensities along the exchange time. The behavior of these C-terminal residues suggested that they might experience protection during the first exchange period, which was also indicated by the peak intensities of first HSQC spectrum of the oligomer sample compared with the monomer reference [Figure 3.36. A]. But, like Ser129, the same situation was also observed for Ser9 at N-terminus, which could be due to the effect of residue side chain. This can also indicate that under current conditions, the differentiation between residues from different parts of αS oligomers were still not significant and far from the precise required for quantitative analysis. Especially, the side effects from individual side-chain and their neighbor residues still largely affected the exchange process and might be more pronounced than the structural effects that we expected to observe.

Comparing to the results of H/D exchange for fibrils of E46K and A53T αS fibrils, the compounds-stabilized oligomers displayed much weaker protection against solvent exchange. Even under exchange condition i.e. 70% D_2O and 5 minutes forward exchange time, we still didn't observe the expected difference of protection at different regions of αS. In αS fibrils, hydrogen bond is a major factor that protect amide proton against solvent exchange. Thus, the weaker protection of the oligomers suggests that the compounds-stabilized oligomers don't contain the regions that are enriched in hydrogen bonds.

Another factor we need to take into account was that after 3 days aggregation with compounds under the given condition, maximally 30% αS monomers would be converted into NMR-invisible oligomers measured by the 1D NMR monomer-consumption assay. Due to the heterogeneity and continuum distribution of oligomeric

species, the effective population of oligomers that finally contributed to our observation during the exchange could be far less than 30% of total amount of αS. Thus the corresponding signals from oligomers were not enough to be distinguished from dominating monomer signals.

In summary, we optimized H/D exchange methods for probing conformation of the compounds-stabilized αS oligomers. After the stepwise improvement for each experimental condition, we observed that the residues from NAC region displayed slight solvent protection. But the general protection of the compounds-stabilized oligomers was much weaker than that of fibrils, suggesting that the compounds-stabilized oligomers likely don't contain strongly hydrogen-bonded regions like fibrils.

4 Discussion

4.1 Functional relevance of alpha-Synuclein phosphorylation

4.1.1 The effect of PD-associated mutations on the phosphorylation of α-Synuclein

Although αS phosphorylation has been implicated in the pathogenesis of PD, little is known about effects of PD-associated mutations (A30P, A53T and E46K) on the phosphorylation of αS, or *vice-versa*. The aim of this section was to address this gap in knowledge and to provide insights into the impact of the PD-associated mutations on phosphorylation of αS at S87 and S129 *in vitro.* This was achieved by real-time NMR method and by employing kinases that are known to specifically and efficiently phosphorylate αS at these residues, namely PLK2 (S129) and CK1 (S87 and S129).

Our quantitative analysis of phosphorylation kinetics revealed that *wt*-αS was phosphorylated at S129 faster and slightly higher levels than all three genetic variants by using the same kinase and protein concentrations (Figures 3.1.1 and 3.1.2). Analogous findings regarding the *in vitro* phosphorylation of the pathogenic A30P and A53T αS by CK2 were reported previously (Ishii et al, 2007). Both A30P and A53T were reported to be phosphorylated *in vitro* at a slower rate compared to *wt*-αS. It is noteworthy that the extent of CK2-mediated phosphorylation of αS does not exceed 5-10%. However, we observed that none of the PD mutants seemed to influence the kinetics or extent of phosphorylation at S87 (Fig. 2B).

The above observations raise questions about why the disease-related mutants affect the levels of phosphorylation of S129 but not S87. The answer to this question may lie in differences in the structural consequences of the S87 and S129 phosphorylation. The previous studies indicated that αS phosphorylation at S87, but not S129, interferes with αS binding to membranes (Paleologou et al, 2010). It is also likely that the conformational changes resulting from the amino acid substitution in the

disease mutants affect their interaction with kinases and/or phosphatases. It has previously been shown that the A30P mutation disrupts a region of residual helical structure that exists in the *wt* protein, whereas the A53T mutation results in a slight enhancement of a small region around the site of mutation with a preference for extended conformations (Bussell & Eliezer, 2001). Furthermore, the A30P and A53T mutations slightly weaken transient interactions between the acidic C-terminal tail of αS and its N-terminal region (Bertoncini et al, 2005b). In contrast, the E46K mutation enhances such contacts (Rospigliosi et al, 2009).

4.1.2 Functional relevance of the Ser129 phosphorylation of α-Synuclein

Several posttranslational modifications of αS have been described, including phosphorylation, nitration, ubiquitination, and truncations, but the role of these modifications in modulating the physiologic and/or pathological properties of α-syn remains poorly understood. One can speculate that many αS properties and functions are regulated by its interactions with other proteins and its subcellular localization/targeting, which in turn might be regulated by posttranslational modifications. Therefore, identifying the key molecules responsible for regulating αS post-translational modifications and elucidating their mechanism of action are essential for unraveling the molecular basis of αS function(s) in health and disease.

Of the posttranslational modifications, phosphorylation at the Ser129 is the major modification of αS, which nearly 90% αS in Lewy body was phosphorylated at the Ser129 (Anderson et al, 2006; Fujiwara et al, 2002; Okochi et al, 2000). Therefore, we investigated the selectivity and efficiency of PLKs-mediated phosphorylation of αS. Our kinetics data indicated that both PLK2 and PLK3 could phosphorylate αS with high efficiency and selectivity at the Ser129, especially PLK3 could achieve 100% phosphorylation of the Ser129 within 2.5 hours.

At the same time, the different phosphorylation kinetics of Ser129 by PLK1-3 suggest that “the propensity of PLKs to phosphorylate α-syn is determined by their substrate specificity and sequence complementarities between the catalytic site of each kinase and the amino acid sequence flanking the phosphorylated serine residue as well

as the conformation of the protein. Sequence analysis and three-dimensional homology modeling studies revealed that PLK2 and PLK3 show the highest pairwise identity of the catalytic domain and ATP binding site. The sequence identity between PLK2 and PLK3 at the catalytic domain and ATP binding site is 68 and 97%, and that of PLK2 and PLK3 to PLK1 is %53 and 86–90%, respectively (Johnson et al, 2007). Furthermore, the consensus sequences of PLK2 and PLK3 are very similar and characterized by the presence of acidic residues within the 3–4 residues flanking the phosphorylation site ((D/E)X(S/T)θ(D/E), where θ denotes a hydrophobic amino acid. PLK1 to 3 have a preference for substrates in which at least one of the three residues flanking the serine residue is negatively charged. Both αS and βS fulfill this criterion. This charge distribution on the substrates complements the electropositive distribution on the substrate binding sites of PLK1 to 3" ((Mbefo et al, 2010), p.2818, co-authored).

As it's already proved that PLK2 and PLK3 were responsible to phosphorylate αS with high specificity and efficiency at Ser129, the next question is whether phosphorylation of Ser129 could affect αS aggregation. This is of crucial aspects to evaluate functional relevance of the Ser129 phosphorylation. Thus, we generated pS129-αS by PLK3 and the mimics of the Ser129 phosphorylation P128E/S129E and M127E/P128E/S129E by genetic mutations. Both the phosphorylated αS and its two mimicking mutants showed very close aggregation kinetics and morphology to *wt* αS, strongly suggesting that the phosphorylation at Ser129 of αS didn't affect the aggregation. Similar finding has also been reported that phosphorylation of Ser129 didn't change the aggregation propensity of αS (Waxman & Giasson, 2011). A structural reason that Ser129 phosphorylation of αS would not affect its aggregation is that Ser129 is located at αS C-terminus. C-terminal (residue 100-140) is well known for its highly disordered state in both monomeric and fibrillar states. Thus, even embedded into the fibrils, C-terminal of αS still retains its disordered conformation outside the fibril core and thereby spatially offers chance for kinase recognition. This feature is drastic to the Ser87, which is located in central part of NAC and deeply buried inside of the rigid fibril core. Because of this special location, Ser87 is very hard to be accessed by the kinase at its fibrillar state. *Vice versa*, if monomeric αS was phosphorylated at Ser87, then the fibrillization could be blocked due to one strong polar group was

introduced into the core region responsible for the fibril formation (Paleologou et al, 2010).

Moreover, several line of evidence have already pointed out that αS fibrils could be phosphoryalted by PLK1-3 in vitro (Mbefo et al) and *in vivo* (Waxman & Giasson, 2011). These findings indicate that αS could also be phosphorylated after they aggregated into fibrils in Lewy body. Therefore, we speculate that the aggregation and the phosphorylation of Ser129 are two independent events in physiological scenario of αS. This indicates that pathological effects of the Ser129 phosphorylation of αS might not rely on modifying pathway of its aggregation. The question that why 90% αS deposited in Lewy Body were phosphorylated at the Ser129 still needs to be further addressed in future research.

4.2 Rab proteins bind to alpha-Synuclein and modulate its aggregation

Lindquist group found: (1) Rab1, Rab3a and Rab8a could suppress the disruption of vesicle trafficking at multiple steps caused by αS; (2) The cellular Rab homeostasis was disturbed by αS (Cooper et al, 2006; Gitler et al, 2008). To unearth the molecular mechanisms underlying these findings, we implemented the protein interaction studies for αS and the different Rab proteins by NMR spectroscopy and the aggregation assays for αS in the presence of Rab proteins.

4.2.1 Rab8a binds to monomeric αS

4.2.1.1 Rab8a binds to C-terminus of αS

NMR titration identified that only Rab8a binds to monomeric αS in solution, however Rab1b and Rab3a lack binding. At the same time, our investigations revealed that both GDP- and GppNHp-bound Rab8a could bind to C-terminal of αS, but interestingly Rab8a(GDP) binds to αS with a stronger affinity than Rab8a(GppNHp). By sequence analysis for Rab8a, we found that Rab8a was relatively positive-charged and predicted that both C-terminal loop and N-terminally folded part of Rab8a were capable of

binding to αS independently. This has been proved by our NMR titration of C-terminally truncated Rab8a-δC and the Rab8a C-terminal peptide into ^{15}N-αS. As addressed in the literature of Lindquist, they found that only Rab3a and Rab8a similar to Rab1 could protect against cellular toxicity induced by αS in primary rat midbrain cultures and *C. elegans.* (Gitler et al, 2008). In *C. elegans.,* Rab8a uniquely displayed the strongest rescuing effect characterized by extending lifespan of the worms. Correlating our NMR titration data, it therefore suggests that the molecular interaction between αS and Rab8a might play an important role in the rescuing mechanism of Rab8a against αS toxicity in the animal models.

Even the weaker amelioration to the αS toxicity displayed by Rab1 and Rab3a in *C. elegans.*, it's noteworthy that these two Rab proteins can also suppress the αS toxicity in rat midbrain culture as similar extent as Rab8a. This suggests that these 3 Rabs are capable of protecting the αS-induced toxicities with close extent but probably with different mechanisms. One speculation could be that αS indirectly interacts with effector or regulator proteins of Rab1 and Rab3a rather than the direct binding. Recent study demonstrated that vesicle trafficking was modulated by the interaction between αS and prenylated Rab acceptor protein 1(PRA1) (Lee et al, 2011). This protein interaction was proposed to inhibit the recycling between GDP and GTP bound Rab and thereby interfered the related vesicle trafficking. PRA1 is a protein comprising both transmembrane and cytosol domains and located at ER and Golgi. It interacts with prenylated Rab-GTPases and facilitates Rabs anchored at the membrane at active GTP-bound state to play its function on regulating vesicle trafficking (Figueroa et al, 2001; Hutt et al, 2000). Particularly, it's shown that PRA1 binds to Rab1, Rab3 and Rab5 (Bucci et al, 1999; Martincic et al, 1997).

Another speculation is that Rab1 and Rab3a modified the αS toxicities by modulating αS aggregation rather than direct interactions with αS monomers. This issue will be discussed in section 4.2.2.

4.2.1.2 αS binds to the Switch I region of Rab8a

The interaction mechanism of Rab8a and αS was further coherently shown by titrating αS into ^{15}N-Rab8a and we thereby mapped the binding sites on Rab8a. There were two

regions of Rab8a, Switch I region and C-terminus, mainly involved in the binding to αS. For Switch I region, we observed increased chemical shift perturbation and enhanced intensity as the response to the addition of αS [Figure 3.2.20], indicating that αS binds and restricts the chemical exchange of this region. Switch I is an important region responsible for interactions of Rab8a with guanine nucleotide exchange factors (GEFs) and effector proteins (Itzen & Goody, 2011). As a common feature, the GEFs and effectors interacts with specific sites of Switch I and Switch II region and hence induce the significant structural changes to these two regions and the interswitch region. Therefore, the switch regions were enriched in potent binding sites for different binding partners and they are structurally sensitive to external bindings. K_d measured for Rab8a(GDP) binding to αS quantitatively depicted the binding strength for this protein-protein interaction. As the K_d for Rab8a binding to αS is at the order of ~100μM, this is normally in the range of weak binding and much weaker than the common binding partners like GEFs and effectors in the Kd range of nM. Therefore, in real systems like neurons, αS likely needs to compete with these stronger binding partners of Rab8a. However, αS is much more abundant than GTPases in cells. The large excess of αS could favor the binding to Rab8a. Especially, under the pathological conditions, αS would progressively accumulate at the vesicles.

According to the definition of the Switch regions, Switch I and Switch II regions experience significant structural changes between GDP and GTP states as a common feature conserved in Ras family and thus these two regions were named with “Switch” (Lee et al, 2009; Milburn et al, 1990; Schlichting et al, 1990). Our titration data show that Switch I region of Rab-GDP was significantly affected by the binding of αS and the following interswitch region also display slight increase in peak intensities [Figure 3.2.20]. This observation suggests that a major binding site was located in Switch I region and the interswitch region was also allosterically modified by the structural change in Switch I. Notably, the conformational nucleotide-dependence of the switch regions describes that for GTP state, Switch regions usually adopts more structured conformation and expose the hydrophobic patch to favor the binding of effectors. Contrarily, Switch regions present as more disordered conformation at GDP state (Itzen & Goody, 2011). Thus, this conformational nucleotide-dependence can provide the

structural basis to understand the preference for αS binding to Rab8a as we identified that Switch I region of Rab8a serves as major binding site for αS.

As described in section 3.2.2.1, the K_d for Rab8a(GppNHp) binding to αS is approximately 2.5 fold higher than the binding of Rab8a(GDP) to αS, suggesting that Rab8a(GDP) possesses a stronger binding affinity to αS than Rab8a(GppNHp). And, this difference was also unambiguously shown in the NMR titration of C-terminally truncated Rab8a(6-176) into ^{15}N-αS as shown in section 3.2.2.3 [Figure 3.2.6]. For all the molar ratios that we used for titrating Rab8a(6-176) into ^{15}N-αS, Rab8a-δC(GDP) induced larger chemical shift perturbation to αS than Rab8a-δC(-GppNHp). Taken together, these observations indicate that there is a structural preference for αS binding to folded part of Rab8a. Importantly, as we identified that Switch I region of Rab8a was a major site for αS binding, this structural preference can attribute to the significant nucleotide-dependence of conformation of the Switch regions and the interswitch region.

Moreover, more disordered conformations are commonly present to Switch regions at GDP state might be more favorable for binding of αS C-terminal, whereas more structured conformation of Switch regions at GTP state is usually favorable for effector protein binding (Itzen & Goody, 2011). There are two functional relevance of this structural preference of Rab8a binding to αS can be taken into account. αS preferentially binds to Rab8a(GDP), which leads the active Rab8a, namely Rab8a(GppNHp), to be less affected by the presence of αS. This serves as a protection mechanism to effects of αS on normal function of Rab8a, which supports the existing results that over-expression of Rab8a can suppress the cellular toxicity of αS. However, there should be a well-balanced equilibrium existing between the GDP- and GTP-bound Rab8a. If large excess of αS is present in the cytosol it could bind to Rab8a-GDP and disturb the equilibrium of Rab8a between the GDP and GTP states and. Thus the reduced pool of Rab8a(GTP) can cause the trafficking deficits which could be viewed as one phenotype of αS-induced cellular toxicity.

4.2.1.3 αS binds to the C-terminus of Rab8a

Another major binding site is C-terminus of Rab8a (Asp176-Arg205). We considered this region due to its positive net charge, which is capable of compensating the negative

charges enriched in the C-terminal region of αS. We further identify this charge-driven interaction mechanism by our NMR titration assays. Titration of the synthesized C-terminus peptide of Rab8a into ^{15}N-αS could reproduce the effects of full-length Rab8a binding to αS [Figure3.2.4]. Correspondingly, this interaction has also been observed at C-terminus of Rab8a when we titrate αS into the full-length ^{15}N-Rab8a [Figure3.2.20]. Especially, the binding of αS restricted the chemical exchange of Rab8a C-terminal reflected by the intensity plot at 8:1 molar ratio of αS to Rab8a(GDP), which was similar to the response of Switch I region of Rab8a-GDP. The C-terminus of Rab8a is structurally disordered and functionally responsible for the membrane-anchoring through prenylation of the cysteine in the CVLL motif. The ^{1}H-^{15}N HSQC spectra of the peptide and full-length Rab8a were not fully overlapped, suggesting that this terminal region possesses contacts with other parts of protein. But, in comparison to the binding of αS to Switch I region in the N-terminally folded part, the C-terminus of Rab8a is highly disordered loop and less affected by the different nucleotide binding. Hence, even at GTP state this C-terminal region can still largely contribute to the interaction between Rab8a and αS, although the conformation of Switch I region is unfavorable for the binding of αS. Taken together, the C-terminus of Rab8a play an important role in the interaction of Rab8a and αS due to its positive net-charge and relatively conformational independence of the nucleotide-binding. The characters of this C-terminus enable Rab8a to bind to αS at both GDP and GTP states. Furthermore, due to the binding of αS, the structural contacts between disordered C-terminal and the structured part of Rab8a might be affected and the thereby the external perturbation could be partially introduced to the tertiary structure of Rab8a.

Additionally, we found that both Rab8a-δC and the C-terminal peptide of Rab8a can bind to αS. But, we also observed that the binding strengths of these two fractions to αS were weaker than the full-length protein according to the chemical shift perturbation. Therefore, these observations suggest that the Switch I region and C-terminus of Rab8a are simultaneously contributing to the binding of full-length Rab8a to αS.

4.2.1.4 The Ser129 phosphorylation enhances the binding of αS to Rab8a

Phosphorylation of αS at Ser129 is one of most common posttranslational modifications to αS. As we discussed in section 3.1 and 4.1, the functional role of this phosphorylation is still less defined. Within the scope of this dissertation, two major questions for the Ser129 phosphorylation of αS remain to us: 1) what are the physiological functions of this phosphorylation; 2) what is the pathological relevance of this phosphorylation in synucleinopathies.

Herein, base on the NMR titration, we found that the Ser129 phosphorylation enhanced the binding of αS to Rab8a in comparison to *wt*-αS [Figure 3.2.4]. The phosphorylation modified the side chain of Ser129 by introducing one negative charge. The length of side chain of Ser129 was increased and the phosphate group attached on the end of Ser129 side chain possesses stronger electronegativity than side chains of normal amino acids. These factors can be the reasons for the binding enhancement.

To date, most of studies on the Ser129 phosphorylation of αS were mainly addressing the questions based on the level of cell culture and other animal models. These assays can study the Ser129 phosphorylation in more physiological environments. But, they are less efficient to identify and determine the specific mechanism at molecular level (Braithwaite et al). Recently, V. Sancenon *et al.* reported that phosphorylation of αS at Ser129 could reduce vesicle trafficking defects caused by αS (Sancenon et al, 2012). In this paper, the authors also reported that the level of Rab5 was increased as a marker of the endosome abnormality occurred in this pathological process. This implicate that there might be a pathological connection between Rab-GTPases and αS in the scenario of vesicle trafficking deficits induced by αS. However, the kinases used in this paper were CK family kinases. CKs normally phosphorylate αS not only at Ser129 but also Ser87 as we described in section 3.1.1. Thus, it should not be excluded that the effects observed in the paper might also be result from the Ser87 phosphorylation. Moreover, the impacts of the Ser129 phosphorylation on the vesicle trafficking deficits were defined based on genetic background and the specific interactions involved in the observations were not recognized in the paper. Compensating to these two points, our *in vitro* investigation was based on αS with the phosphorylation specifically at Ser129 by PLK3. At the same time, our investigation

identified the enhancement effects of Ser129 phosphorylation on αS-Rab8a interaction unambiguously by NMR spectroscopy at atomic resolution. Hence, this enhancement mechanism observed by us suggests that the Ser129 phsophorylation of αS likely plays an important role in the interaction with Rab8a and thereby further mediates αS toxicity in the context of vesicle trafficking disrupted by the large accumulation of αS. Additionally, this is also the first specific indication based on protein-protein interaction to demonstrate that how phosphorylation at Ser129 of αS mechanistically mediates the functions of αS.

4.2.1.5 Overview for the molecular interaction of αS and Rab8a

In section 4.2.1.1 – 4.2.1.4, we in-depth discussed the mechanism of the interaction between αS and Rab8a. Rab8a binds to αS C-terminal through its C-terminus and Switch I region and the electrostatic interaction is a major driven force for the binding. This binding has been well characterized from both αS and Rab8a sides. At the same time, this binding displays nucleotide-dependence mechanism that Rab8a-GDP binds to αS stronger than Rab8a-GppNHp. As the Switch I region of Rab8a was identified as a major binding site, this mechanism can attribute to the structural preference of the Switch I region for αS binding. Furthermore, we identified that the phosphorylation of αS Ser129 could enhance the binding between αS and Rab8a, which is as a specific indication of the functional relevance of the Serr129 phosphorylation of αS.

In concert with our *in vitro* investigation, the *in vivo* assays have been undertaken by our collaborator Prof. Dr. Tiago F. Outeiro in his lab. Both αS and Rab8a were co-expressed in the model system of H4 neuroglioma cells (McLean et al, 2000) and co-localization of these two proteins has been observed. Hence, the co-localization suggests that these two proteins have potential interactions in the cells, which is in agreement with our *in vitro* finding. Furthermore, to identify the deeper mechanism that the Ser129 phosphorylation mediates the interplay between αS and Rab8a, one phosphorylation mimic S129D αS has been proposed by us to test its co-localization with Rab8a *in vivo* and interaction with Rab8a *in vitr*o.

Up to now, the specific protein-protein interactions characterized from both interaction partners at atomic resolution for αS are still rare. Thus, our studies are not

only helpful in understanding the rescuing mechanism of Rab8a against the αS toxicities, but also extend our knowledge respecting to general principles for the αS-participating protein-protein/ligand interactions.

4.2.2 Rab proteins modulate the αS aggregation

Investigating α-Synuclein aggregation is one important approach to evaluate the physiologic and pathologic relevance of αS under the given conditions. We found that Rab1b and Rab3a didn't bind to αS monomers but modulated αS aggregation. Rab8a can bind to αS as well as modulate αS aggregation. The effect of Rab8a on αS aggregation could be reproduced by its C-terminal peptide. Moreover, these 3 Rabs adjusted αS aggregation mainly in a dose-independent manner. To analyze the molecular mechanism of the 3 Rab proteins underlying their aggregation modulation effects, we take into account two types of molecular interactions: 1) the interaction of Rabs with monomeric αS; 2) the interaction of Rab with aggregation intermediates of αS.

4.2.2.1 Rab8a modulates αS aggregation

Firstly, our titrations indicate that both GDP-bound and GTP-bound Rab8a can bind to αS C-terminal and introduce the structural perturbation to the local conformation of αS C-terminal. At the same time, Rab8a can offer multiple binding sites, Switch I and C-terminus for αS, suggesting that Rab8a likely interact with αS by 1:2 ratio of Rab8a/αS. Thus, local concentration of αS around Rab8a might be increased due to this binding. The increase of αS local concentration could ficiliate nucleation and thereby shortening the lag phase.

Furthermore, the binding of Rab8a to αS C-terminus might modify the long-range interactions between N and C termini of αS. As the long-rang interactions are important to maintain the protein conformation and inhibit aggregation of αS (Bertoncini et al, 2005b; Dedmon et al, 2005c), the presence of Rab8a might affect αS aggregation by modifying the long-range interactions due to its binding. In particular, this aggregation modulation mechanism of Rab8a by interacting with αS C-terminal through the electrostatic interactions was confirmed by the aggregation assay of αS with

the addition of the positively charged Rab8a C-terminal peptide [Figure 3.2.10]. This modulation mechanism is similar to the case that αS aggregation is mediated by positively charged polyamines (Fernandez et al, 2004). Furthermore, consistent with the observations by W. Hoyer *et al*. (Hoyer et al, 2004), our results indicate that C-terminal is important in modulating αS aggregation although it's disordered and absent in fibril core.

The distinction between polyamines and Rab8a should be noticed. Polyamines are small molecules but Rab8a is a protein relatively larger than αS. This suggests that even Rab8a impacts on αS aggregation in a polyamines-like manner, it also possessed some other characters specially modulating the aggregation in the way different to polyamines. Correlating with the binding of Rab8a to αS, C-terminus of Rab8a might act in a polyamine-like manner to modulate αS aggregation. In addition, the globular part can also bind to αS C-terminus and potentially affect the aggregation as well. Thus the full-length Rab8a that is a combination of its globular part and C-terminal loop might interact with αS and adjust its aggregation by a more collective way.

4.2.2.2 Rab1b and Rab3a modulate αS aggregation

From the interaction studies by NMR, we found that no molecular interactions between monomeric αS and Rab1b/Rab3a. But, they did enhance the αS aggregation by shortening the lag phase and significantly prompting the elongation. In addition, when the fibrillar αS was titrated into ^{15}N-Rab1b-δC we did not observe the pronounced perturbation to Rab1b either. Therefore, it's likely that Rab1b binds to αS aggregation intermediates. This interaction might rely on the fact that surface or shape of Rab1b fit to conformation of αS oligomers, which enables Rab1b to interact with the αS oligomers. Similarly, HSP70 were reported to selectively interact with αS aggregation intermediates and affect the αS aggregation (Dedmon et al, 2005a; Huang et al, 2006; Roodveldt et al, 2009).

At the same time, we observed that all 3 Rabs could enhance the elongation rate of αS significantly. This might originate from the specific protein conformation which is conserved amongst the members of Rab-GTPases family. The aggregation control of αS with BSA also suggests that the aggregation mediation effects of Rab1b should be a

result specifically from Rab1b. Furthermore, 3 Rabs affected the αS aggregation mainly by a dose-independent manner within the concentration ranges that we applied. The addition of 0.3 to 3 molar equivalents of Rabs did not cause significantly difference in the aggregation behavior of αS. As Rab1b and Rab3a were suggested to selectively interact with αS aggregation intermediates, the concentration of Rabs even as half of the αS monomer concentration is still likely beyond the concentration of the αS intermediates because the oligomeric species of αS is populated much less than monomers in solution (Conway et al, 2000). Therefore, similar to the case of HSP70 (Dedmon et al, 2005a), there is putatively a critical concentration for Rabs with respect to αS concentration to play its role in modulating αS aggregation, particularly for Rab1b and Rab3a. If the concentration of Rabs is higher than this critical value, it is speculated that the amount of Rabs is enough to catalyze the fibril growth of αS through binding to the αS oligomers formed during the lag phase.

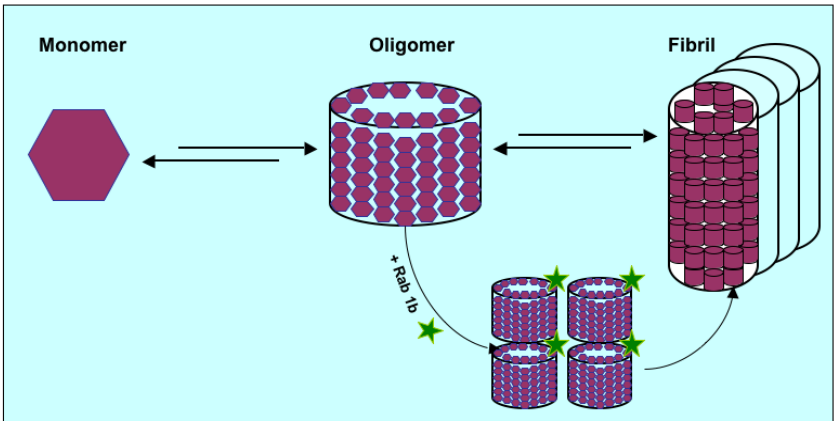

Figure 4.2.1 Putative role of Rab1b in modulating αS aggregation. The aggregation pathway consisting of the oligomerization and fibrillization has bee depicted, in where Rab1b selectively binds to the oligomeric species and favors the assembly of the oligomers into fibrils.

Taken together, we speculate that Rab1b and Rab3a modulate αS aggregation by interacting with αS oligomers and facilitate the assembly of oligomers to larger oligomeric species or directly into the fibrils [Figure 4.2.1]. This can explain why the Rabs could modify aggregation by both shortening lag phase and prompting fibril growth. Rab8a due to its binding to monomeric αS might perform a different mechanism in modulating αS aggregation in comparison to Rab1b and Rab3a.

4.2.2.3 Pathological implications of Rabs modulating αS aggregation

Vesicle trafficking deficits caused by αS have been implicated in the Synucleinopathies. Elevated expression of αS was reported to affect the vesicle trafficking from ER to Golgi as the vesicle docking and fusion to Golgi membrane were blocked and the accumulation of undocked vesicles grew into massive intracellular clusters (Cooper et al, 2006; Gitler et al, 2008). Rab1 is responsible for modulating the vesicle trafficking between ER and Golgi. The overproduction of Rab1 gene *in vivo* was observed to suppress the trafficking disruption casued by αS. (Cooper et al, 2006) In addition, Rab8a, which is located at the post-Golgi vesicles and Rab3a, which is expressed specifically in neurons, could also suppress this cellular toxicity of αS by their overexpression, suggesting that αS broadly affects multiple steps of vesicle trafficking in cells (Gitler et al, 2008). Furthermore, recent study points out that αS aggregation induced the aggregation of many Rab-GTPases in the model system of *S. cerevisiae* (Soper et al, 2011), as the direct evidence of the interactions between αS and Rab proteins *in vivo*. Thus, the tight interplays between αS and the Rab proteins have been implicated in the scenario of vesicular trafficking.

Both the Rab1 mutation (Wilson et al, 1994) and the overexpression of αS (Gosavi et al, 2002) could cause the Golgi fragmentation (Cooper et al, 2006). This reflects a deleterious relationship that αS can reproduce the harmful effects of the Rab1 malfunction caused by the critical mutation. Conversely, this also partially explains that Rab1 was capable of rescuing the toxic effects of αS involved in the ER-Golgi transport. The mechanism of αS-induced deficits of vesicle trafficking and cellular compartment fragmentation might be attributed to the high affinity of αS to acidic phospholipid-rich membranes and the prone of misfolding and oligomerization (Cooper et al, 2006). In vitro biophysical studies found that the binding of αS monomers to the artificial vesicle, SUV, can render the deformation of SUV membrane (Bodner et al, 2009), implicating that the attenuated membrane intactness likely account for the vesicle dysfunction induced by αS. Meanwhile, αS oligomers have been reported to possess pore-forming propensity in the membranes (Kim et al, 2009). The mitochondria fragmentation has been observed as a result of the αS oligomerization as well (Exner et al, 2012; Kamp et al, 2010), which the fragmentation is probably similar in the toxic mechanism leading to

the Golgi fragmentation by αS and speculated as one general phenotype of αS oligomers-induced toxicities. Thus, the vesicle trafficking disruptions caused by αS (Cooper et al, 2006; Gitler et al, 2008) might be as the results of αS binding to the vesicle membranes and the pore-forming effects of αS oligomers.

Comparing to the soluble monomers and oligomers of αS, αS fibrils possesses lower affinity to membrane and less cellular toxicity than the oligomeric species. Taken together, therefore, one molecular mechanism for the αS-toxicity suppression by the Rabs is proposed: Rabs lowered the populations of αS oligomers by enhancing their conversation into fibrils and thereby the toxicity of αS was reduced.

4.3 Conserved fibril core and its implications to the conformation of alpha-Synuclein oligomers

4.3.1 Molecular structure and supermolecular assembly of αS fibrils

One central question of our study is to find the impact of 3 mutations A30P, E46K and A53T on the αS fibril structure. To address this question, we need to determine if these 3 mutation sites are located in a structured β-sheet or in loop. At the same time, it also needs to answer if the arrangement of β-sheets inside fibril core would be changed by these 3 mutations.

The locations of the 46th and 53rd residue inside αS fibrils

Herein, we determine a conserved fibril core which exists between E46K and A53T αS fibrils by using solution NMR based H/D exchange. Particularly, for both mutants, the 46th residue was likely located in a loop region that between the first and second β-sheet. This is close to the observation for *wt* and A30P αS fibrils by combination of H/D exchange and HR-MARS (Cho et al, 2011). Riek group used solution NMR based H/D exchange together with ssNMR for rigid core region and cryo-EM for assembly of filaments depicted the inner arrangement of β-sheets inside core and the possible fold of *wt* αS fibrils of both twisted and straight type of fibrils (Vilar et al, 2008). In this comprehensive study, the location of E46 was also identified in a loop region. Similar speculation that E46K was located in a loop region was

proposed based on the ssNMR experiments for the fibrils of *wt* αS as well (Heise et al, 2005). However, the indication from this ssNMR analysis is less unambiguous due to the incomplete assignments especially for the E46 and its neighbor region.

With improved resolution, the residues located in ambient region of E46 in *wt* αS fibrils and K46 in E46K αS fibrils were assigned by ssNMR (Comellas et al, 2011). Based on the analysis of carbon chemical shifts of the ambient region for both *wt* and E46K αS, the mutation site of E46K was located in a structured region, the first β-sheet of fibril core. Meanwhile, the sequence for residue 40-51 completely conserved between human αS and mouse αS. With improved resolution achieved by uniformly [^{13}C, ^{15}N], [1-^{13}C]glucose and [2-^{13}C]glucose labeled mouse αS fibrils, this segment was fully assigned and the result also demonstrated that residue E46 was located in first β-sheet inside fibril core (Lv et al). Thus, the agreement has still been not reached for the location of 46th residue inside αS fibrils. The related reasons that need to be considered for this discrepancy can be listed as: 1) the fibril samples for NMR measurements were generated under different solution conditions and thus might be differed partially between each other (Hoyer et al, 2002); 2) significantly structural heterogeneity of αS fibrils has been witnessed by biphasic H/D exchange curves by solution NMR (Vilar et al, 2008) and doubling peaks for certain residues by ssNMR (Heise et al, 2005; Vilar et al, 2008), which is highly correlated different fibril morphologies. Especially, the region 44-75 where E46 is located was indicated with more flexibility and less structural homogeneity in recent ssNMR study on αS fibril structure (Gath et al, 2012); 3) the methodological differences. For solution NMR based H/D exchange, the essence is to distinguish the solvent-exposured/protected regions of fibrils. But some structured parts in the fold of αS fibrils might enjoy a interface with solvent and some loop regions might locate between the interface of two protofilaments and thereby less accessible by solvents (Comellas et al, 2011). ssNMR can achieve the in-situ analysis of fibril structure which is superior to H/D exchange method based on solution NMR, but the resolution and sensitivity of ssNMR can be affected by internal dynamics and heterogeneity of fibrils (Kloepper et al, 2007).

Different with the case of E46K, a better agreement for the location of mutation A53T in the fibril core has been reached. We identify that, for fibrils of both E46K and

A53T αS mutants, the locations of 53rd residue are in second β-sheets in fibril core. This observation is close to other structural studies mentioned above (Cho et al, 2011; Comellas et al, 2011; Heise et al, 2005; Lv et al; Vilar et al, 2008).

The impacts of the familiar mutations on αS fibril core structures

The structural comparison for E46K and A53T αS fibrils are based on our H/D exchange results which point out that a conserved fibril core for them with respect to the basic arrangement of β-sheets and the boundaries of core. A very similar observation was obtained for *wt* and A30P methods by similar method (Cho et al, 2011). This indicates that fibril core region is conserved between *wt* αS and 3 familiar mutants. For the residues located at the starting and ending boundaries of fibril core, most of structural studies figure out fairly close result as we observed. And the boundaries which were started at ~37th residue and ended at ~97 residue were also further confirmed by the other techniques like EPR (Chen et al, 2007), Mass spectrum (Del Mar et al, 2005).

The central question of our study is to address that how the familiar mutations affect fibril structure. Particularly, E46K and A53T are in the core region of fibrils, unlike A30P is located in N-terminal loop. Our data suggest that there are minor changes caused by these two mutations on fibril structures. According to the chemical shift analysis, E46K and A53T mutations were reported to induce major and minor perturbation to fibril structure and attributed to their different side chains (Comellas et al, 2011). But, there was no further evidence from this work to point out mutation-induced change of β-sheets arrangement, suggesting that these two mutations probably impacted more on the local conformation around the single mutation points. One early result suggested that mutation A53T significantly affected on the fibril structure in comparison to *wt*-αS (Heise et al, 2008). However, the critical regions for plausible comparison like residue50-60, 76-80 were not assigned for A53T fibrils.

The role of different segments in the fibril formation

Inspecting the H/D exchange results, we found that the 4th β-sheet(70-81) experienced relatively stronger protection against solvent, indicating that this region is located in the center of the fibril fold. Meanwhile, the short β-sheet (63-65) and the fifth

β-sheet (86-96) as the neighboring region of 4th β-sheet also displayed stronger protections [Figure 3.3.3]. These regions occupy most of NAC region of αS known as pivot area responsible for aggregation. Particularly the β3 and β4 defined by our H/D exchange are highly overlapped with the β3 and β4 defined by Riek group (Vilar et al, 2008), where they indicated these two β-sheets are pivotal for fibril formations. The similar conclusions by other methods also point to that the certain segments in this region are centrally responsible for fibrillization(el-Agnaf & Irvine, 2002; El-Agnaf et al, 1998; Giasson et al, 2001; Madine et al, 2008).

Interestingly, in our studies although N-terminal residues (1-35) adopts a random coil conformation out of rigid fibril core, part of these residues still showed more protection compared to C-terminal, particularly the region 18~25. A recently ssNMR study on αS fibrils suggested that the fibril core started from the first residue of N-terminus (Gath et al, 2012). Although this finding is drastic to other structural investigation for αS fibrils performed before, it still implicates the presence of potentially tight contact between N-terminal residues and fibril core. In agreement to this, Rienstra group recently evaluated the impact of A30P mutation on αS fibril structure by ssNMR and identified that the fibril structure was mostly conserved between A30P and αS fibril. Nevertheless, this study found that due to mutation from Ala to Pro at 30th residue, the non-ignorable chemical shift perturbation with a average value of 0.5ppm was observed for Val55-Val63 (Lemkau et al, 2012), suggesting that A30P interacts with this region either intra or intermolecularly or by some indirect means. Moreover, correlated with this observation, N-terminally truncated αS was found to have a longer lag phase compared with *wt* αS (Zibaee et al, 2007).

Except molecular structure of single αS present in the fibrils, another intriguing question is how amino acid sequence affects the morphology of amyloid fibrils. As shown in Figure 3.3.1, the morphologies of E46K and A53T αS fibrils reflected by EM were fairly different. However, according to our H/D exchange data, the molecular structures of two mutants in the fibrils are similar. Although, EM images and H/D exchange address the structural arrangement at different level, they collectively suggest that familiar mutation impacts on ultrastructural arrangement of protofilaments rather than molecular structure of single protein. Therefore, at the end, several progress still

need to be made in 1) determining side chain conformation of the key residues in fibril core; 2) determining the N-terminal conformation of αS in fibril sample and map the potential contacts between N-terminal and fibril core region of αS since N-terminus of αS play an important role in modulating fibril formation; 3) clearly identifying the polymorphism existing in the fibrils.

4.3.2 Structural relationship of αS fibrils and oligomers and the prospective for structural study of αS oligomers

Structural correlation between αS fibrils and oligomers

As discussed above, N-terminus of αS potently act as a role in promoting the fibril formation as the tight interplay between it and fibril core has been implied by structural analysis and aggregation kinetics. And, *vice versa*, αS N-terminus is important for the fibrillization and might reduce the oligomeric species by assembling them into fibrils, which accordingly the N-terminal truncation led to longer lag phase (Zibaee et al, 2007). Therefore, it's more likely that N-terminus of αS is capable to regulate fibril formation of αS.

Low resolution model of αS oligomers and fibrils indicates that on-pathway oligomers of αS are the building blocks for αS fibrils (Giehm et al, 2011a). Our H/D exchange data for the oligomers also tentatively indicated the residues involved in the structured regions of fibril core could show certain degree of protection in the oligomer sample. Similar to this observation on the αS oligomers, recent progress in structural study of Aβ aggregates collectively by solution NMR and ssNMR revealed that there is close structural relationship amongst Aβ oligomers, protofilaments and mature fibrils (Fawzi et al, 2011; Lopez Del Amo et al, 2012; Scheidt et al, 2012). Therefore, there might be correlation of αS oligomer conformation and fibril structure as well. However, until now, there is no clear model to define the details that how oligomers are converted into fibrils. Particularly, the lack of structural information of αS oligomers at atomic resolution largely hampers to set reasonable link between oligomers and fibrils. In our H/D exchange experiment which was optimized for the compounds-stabilized αS oligomers, one major obstacle is presence of the oligomers as a mixture with αS

monomers and thus hard to be purified, concentrated. At the same time, the polymorphisms of the oligomers present in terms of size distribution and structural heterogeneity. Both characters render our experiment with lower sensitivity specific to the oligomers and experimental design.

Prospective for structural study of αS oligomers

As the predominant advantage of NMR is revealing the atomic resolution, probing αS oligomer conformation with at least residue-specific resolution is still of the core tasks pursued in the future research. Based on the experience I attained for structural study of αS oligomers, several envisions would be made for the following-up studies. 1) Further optimization of H/D exchange for the oligomers by searching proper solution conditions and time span for forward exchange period and improving data processing to enhance data sensitivity for the data fraction that encods information of the oligomer conformation. 2) Performing the relaxation dispersion experiments to catch wider time scale dynamics involved in conformational exchange between αS oligomers and monomers.

Alternatively, other methods would also be of options to access this end. Considering the relative lower population of the oligomers in the mixture of monomers and oligomers, reasonable purification and separation for oligomers are still desirable. Lashuel's group purified αS oligomers by Superose 6 column of size exclusion chromatography and obtained homogeneous, stable and off-pathway oligomers with size of 10~14mer and diameter of ~21nm (Hinault et al, 2010). Another feasible approach is to generate oligomers from mature fibrils. αS fibrils can be reverted back to oligomers through cold-dissociation approach, which was capable to reach ~70% of total amount staying at oligomeric state under super-cooling condition (Kim et al, 2009; Kim et al, 2008). Moreover, other compounds such as Dopamine (Cappai et al, 2005), EGCG (Ehrnhoefer et al, 2008) which were able to inhibit fibril formation and stabilize αS oligomers can also be the choices to generate αS oligomers for structural analysis.

With optimal sample condition, the following issue is to choose experimental strategy of NMR spectroscopy to characterize conformation of αS oligomers. In recent years, Clore group characterize amyloid-β oligomers by applying selective saturation oligomer-bound monomer together with comparison of apparent R_2 values between the bound and free monomers. Thereby chemical exchange process up to 1 second timescale between observable monomers and NMR-invisible oligomers can be mapped and residue-specific dynamics containing oligomer conformation can be probed (Fawzi et al, 2011; Fawzi et al, 2010; Fawzi et al, 2012). This is an option to test our oligomer sample. But, the difference for Aβ and αS should be noticed. Aβ is a short peptide with high hydrophobicity, however αS comprises not only hydrophobic region i.e. NAC but also amphiphilic N-terminal and acidic C-terminal which effectively modulate the oligomerization and fibrillization. Thus, the association of αS monomers to the oligomers is likely not tight as Aβ. Hence kinetics of the chemical exchange process between αS monomers and oligomers could largely be different with the Aβ case, which might be out the time scale of ~10ms-1s allowing to be detected by the method of Clore (Fawzi et al, 2012).

Complementary to this method, relaxation dispersion as mentioned is one option to describe the dynamics within a wider timescale (50μs-10ms) (Ishima & Torchia, 2006). Another choice is paramagnetic relaxation enhancement (PRE) to detect the transient complex formation within time scale 250-500μs (Clore & Iwahara, 2009). Intermolecular PRE was already been detected between N-terminal of one αS and C-terminal of another αS in concentration-dependent manner (Wu & Baum). The intermolecular PRE has been identified by placing paramagnetic tag MTSL at A19C and G132C of αS, which ^{15}N-labelled αS mixed with unlabeled αS with MTSL tag. A position-dependence of this intermolecular PRE has also been indicated by less significant effect for MTSL at A90C position since it's located at the distal side of the interface of intermolecular contact. Recently, the groups of Klenerman and Dobson successfully accessed the structural information of αS oligomers and identified the conversation between oligomers of different size by placing fluorescence tag at the 90th residue (Cremades et al, 2012). Therefore, it's likely to detect dynamics of chemical exchange between αS monomers and oligomers by placing paramagnetic tag at proper

position. For instance, placing MTSL tag at A90C of αS would not cause significant PRE at neighboring αS monomers. But, after the preliminary aggregation for mixture of ^{14}N-A90C αS with MTSL and ^{15}N-αS, the hydrophobic segments of αS would get close to neighboring αS during oligomerization and ^{15}N-αS would feel the PRE from neighboring ^{14}N-A90C αS with MTSL within oligomers. If free αS monomers are experiencing intensive chemical exchange with oligomer-bound monomers, there would be possibility that the PRE effect on bound αS is detectable after it quickly dissociates from oligomers assuming the time scale of this process fits to detect the encoded PRE effects.

4.4 Structural and functional importance of alpha-Synuclein C-terminus

The C-terminus of αS (98-140) displays distinct structural properties and functional significance within the scope of this dissertation. Therefore, herein a brief summary is exerted by linking the roles of αS C-terminal defined in different topics of this dissertation. The further implications respecting to the previously less-highlighted features of the C-terminal thereby would be proposed.

Structural reasons for the hyperphosphorylation at Ser129 of αS

In the first section, the phosphorylation of αS, we studied the Ser phosphorylation at Ser87 and Ser129. Kinetic studies of the phosphorylation by both CKI and PLKs points out that the 3 familiar mutations of αS didn't alter the phosphorylation kinetics of Ser87, but slightly modified the kinetics of Ser129. Comparing with CKI, the PLK family kinases phosphorylated αS specifically at Ser129, particularly PLK2 and PLK3 display high efficiency in phosphorylation kinetics both *in vitro* and *in vivo*. Furthermore, we performed the aggregation assays for the phosphorylated-Ser129 αS and for the two Ser-to-Glu mutants that mimic the Ser129 phosphorylation. Our results indicated that the aggregation propensity of αS was not significantly modified by the phosphorylation at Ser129, drastically in contrast to the aggregation of αS with the Ser87 phosphorylation (Paleologou et al). The related

evidences also point out that PLKs are capable of phosphorylating the αS fibrils at Ser129 (Mbefo et al).

Linking to our H/D exchange data for the fibrils of the two familiar mutants of αS, C-terminal of αS is a special region that doesn't participate in the fibril formation and maintains in highly disordered conformation in both monomers and fibrils. This structural feature can address that why approximately 90% αS was identified with the Ser129 phosphorylation in the Lewy body (Fujiwara et al, 2002), which is because the αS C-terminal can be readily accessed and recognized by the kinases at both monomeric and fibrillar states. Furthermore, the fact that the post-translational modifications are enriched in C-terminal region (Oueslati et al, 2010b) might be as a consequence of the evolution, where the probability of the posttranslational modifications was maximized for αS as the sites located in the C-terminal which could be readily accessed even for αS fibrils.

C-terminus of αS is important in the protein-protein interactions

The dominant negative charges at the C-terminus of αS are recognized to be important for stabilizing monomer conformation and modulating the fibril formation (Levitan et al, 2011). Our interaction studies for αS and the Rab proteins provide a solid case to understand the role of C-terminal charges in modulating the protein-protein interactions. For instance, Rab8a performs a polyamines-like manner (Fernandez et al, 2004) to interact with αS C-terminal mainly through the electrostatic interaction. Moreover, it's reported that PLKs possess dominantly positive net-charge over the whole proteins (PLK1: +15, PLK2: +19, PLK3: +15.5, PLK4: +8) (Johnson et al, 2007). At the same time, as described in section 4.1, PLK1 to -3 have a preference for substrates in which at least one of the three residues flanking the serine residue is negatively charged. These two points might shed light to the phosphorylation specificity of PLKs to the C-terminal Ser129 but not the NAC Ser87.

Except the positively charged C-terminus of Rab8a, its folded part can also bind to αS C-terminus in conformational preference mechanism that Rab8a-GDP displays a stronger affinity than Rab8a-GppNHp binding to αS. This indicates that αS prefers to bind to GDP-state Rab8a and can be attributed to significant nucleotide-dependence of

Rab-GTPases conformation, particularly on the Switch regions (Itzen & Goody, 2011; Lee et al, 2009). Thus, this observation extends our understanding that αS C-terminus binds to other proteins not only upon the charges but also the structural preference.

The role of αS C-terminus in modulating the aggregation

Due to the binding of Rab8a to αS C-terminus, the aggregation of αS was improved by the presence of Rab8a in a polyamine-like manner that the lag phase was significantly shortened and fibril formation was also enhanced (Fernandez et al, 2004). The same effects have been achieved previously by C-terminal truncation of αS (Hoyer et al, 2004; Kim et al, 2002; Levitan et al, 2011), which is in contrast to that the N-terminal truncation would increase lag phase of aggregation (Zibaee et al, 2007). Taken together, these evidences collectively suggest that the αS C-terminus potentially plays a role in modulating the αS oligomerization.

5 Summary and outlook

In this study, we investigated the serine phosphorylation of αS, interactions of αS with three Rab-GTPases, and the structure of αS aggregates.

Summary

1. Serine phosphorylation

   (1) Three familial mutations A30P, E46K, and A53T slightly affect the phosphorylation kinetics of Ser129, but do not affect that of Ser87.

   (2) PLKs selectively and efficiently phosphorylate αS at Ser129. PLK3 fully phosphorylate αS at Ser129 within 2.5 hours under our assay conditions.

   (3) Phosphorylation of Ser129 does not affect αS aggregation.

2. Interactions of αS with three Rab-GTPases

   (1) Rab8a at both GDP- and GppNHp-bound states binds to monomeric αS at its C-terminus in solution.

   (2) Both Rab8a-δC and the C-terminal peptide of Rab8a bind to αS C-terminus as well.

   (3) Rab8a(GDP) binds to αS more strongly than Rab8a(GppNHp) and this is reproduced by Rab8a-δC.

   (4) The Switch I region and the C-terminal loop of Rab8a are two major binding sites for αS.

   (5) Both Rab8a and its C-terminal peptide can enhance αS aggregation.

   (6) Rab1b and Rab3a do not bind to monomeric αS, but they enhance αS aggregation.

3. Structure of αS aggregates

(1) H/D exchange for fibrils of E46K and A53T αS indicates a conserved fibril core.

(2) H/D exchange for the compounds-stabilized oligomers of αS suggests that these oligomers do not contain large amount of hydrogen-bonded regions like αS fibrils.

Outlook

To further characterize the comprehensive interplays between αS and the Rab proteins, we propose to implement:

1) αS aggregation assays in the presence of the C-terminal peptides of Rab1b, Rab3a and Rab3a, to clarify the role of each fragment of the protein in modulating aggregation;

2) αS aggregation assays with Rab8a-δC to exactly determine its role in aggregation modulation;

3) NMR titration of Rab8a and S129D αS to evaluate the effect of the Ser129 phosphorylation on molecular interaction;

4) aggregation assays of phosphorylated Ser129 αS in the presence of Rab8a;

5) related *in vivo* assays to study the αS-Rab8a co-localization, the aggregation of αS in the presence of Rab8a and the impacts of Ser129 phosphorylation on the interplay between αS and Rab8a (undertaken in Prof. Dr. Tiago F. Outeiro's lab);

6) interaction study for αS oligomers and the Rab proteions.

6 References

Abeliovich A, Schmitz Y, Farinas I, Choi-Lundberg D, Ho WH, Castillo PE, Shinsky N, Verdugo JM, Armanini M, Ryan A, Hynes M, Phillips H, Sulzer D, Rosenthal A (2000) Mice lacking alpha-synuclein display functional deficits in the nigrostriatal dopamine system. *Neuron* **25**(1)**:** 239-252

Anderson JP, Walker DE, Goldstein JM, de Laat R, Banducci K, Caccavello RJ, Barbour R, Huang J, Kling K, Lee M, Diep L, Keim PS, Shen X, Chataway T, Schlossmacher MG, Seubert P, Schenk D, Sinha S, Gai WP, Chilcote TJ (2006) Phosphorylation of Ser-129 is the dominant pathological modification of alpha-synuclein in familial and sporadic Lewy body disease. *The Journal of biological chemistry* **281**(40)**:** 29739-29752

Angot E, Steiner JA, Hansen C, Li JY, Brundin P (2010) Are synucleinopathies prion-like disorders? *Lancet neurology* **9**(11)**:** 1128-1138

Artimo P, Jonnalagedda M, Arnold K, Baratin D, Csardi G, de Castro E, Duvaud S, Flegel V, Fortier A, Gasteiger E, Grosdidier A, Hernandez C, Ioannidis V, Kuznetsov D, Liechti R, Moretti S, Mostaguir K, Redaschi N, Rossier G, Xenarios I, Stockinger H (2012) ExPASy: SIB bioinformatics resource portal. *Nucleic acids research* **40**(W1)**:** W597-W603

Auluck PK, Caraveo G, Lindquist S alpha-Synuclein: membrane interactions and toxicity in Parkinson's disease. *Annual review of cell and developmental biology* **26:** 211-233

Auluck PK, Caraveo G, Lindquist S (2010) alpha-Synuclein: membrane interactions and toxicity in Parkinson's disease. *Annual review of cell and developmental biology* **26:** 211-233

Azeredo da Silveira S, Schneider BL, Cifuentes-Diaz C, Sage D, Abbas-Terki T, Iwatsubo T, Unser M, Aebischer P (2009) Phosphorylation does not prompt, nor prevent, the formation of alpha-synuclein toxic species in a rat model of Parkinson's disease. *Human molecular genetics* **18**(5)**:** 872-887

Bartels T, Choi JG, Selkoe DJ (2011) alpha-Synuclein occurs physiologically as a helically folded tetramer that resists aggregation. *Nature* **477**(7362)**:** 107-110

Bax A, Grzesiek S (1993) Methodological Advances in Protein Nmr. *Accounts of Chemical Research* **26**(4)**:** 131-138

Ben Gedalya T, Loeb V, Israeli E, Altschuler Y, Selkoe DJ, Sharon R (2009) Alpha-synuclein and polyunsaturated fatty acids promote clathrin-mediated endocytosis and synaptic vesicle recycling. *Traffic (Copenhagen, Denmark)* **10**(2)**:** 218-234

Bertoncini CW, Fernandez CO, Griesinger C, Jovin TM, Zweckstetter M (2005a) Familial mutants of alpha-synuclein with increased neurotoxicity have a destabilized conformation. *The Journal of biological chemistry* **280**(35)**:** 30649-30652

Bertoncini CW, Jung YS, Fernandez CO, Hoyer W, Griesinger C, Jovin TM, Zweckstetter M (2005b) Release of long-range tertiary interactions potentiates aggregation of natively unstructured alpha-synuclein. *Proceedings of the National Academy of Sciences of the United States of America* **102**(5)**:** 1430-1435

Bisaglia M, Mammi S, Bubacco L (2009) Structural insights on physiological functions and pathological effects of alpha-synuclein. *Faseb J* **23**(2)**:** 329-340

Bleimling N, Alexandrov K, Goody R, Itzen A (2009) Chaperone-assisted production of active human Rab8A GTPase in Escherichia coli. *Protein Expr Purif* **65**(2)**:** 190-195

Bodner CR, Dobson CM, Bax A (2009) Multiple tight phospholipid-binding modes of alpha-synuclein revealed by solution NMR spectroscopy. *Journal of molecular biology* **390**(4)**:** 775-790

Bodner CR, Maltsev AS, Dobson CM, Bax A (2010) Differential phospholipid binding of alpha-synuclein variants implicated in Parkinson's disease revealed by solution NMR spectroscopy. *Biochemistry* **49**(5)**:** 862-871

Braak H, Del Tredici K, Bratzke H, Hamm-Clement J, Sandmann-Keil D, Rub U (2002) Staging of the intracerebral inclusion body pathology associated with idiopathic Parkinson's disease (preclinical and clinical stages). *Journal of neurology* **249 Suppl 3:** III/1-5

Braithwaite SP, Stock JB, Mouradian MM alpha-Synuclein phosphorylation as a therapeutic target in Parkinson's disease. *Reviews in the neurosciences* **23**(2)**:** 191-198

Braithwaite SP, Stock JB, Mouradian MM (2012) alpha-Synuclein phosphorylation as a therapeutic target in Parkinson's disease. *Reviews in the neurosciences* **23**(2)**:** 191-198

Brundin P, Melki R, Kopito R Prion-like transmission of protein aggregates in neurodegenerative diseases. *Nature reviews* **11**(4)**:** 301-307

Brundin P, Melki R, Kopito R (2010) Prion-like transmission of protein aggregates in neurodegenerative diseases. *Nature reviews* **11**(4)**:** 301-307

Brundin P, Olsson R (2011) Can alpha-synuclein be targeted in novel therapies for Parkinson's disease? *Expert review of neurotherapeutics* **11**(7)**:** 917-919

Bucci C, Chiariello M, Lattero D, Maiorano M, Bruni CB (1999) Interaction cloning and characterization of the cDNA encoding the human prenylated rab acceptor (PRA1). *Biochemical and biophysical research communications* **258**(3)**:** 657-662

Bussell R, Jr., Eliezer D (2001) Residual structure and dynamics in Parkinson's disease-associated mutants of alpha-synuclein. *J Biol Chem* **276**(49)**:** 45996-46003

Butterfield SM, Lashuel HA Amyloidogenic protein-membrane interactions: mechanistic insight from model systems. *Angewandte Chemie (International ed* **49**(33)**:** 5628-5654

Cabin DE, Shimazu K, Murphy D, Cole NB, Gottschalk W, McIlwain KL, Orrison B, Chen A, Ellis CE, Paylor R, Lu B, Nussbaum RL (2002) Synaptic vesicle depletion correlates with attenuated synaptic responses to prolonged repetitive stimulation in mice lacking alpha-synuclein. *J Neurosci* **22**(20)**:** 8797-8807

Cappai R, Leck SL, Tew DJ, Williamson NA, Smith DP, Galatis D, Sharples RA, Curtain CC, Ali FE, Cherny RA, Culvenor JG, Bottomley SP, Masters CL, Barnham KJ, Hill AF (2005) Dopamine promotes alpha-synuclein aggregation into SDS-resistant soluble oligomers via a distinct folding pathway. *Faseb J* **19**(10)**:** 1377-1379

Carulla N, Zhou M, Giralt E, Robinson CV, Dobson CM (2010) Structure and intermolecular dynamics of aggregates populated during amyloid fibril formation studied by hydrogen/deuterium exchange. *Accounts of chemical research* **43**(8)**:** 1072-1079

Caughey B, Lansbury PT (2003) Protofibrils, pores, fibrils, and neurodegeneration: separating the responsible protein aggregates from the innocent bystanders. *Annual review of neuroscience* **26:** 267-298

Cavanagh J, Fairbrother W, Palmer III A, Rance M, Skelton N. (2007) Protein NMR Spectroscopy (Second Edition) Elsevier Inc. , p. 757.

Chandra S, Gallardo G, Fernandez-Chacon R, Schluter OM, Sudhof TC (2005) Alpha-synuclein cooperates with CSPalpha in preventing neurodegeneration. *Cell* **123**(3)**:** 383-396

Chaudhuri KR, Healy DG, Schapira AH (2006) Non-motor symptoms of Parkinson's disease: diagnosis and management. *Lancet neurology* **5**(3)**:** 235-245

Chen L, Feany MB (2005) Alpha-synuclein phosphorylation controls neurotoxicity and inclusion formation in a Drosophila model of Parkinson disease. *Nature neuroscience* **8**(5)**:** 657-663

Chen L, Periquet M, Wang X, Negro A, McLean PJ, Hyman BT, Feany MB (2009) Tyrosine and serine phosphorylation of alpha-synuclein have opposing effects on neurotoxicity and soluble oligomer formation. *The Journal of clinical investigation* **119**(11)**:** 3257-3265

Chen M, Margittai M, Chen J, Langen R (2007) Investigation of alpha-synuclein fibril structure by site-directed spin labeling. *The Journal of biological chemistry* **282**(34)**:** 24970-24979

Cho MK, Kim HY, Bernado P, Fernandez CO, Blackledge M, Zweckstetter M (2007) Amino acid bulkiness defines the local conformations and dynamics of natively unfolded alpha-synuclein and tau. *Journal of the American Chemical Society* **129**(11)**:** 3032-3033

Cho MK, Kim HY, Fernandez CO, Becker S, Zweckstetter M (2011) Conserved core of amyloid fibrils of wild type and A30P mutant alpha-synuclein. *Protein Sci* **20**(2)**:** 387-395

Chung CY, Koprich JB, Hallett PJ, Isacson O (2009) Functional enhancement and protection of dopaminergic terminals by RAB3B overexpression. *Proceedings of the National Academy of Sciences of the United States of America* **106**(52)**:** 22474-22479

Clore GM, Iwahara J (2009) Theory, practice, and applications of paramagnetic relaxation enhancement for the characterization of transient low-population states of biological macromolecules and their complexes. *Chemical reviews* **109**(9)**:** 4108-4139

Comellas G, Lemkau LR, Nieuwkoop AJ, Kloepper KD, Ladror DT, Ebisu R, Woods WS, Lipton AS, George JM, Rienstra CM (2011) Structured regions of alpha-synuclein fibrils include the early-onset Parkinson's disease mutation sites. *Journal of molecular biology* **411**(4)**:** 881-895

Conway KA, Harper JD, Lansbury PT (1998) Accelerated in vitro fibril formation by a mutant alpha-synuclein linked to early-onset Parkinson disease. *Nature medicine* **4**(11)**:** 1318-1320

Conway KA, Lee SJ, Rochet JC, Ding TT, Williamson RE, Lansbury PT, Jr. (2000) Acceleration of oligomerization, not fibrillization, is a shared property of both alpha-

synuclein mutations linked to early-onset Parkinson's disease: implications for pathogenesis and therapy. *Proceedings of the National Academy of Sciences of the United States of America* **97**(2)**:** 571-576

Cookson MR (2009) alpha-Synuclein and neuronal cell death. *Molecular neurodegeneration* **4:** 9

Cookson MR, van der Brug M (2008) Cell systems and the toxic mechanism(s) of alpha-synuclein. *Experimental neurology* **209**(1)**:** 5-11

Cooper AA, Gitler AD, Cashikar A, Haynes CM, Hill KJ, Bhullar B, Liu K, Xu K, Strathearn KE, Liu F, Cao S, Caldwell KA, Caldwell GA, Marsischky G, Kolodner RD, Labaer J, Rochet JC, Bonini NM, Lindquist S (2006) Alpha-synuclein blocks ER-Golgi traffic and Rab1 rescues neuron loss in Parkinson's models. *Science (New York, NY* **313**(5785)**:** 324-328

Craik DJ, Wilce JA (1997) Studies of protein-ligand interactions by NMR. *Methods Mol Biol* **60:** 195-232

Cremades N, Cohen SI, Deas E, Abramov AY, Chen AY, Orte A, Sandal M, Clarke RW, Dunne P, Aprile FA, Bertoncini CW, Wood NW, Knowles TP, Dobson CM, Klenerman D (2012) Direct observation of the interconversion of normal and toxic forms of alpha-synuclein. *Cell* **149**(5)**:** 1048-1059

Dalfo E, Barrachina M, Rosa JL, Ambrosio S, Ferrer I (2004a) Abnormal alpha-synuclein interactions with rab3a and rabphilin in diffuse Lewy body disease. *Neurobiology of disease* **16**(1)**:** 92-97

Dalfo E, Gomez-Isla T, Rosa JL, Nieto Bodelon M, Cuadrado Tejedor M, Barrachina M, Ambrosio S, Ferrer I (2004b) Abnormal alpha-synuclein interactions with Rab proteins in alpha-synuclein A30P transgenic mice. *Journal of neuropathology and experimental neurology* **63**(4)**:** 302-313

Davidson WS, Jonas A, Clayton DF, George JM (1998) Stabilization of alpha-synuclein secondary structure upon binding to synthetic membranes. *The Journal of biological chemistry* **273**(16)**:** 9443-9449

de Rijk MC, Launer LJ, Berger K, Breteler MM, Dartigues JF, Baldereschi M, Fratiglioni L, Lobo A, Martinez-Lage J, Trenkwalder C, Hofman A (2000) Prevalence of Parkinson's disease in Europe: A collaborative study of population-based cohorts. Neurologic Diseases in the Elderly Research Group. *Neurology* **54**(11 Suppl 5)**:** S21-23

Dedmon MM, Christodoulou J, Wilson MR, Dobson CM (2005a) Heat shock protein 70 inhibits alpha-synuclein fibril formation via preferential binding to prefibrillar species. *Journal of Biological Chemistry* **280**(15)**:** 14733-14740

Dedmon MM, Christodoulou J, Wilson MR, Dobson CM (2005b) Heat shock protein 70 inhibits alpha-synuclein fibril formation via preferential binding to prefibrillar species. *The Journal of biological chemistry* **280**(15)**:** 14733-14740

Dedmon MM, Lindorff-Larsen K, Christodoulou J, Vendruscolo M, Dobson CM (2005c) Mapping long-range interactions in alpha-synuclein using spin-label NMR and ensemble molecular dynamics simulations. *Journal of the American Chemical Society* **127**(2)**:** 476-477

Del Mar C, Greenbaum EA, Mayne L, Englander SW, Woods VL, Jr. (2005) Structure and properties of alpha-synuclein and other amyloids determined at the amino acid level. *Proceedings of the National Academy of Sciences of the United States of America* **102**(43)**:** 15477-15482

Di Giovanni S, Eleuteri S, Paleologou KE, Yin G, Zweckstetter M, Carrupt PA, Lashuel HA (2010) Entacapone and tolcapone, two catechol O-methyltransferase inhibitors, block fibril formation of alpha-synuclein and beta-amyloid and protect against amyloid-induced toxicity. *The Journal of biological chemistry* **285**(20)**:** 14941-14954

Dolgin E (2012) First therapy targeting Parkinson's proteins enters clinical trials. *Nature medicine* **18**(7)**:** 992-993

Dumas JJ, Zhu Z, Connolly JL, Lambright DG (1999) Structural basis of activation and GTP hydrolysis in Rab proteins. *Structure* **7**(4)**:** 413-423

Dyson HJ, Wright PE (2004) Unfolded proteins and protein folding studied by NMR. *Chemical Reviews* **104**(8)**:** 3607-3622

Dyson HJ, Wright PE (2005) Intrinsically unstructured proteins and their functions. *Nature reviews* **6**(3)**:** 197-208

Ehrnhoefer DE, Bieschke J, Boeddrich A, Herbst M, Masino L, Lurz R, Engemann S, Pastore A, Wanker EE (2008) EGCG redirects amyloidogenic polypeptides into unstructured, off-pathway oligomers. *Nature structural & molecular biology* **15**(6)**:** 558-566

el-Agnaf OM, Irvine GB (2002) Aggregation and neurotoxicity of alpha-synuclein and related peptides. *Biochemical Society transactions* **30**(4)**:** 559-565

El-Agnaf OM, Jakes R, Curran MD, Middleton D, Ingenito R, Bianchi E, Pessi A, Neill D, Wallace A (1998) Aggregates from mutant and wild-type alpha-synuclein proteins and NAC peptide induce apoptotic cell death in human neuroblastoma cells by formation of beta-sheet and amyloid-like filaments. *FEBS letters* **440**(1-2)**:** 71-75

Exner N, Lutz AK, Haass C, Winklhofer KF (2012) Mitochondrial dysfunction in Parkinson's disease: molecular mechanisms and pathophysiological consequences. *The EMBO journal* **31**(14)**:** 3038-3062

Falsone SF, Kungl AJ, Rek A, Cappai R, Zangger K (2009) The molecular chaperone Hsp90 modulates intermediate steps of amyloid assembly of the Parkinson-related protein alpha-synuclein. *The Journal of biological chemistry* **284**(45)**:** 31190-31199

Fauvet B, Fares MB, Samuel F, Dikiy I, Tandon A, Eliezer D, Lashuel HA (2012a) Characterization of Semisynthetic and Naturally Nalpha-Acetylated alpha-Synuclein in Vitro and in Intact Cells: IMPLICATIONS FOR AGGREGATION AND CELLULAR PROPERTIES OF alpha-SYNUCLEIN. *The Journal of biological chemistry* **287**(34)**:** 28243-28262

Fauvet B, Mbefo MK, Fares MB, Desobry C, Michael S, Ardah MT, Tsika E, Coune P, Prudent M, Lion N, Eliezer D, Moore DJ, Schneider B, Aebischer P, El-Agnaf OM, Masliah E, Lashuel HA (2012b) alpha-Synuclein in Central Nervous System and from Erythrocytes, Mammalian Cells, and Escherichia coli Exists Predominantly as Disordered Monomer. *Journal of Biological Chemistry* **287**(19)**:** 15345-15364

Fawzi NL, Ying J, Ghirlando R, Torchia DA, Clore GM (2011) Atomic-resolution dynamics on the surface of amyloid-beta protofibrils probed by solution NMR. *Nature* **480**(7376)**:** 268-272

Fawzi NL, Ying J, Torchia DA, Clore GM (2010) Kinetics of amyloid beta monomer-to-oligomer exchange by NMR relaxation. *Journal of the American Chemical Society* **132**(29)**:** 9948-9951

Fawzi NL, Ying J, Torchia DA, Clore GM (2012) Probing exchange kinetics and atomic resolution dynamics in high-molecular-weight complexes using dark-state exchange saturation transfer NMR spectroscopy. *Nature protocols* **7**(8)**:** 1523-1533

Fernandez CO, Hoyer W, Zweckstetter M, Jares-Erijman EA, Subramaniam V, Griesinger C, Jovin TM (2004) NMR of alpha-synuclein-polyamine complexes elucidates the mechanism and kinetics of induced aggregation. *Embo J* **23**(10)**:** 2039-2046

Figueroa C, Taylor J, Vojtek AB (2001) Prenylated Rab acceptor protein is a receptor for prenylated small GTPases. *The Journal of biological chemistry* **276**(30)**:** 28219-28225

Fink AL (2006) The aggregation and fibrillation of alpha-synuclein. *Accounts of Chemical Research* **39**(9)**:** 628-634

Fredenburg RA, Rospigliosi C, Meray RK, Kessler JC, Lashuel HA, Eliezer D, Lansbury PT, Jr. (2007) The impact of the E46K mutation on the properties of alpha-synuclein in its monomeric and oligomeric states. *Biochemistry* **46**(24)**:** 7107-7118

Fujiwara H, Hasegawa M, Dohmae N, Kawashima A, Masliah E, Goldberg MS, Shen J, Takio K, Iwatsubo T (2002) alpha-Synuclein is phosphorylated in synucleinopathy lesions. *Nature cell biology* **4**(2)**:** 160-164

Gao G, Williams JG, Campbell SL (2004) Protein-protein interaction analysis by nuclear magnetic resonance spectroscopy. *Methods Mol Biol* **261:** 79-92

Gath J, Habenstein B, Bousset L, Melki R, Meier BH, Bockmann A (2012) Solid-state NMR sequential assignments of alpha-synuclein. *Biomolecular NMR assignments* **6**(1)**:** 51-55

Giasson BI, Duda JE, Murray IV, Chen Q, Souza JM, Hurtig HI, Ischiropoulos H, Trojanowski JQ, Lee VM (2000) Oxidative damage linked to neurodegeneration by selective alpha-synuclein nitration in synucleinopathy lesions. *Science (New York, NY* **290**(5493)**:** 985-989

Giasson BI, Murray IV, Trojanowski JQ, Lee VM (2001) A hydrophobic stretch of 12 amino acid residues in the middle of alpha-synuclein is essential for filament assembly. *The Journal of biological chemistry* **276**(4)**:** 2380-2386

Giehm L, Svergun DI, Otzen DE, Vestergaard B (2011a) Low-resolution structure of a vesicle disrupting α-synuclein oligomer that accumulates during fibrillation. *Proceedings of the National Academy of Sciences of the United States of America* **108**(8)**:** 3246-3251

Giehm L, Svergun DI, Otzen DE, Vestergaard B (2011b) Low-resolution structure of a vesicle disrupting alpha-synuclein oligomer that accumulates during fibrillation. *Proceedings of the National Academy of Sciences of the United States of America* **108**(8)**:** 3246-3251

Gitler AD, Bevis BJ, Shorter J, Strathearn KE, Hamamichi S, Su LJ, Caldwell KA, Caldwell GA, Rochet JC, McCaffery JM, Barlowe C, Lindquist S (2008) The Parkinson's disease protein alpha-synuclein disrupts cellular Rab homeostasis.

Proceedings of the National Academy of Sciences of the United States of America **105**(1)**:** 145-150

Golbe LI, Di Iorio G, Bonavita V, Miller DC, Duvoisin RC (1990) A large kindred with autosomal dominant Parkinson's disease. *Ann Neurol* **27**(3)**:** 276-282

Gomez-Tortosa E, Newell K, Irizarry MC, Sanders JL, Hyman BT (2000) alpha-Synuclein immunoreactivity in dementia with Lewy bodies: morphological staging and comparison with ubiquitin immunostaining. *Acta neuropathologica* **99**(4)**:** 352-357

Gorbatyuk OS, Li S, Sullivan LF, Chen W, Kondrikova G, Manfredsson FP, Mandel RJ, Muzyczka N (2008) The phosphorylation state of Ser-129 in human alpha-synuclein determines neurodegeneration in a rat model of Parkinson disease. *Proceedings of the National Academy of Sciences of the United States of America* **105**(2)**:** 763-768

Gosavi N, Lee HJ, Lee JS, Patel S, Lee SJ (2002) Golgi fragmentation occurs in the cells with prefibrillar alpha-synuclein aggregates and precedes the formation of fibrillar inclusion. *The Journal of biological chemistry* **277**(50)**:** 48984-48992

Greenbaum EA, Graves CL, Mishizen-Eberz AJ, Lupoli MA, Lynch DR, Englander SW, Axelsen PH, Giasson BI (2005) The E46K mutation in alpha-synuclein increases amyloid fibril formation. *The Journal of biological chemistry* **280**(9)**:** 7800-7807

Guex N, Peitsch MC (1997) SWISS-MODEL and the Swiss-PdbViewer: an environment for comparative protein modeling. *Electrophoresis* **18**(15)**:** 2714-2723

Halliday GM, Holton JL, Revesz T, Dickson DW (2011) Neuropathology underlying clinical variability in patients with synucleinopathies. *Acta neuropathologica* **122**(2)**:** 187-204

Hansen C, Angot E, Bergstrom AL, Steiner JA, Pieri L, Paul G, Outeiro TF, Melki R, Kallunki P, Fog K, Li JY, Brundin P alpha-Synuclein propagates from mouse brain to grafted dopaminergic neurons and seeds aggregation in cultured human cells. *The Journal of clinical investigation* **121**(2)**:** 715-725

Hardy J (2010) Genetic Analysis of Pathways to Parkinson Disease. *Neuron* **68**(2)**:** 201-206

Hardy J, Lewis P, Revesz T, Lees A, Paisan-Ruiz C (2009) The genetics of Parkinson's syndromes: a critical review. *Curr Opin Genet Dev* **19**(3)**:** 254-265

Hartl FU, Bracher A, Hayer-Hartl M (2011) Molecular chaperones in protein folding and proteostasis. *Nature* **475**(7356)**:** 324-332

Hartl FU, Hayer-Hartl M (2009) Converging concepts of protein folding in vitro and in vivo. *Nature structural & molecular biology* **16**(6)**:** 574-581

Hawkes CH, Del Tredici K, Braak H (2007) Parkinson's disease: a dual-hit hypothesis. *Neuropathology and applied neurobiology* **33**(6)**:** 599-614

Heise H, Celej MS, Becker S, Riedel D, Pelah A, Kumar A, Jovin TM, Baldus M (2008) Solid-state NMR reveals structural differences between fibrils of wild-type and disease-related A53T mutant alpha-synuclein. *Journal of molecular biology* **380**(3)**:** 444-450

Heise H, Hoyer W, Becker S, Andronesi OC, Riedel D, Baldus M (2005) Molecular-level secondary structure, polymorphism, and dynamics of full-length alpha-synuclein fibrils studied by solid-state NMR. *Proceedings of the National Academy of Sciences of the United States of America* **102**(44)**:** 15871-15876

Hejjaoui M, Butterfield S, Fauvet B, Vercruysse F, Cui J, Dikiy I, Prudent M, Olschewski D, Zhang Y, Eliezer D, Lashuel HA (2012) Elucidating the role of C-terminal post-translational modifications using protein semisynthesis strategies: alpha-synuclein phosphorylation at tyrosine 125. *Journal of the American Chemical Society* **134**(11)**:** 5196-5210

Hinault MP, Cuendet AF, Mattoo RU, Mensi M, Dietler G, Lashuel HA, Goloubinoff P (2010) Stable alpha-synuclein oligomers strongly inhibit chaperone activity of the Hsp70 system by weak interactions with J-domain co-chaperones. *The Journal of biological chemistry* **285**(49)**:** 38173-38182

Hou X, Hagemann N, Schoebel S, Blankenfeldt W, Goody RS, Erdmann KS, Itzen A (2011) A structural basis for Lowe syndrome caused by mutations in the Rab-binding domain of OCRL1. *Embo J* **30**(8)**:** 1659-1670

Hoyer W, Antony T, Cherny D, Heim G, Jovin TM, Subramaniam V (2002) Dependence of alpha-synuclein aggregate morphology on solution conditions. *Journal of molecular biology* **322**(2)**:** 383-393

Hoyer W, Cherny D, Subramaniam V, Jovin TM (2004) Impact of the acidic C-terminal region comprising amino acids 109-140 on alpha-synuclein aggregation in vitro. *Biochemistry* **43**(51)**:** 16233-16242

Huang CJ, Cheng H, Hao SF, Zhou H, Zhang XJ, Gao JN, Sun QH, Hu HY, Wang CC (2006) Heat shock protein 70 inhibits alpha-synuclein fibril formation via interactions with diverse intermediates. *Journal of molecular biology* **364**(3)**:** 323-336

Hutagalung AH, Novick PJ (2011) Role of Rab GTPases in membrane traffic and cell physiology. *Physiological reviews* **91**(1)**:** 119-149

Hutt DM, Da-Silva LF, Chang LH, Prosser DC, Ngsee JK (2000) PRA1 inhibits the extraction of membrane-bound rab GTPase by GDI1. *The Journal of biological chemistry* **275**(24)**:** 18511-18519

Huynh T (2011) The Parkinson's disease market. *Nature reviews* **10**(8)**:** 571-572

Inglis KJ, Chereau D, Brigham EF, Chiou SS, Schobel S, Frigon NL, Yu M, Caccavello RJ, Nelson S, Motter R, Wright S, Chian D, Santiago P, Soriano F, Ramos C, Powell K, Goldstein JM, Babcock M, Yednock T, Bard F, Basi GS, Sham H, Chilcote TJ, McConlogue L, Griswold-Prenner I, Anderson JP (2009) Polo-like kinase 2 (PLK2) phosphorylates alpha-synuclein at serine 129 in central nervous system. *The Journal of biological chemistry* **284**(5)**:** 2598-2602

Ishii A, Nonaka T, Taniguchi S, Saito T, Arai T, Mann D, Iwatsubo T, Hisanaga S, Goedert M, Hasegawa M (2007) Casein kinase 2 is the major enzyme in brain that phosphorylates Ser129 of human alpha-synuclein: Implication for alpha-synucleinopathies. *FEBS Lett* **581**(24)**:** 4711-4717

Ishima R, Torchia DA (2006) Accuracy of optimized chemical-exchange parameters derived by fitting CPMG R2 dispersion profiles when R2(0a) not = R2(0b). *Journal of biomolecular NMR* **34**(4)**:** 209-219

Itzen A, Goody RS (2011) GTPases involved in vesicular trafficking: structures and mechanisms. *Seminars in cell & developmental biology* **22**(1)**:** 48-56

Jensen MR, Markwick PR, Meier S, Griesinger C, Zweckstetter M, Grzesiek S, Bernado P, Blackledge M (2009) Quantitative determination of the conformational properties of partially folded and intrinsically disordered proteins using NMR dipolar couplings. *Structure* **17**(9)**:** 1169-1185

Johnson CS (1999) Diffusion ordered nuclear magnetic resonance spectroscopy: principles and applications. *Progress in Nuclear Magnetic Resonance Spectroscopy* **34**(3-4)**:** 203-256

Johnson EF, Stewart KD, Woods KW, Giranda VL, Luo Y (2007) Pharmacological and functional comparison of the polo-like kinase family: insight into inhibitor and substrate specificity. *Biochemistry* **46**(33)**:** 9551-9563

Jung YS, Zweckstetter M (2004a) Backbone assignment of proteins with known structure using residual dipolar couplings. *Journal of biomolecular NMR* **30**(1)**:** 25-35

Jung YS, Zweckstetter M (2004b) Mars -- robust automatic backbone assignment of proteins. *Journal of biomolecular NMR* **30**(1)**:** 11-23

Kamp F, Exner N, Lutz AK, Wender N, Hegermann J, Brunner B, Nuscher B, Bartels T, Giese A, Beyer K, Eimer S, Winklhofer KF, Haass C (2010) Inhibition of mitochondrial fusion by alpha-synuclein is rescued by PINK1, Parkin and DJ-1. *The EMBO journal* **29**(20)**:** 3571-3589

Kang L, Moriarty GM, Woods LA, Ashcroft AE, Radford SE, Baum J (2012) N-terminal acetylation of alpha-synuclein induces increased transient helical propensity and decreased aggregation rates in the intrinsically disordered monomer. *Protein Sci* **21**(7)**:** 911-917

Karpinar DP, Balija MB, Kugler S, Opazo F, Rezaei-Ghaleh N, Wender N, Kim HY, Taschenberger G, Falkenburger BH, Heise H, Kumar A, Riedel D, Fichtner L, Voigt A, Braus GH, Giller K, Becker S, Herzig A, Baldus M, Jackle H, Eimer S, Schulz JB, Griesinger C, Zweckstetter M (2009) Pre-fibrillar alpha-synuclein variants with impaired beta-structure increase neurotoxicity in Parkinson's disease models. *The EMBO journal* **28**(20)**:** 3256-3268

Kessler JC, Rochet JC, Lansbury PT, Jr. (2003) The N-terminal repeat domain of alpha-synuclein inhibits beta-sheet and amyloid fibril formation. *Biochemistry* **42**(3)**:** 672-678

Kim HY, Cho MK, Kumar A, Maier E, Siebenhaar C, Becker S, Fernandez CO, Lashuel HA, Benz R, Lange A, Zweckstetter M (2009) Structural properties of pore-forming oligomers of alpha-synuclein. *Journal of the American Chemical Society* **131**(47)**:** 17482-17489

Kim HY, Cho MK, Riedel D, Fernandez CO, Zweckstetter M (2008) Dissociation of amyloid fibrils of alpha-synuclein in supercooled water. *Angewandte Chemie (International ed* **47**(27)**:** 5046-5048

Kim TD, Paik SR, Yang CH (2002) Structural and functional implications of C-terminal regions of alpha-synuclein. *Biochemistry* **41**(46)**:** 13782-13790

Kloepper KD, Hartman KL, Ladror DT, Rienstra CM (2007) Solid-state NMR spectroscopy reveals that water is nonessential to the core structure of alpha-synuclein fibrils. *The journal of physical chemistry* **111**(47)**:** 13353-13356

Kontaxis G, Clore GM, Bax A (2000) Evaluation of cross-correlation effects and measurement of one-bond couplings in proteins with short transverse relaxation times. *J Magn Reson* **143**(1)**:** 184-196

Kruger R, Kuhn W, Muller T, Woitalla D, Graeber M, Kosel S, Przuntek H, Epplen JT, Schols L, Riess O (1998) Ala30Pro mutation in the gene encoding alpha-synuclein in Parkinson's disease. *Nat Genet* **18**(2)**:** 106-108

Kuwahara T, Tonegawa R, Ito G, Mitani S, Iwatsubo T (2012) Phosphorylation of alpha-synuclein protein at Ser-129 reduces neuronal dysfunction by lowering its membrane binding property in Caenorhabditis elegans. *The Journal of biological chemistry* **287**(10)**:** 7098-7109

Landrieu I, Lacosse L, Leroy A, Wieruszeski JM, Trivelli X, Sillen A, Sibille N, Schwalbe H, Saxena K, Langer T, Lippens G (2006) NMR analysis of a Tau phosphorylation pattern. *J Am Chem Soc* **128**(11)**:** 3575-3583

Lansbury PT, Lashuel HA (2006) A century-old debate on protein aggregation and neurodegeneration enters the clinic. *Nature* **443**(7113)**:** 774-779

Larsen KE, Schmitz Y, Troyer MD, Mosharov E, Dietrich P, Quazi AZ, Savalle M, Nemani V, Chaudhry FA, Edwards RH, Stefanis L, Sulzer D (2006) Alpha-synuclein overexpression in PC12 and chromaffin cells impairs catecholamine release by interfering with a late step in exocytosis. *J Neurosci* **26**(46)**:** 11915-11922

Lashuel HA, Hartley D, Petre BM, Walz T, Lansbury PT, Jr. (2002a) Neurodegenerative disease: amyloid pores from pathogenic mutations. *Nature* **418**(6895)**:** 291

Lashuel HA, Lansbury PT, Jr. (2006) Are amyloid diseases caused by protein aggregates that mimic bacterial pore-forming toxins? *Quarterly reviews of biophysics* **39**(2)**:** 167-201

Lashuel HA, Petre BM, Wall J, Simon M, Nowak RJ, Walz T, Lansbury PT, Jr. (2002b) Alpha-synuclein, especially the Parkinson's disease-associated mutants, forms pore-like annular and tubular protofibrils. *Journal of molecular biology* **322**(5)**:** 1089-1102

Lee HJ, Kang SJ, Lee K, Im H (2011) Human alpha-synuclein modulates vesicle trafficking through its interaction with prenylated Rab acceptor protein 1. *Biochemical and biophysical research communications* **412**(4)**:** 526-531

Lee MT, Mishra A, Lambright DG (2009) Structural mechanisms for regulation of membrane traffic by rab GTPases. *Traffic (Copenhagen, Denmark)* **10**(10)**:** 1377-1389

Lees AJ, Hardy J, Revesz T (2009) Parkinson's disease. *Lancet* **373**(9680)**:** 2055-2066

Lemkau LR, Comellas G, Kloepper KD, Woods WS, George JM, Rienstra CM (2012) Mutant Protein A30P alpha-Synuclein Adopts Wild-type Fibril Structure, Despite Slower Fibrillation Kinetics. *The Journal of biological chemistry* **287**(14)**:** 11526-11532

Lescop E, Kern T, Brutscher B (2010) Guidelines for the use of band-selective radiofrequency pulses in hetero-nuclear NMR: example of longitudinal-relaxation-enhanced BEST-type 1H-15N correlation experiments. *J Magn Reson* **203**(1)**:** 190-198

LeVine H, 3rd (1999) Quantification of beta-sheet amyloid fibril structures with thioflavin T. *Methods in enzymology* **309:** 274-284

Levitan K, Chereau D, Cohen SI, Knowles TP, Dobson CM, Fink AL, Anderson JP, Goldstein JM, Millhauser GL (2011) Conserved C-terminal charge exerts a profound influence on the aggregation rate of alpha-synuclein. *Journal of molecular biology* **411**(2)**:** 329-333

Li JY, Englund E, Holton JL, Soulet D, Hagell P, Lees AJ, Lashley T, Quinn NP, Rehncrona S, Bjorklund A, Widner H, Revesz T, Lindvall O, Brundin P (2008) Lewy bodies in grafted neurons in subjects with Parkinson's disease suggest host-to-graft disease propagation. *Nature medicine* **14**(5)**:** 501-503

Li W, West N, Colla E, Pletnikova O, Troncoso JC, Marsh L, Dawson TM, Jakala P, Hartmann T, Price DL, Lee MK (2005) Aggregation promoting C-terminal truncation of alpha-synuclein is a normal cellular process and is enhanced by the familial Parkinson's disease-linked mutations. *Proceedings of the National Academy of Sciences of the United States of America* **102**(6)**:** 2162-2167

Lim Y, Kehm VM, Lee EB, Soper JH, Li C, Trojanowski JQ, Lee VM (2011) alpha-Syn suppression reverses synaptic and memory defects in a mouse model of dementia with Lewy bodies. *J Neurosci* **31**(27)**:** 10076-10087

Liu CW, Giasson BI, Lewis KA, Lee VM, Demartino GN, Thomas PJ (2005) A precipitating role for truncated alpha-synuclein and the proteasome in alpha-synuclein aggregation: implications for pathogenesis of Parkinson disease. *The Journal of biological chemistry* **280**(24)**:** 22670-22678

Liu J, Zhang JP, Shi M, Quinn T, Bradner J, Beyer R, Chen S, Zhang J (2009) Rab11a and HSP90 regulate recycling of extracellular alpha-synuclein. *J Neurosci* **29**(5)**:** 1480-1485

Liu S, Ninan I, Antonova I, Battaglia F, Trinchese F, Narasanna A, Kolodilov N, Dauer W, Hawkins RD, Arancio O (2004) alpha-Synuclein produces a long-lasting increase in neurotransmitter release. *The EMBO journal* **23**(22)**:** 4506-4516

Lo Bianco C, Shorter J, Regulier E, Lashuel H, Iwatsubo T, Lindquist S, Aebischer P (2008) Hsp104 antagonizes alpha-synuclein aggregation and reduces dopaminergic degeneration in a rat model of Parkinson disease. *The Journal of clinical investigation* **118**(9)**:** 3087-3097

Lopez Del Amo JM, Fink U, Dasari M, Grelle G, Wanker EE, Bieschke J, Reif B (2012) Structural Properties of EGCG-Induced, Nontoxic Alzheimer's Disease Abeta Oligomers. *Journal of molecular biology* **421**(4-5)**:** 517-524

Luk KC, Song C, O'Brien P, Stieber A, Branch JR, Brunden KR, Trojanowski JQ, Lee VM (2009) Exogenous alpha-synuclein fibrils seed the formation of Lewy body-like intracellular inclusions in cultured cells. *Proceedings of the National Academy of Sciences of the United States of America* **106**(47)**:** 20051-20056

Lv G, Kumar A, Giller K, Orcellet ML, Riedel D, Fernandez CO, Becker S, Lange A Structural comparison of mouse and human alpha-synuclein amyloid fibrils by solid-state NMR. *Journal of molecular biology* **420**(1-2)**:** 99-111

Madine J, Doig AJ, Middleton DA (2008) Design of an N-methylated peptide inhibitor of alpha-synuclein aggregation guided by solid-state NMR. *Journal of the American Chemical Society* **130**(25)**:** 7873-7881

Madine J, Middleton DA (2009) TARGETING alpha-SYNUCLEIN AGGREGATION FOR PARKINSON'S DISEASE TREATMENT. *Drugs of the Future* **34**(8)**:** 655-663

Maltsev AS, Ying J, Bax A (2012) Impact of N-terminal acetylation of alpha-synuclein on its random coil and lipid binding properties. *Biochemistry* **51**(25)**:** 5004-5013

Martincic I, Peralta ME, Ngsee JK (1997) Isolation and characterization of a dual prenylated Rab and VAMP2 receptor. *The Journal of biological chemistry* **272**(43)**:** 26991-26998

Mbefo MK, Paleologou KE, Boucharaba A, Oueslati A, Schell H, Fournier M, Olschewski D, Yin G, Zweckstetter M, Masliah E, Kahle PJ, Hirling H, Lashuel HA Phosphorylation of synucleins by members of the Polo-like kinase family. *The Journal of biological chemistry* **285**(4)**:** 2807-2822

Mbefo MK, Paleologou KE, Boucharaba A, Oueslati A, Schell H, Fournier M, Olschewski D, Yin G, Zweckstetter M, Masliah E, Kahle PJ, Hirling H, Lashuel HA (2010) Phosphorylation of synucleins by members of the Polo-like kinase family. *The Journal of biological chemistry* **285**(4)**:** 2807-2822

McFarland NR, Fan Z, Xu K, Schwarzschild MA, Feany MB, Hyman BT, McLean PJ (2009) Alpha-synuclein S129 phosphorylation mutants do not alter nigrostriatal toxicity

in a rat model of Parkinson disease. *Journal of neuropathology and experimental neurology* **68**(5)**:** 515-524

McLean PJ, Ribich S, Hyman BT (2000) Subcellular localization of alpha-synuclein in primary neuronal cultures: effect of missense mutations. *Journal of neural transmission*(58)**:** 53-63

Milburn MV, Tong L, deVos AM, Brunger A, Yamaizumi Z, Nishimura S, Kim SH (1990) Molecular switch for signal transduction: structural differences between active and inactive forms of protooncogenic ras proteins. *Science (New York, NY* **247**(4945)**:** 939-945

Morris GA, Freeman R (1979) Enhancement of Nuclear Magnetic-Resonance Signals by Polarization Transfer. *Journal of the American Chemical Society* **101**(3)**:** 760-762

Mukrasch MD, Markwick P, Biernat J, Bergen M, Bernado P, Griesinger C, Mandelkow E, Zweckstetter M, Blackledge M (2007) Highly populated turn conformations in natively unfolded tau protein identified from residual dipolar couplings and molecular simulation. *Journal of the American Chemical Society* **129**(16)**:** 5235-5243

Mulder FAA, Spronk CAEM, Slijper M, Kaptein R, Boelens R (1996) Improved HSQC experiments for the observation of exchange broadened signals. *Journal of biomolecular NMR* **8**(2)**:** 223-228

Muller MP, Peters H, Blumer J, Blankenfeldt W, Goody RS, Itzen A (2010) The Legionella effector protein DrrA AMPylates the membrane traffic regulator Rab1b. *Science (New York, NY* **329**(5994)**:** 946-949

Murphy DD, Rueter SM, Trojanowski JQ, Lee VM (2000) Synucleins are developmentally expressed, and alpha-synuclein regulates the size of the presynaptic vesicular pool in primary hippocampal neurons. *J Neurosci* **20**(9)**:** 3214-3220

Nalls MA, Plagnol V, Hernandez DG, Sharma M, Sheerin UM, Saad M, Simon-Sanchez J, Schulte C, Lesage S, Sveinbjornsdottir S, Stefansson K, Martinez M, Hardy J, Heutink P, Brice A, Gasser T, Singleton AB, Wood NW (2011) Imputation of sequence variants for identification of genetic risks for Parkinson's disease: a meta-analysis of genome-wide association studies. *Lancet* **377**(9766)**:** 641-649

Nonaka T, Iwatsubo T, Hasegawa M (2005) Ubiquitination of alpha-synuclein. *Biochemistry* **44**(1)**:** 361-368

Notredame C, Higgins DG, Heringa J (2000) T-Coffee: A novel method for fast and accurate multiple sequence alignment. *Journal of molecular biology* **302**(1)**:** 205-217

Okochi M, Walter J, Koyama A, Nakajo S, Baba M, Iwatsubo T, Meijer L, Kahle PJ, Haass C (2000) Constitutive phosphorylation of the Parkinson's disease associated alpha-synuclein. *The Journal of biological chemistry* **275**(1)**:** 390-397

Oschkinat H, Griesinger C, Kraulis PJ, Sorensen OW, Ernst RR, Gronenborn AM, Clore GM (1988) 3-Dimensional Nmr-Spectroscopy of a Protein in Solution. *Nature* **332**(6162)**:** 374-376

Ottiger M, Delaglio F, Bax A (1998) Measurement of J and dipolar couplings from simplified two-dimensional NMR spectra. *J Magn Reson* **131**(2)**:** 373-378

Oueslati A, Fournier M, Lashuel HA (2010a) Role of post-translational modifications in modulating the structure, function and toxicity of alpha-synuclein: implications for Parkinson's disease pathogenesis and therapies. *Progress in brain research* **183:** 115-145

Oueslati A, Fournier M, Lashuel HA (2010b) Role of post-translational modifications in modulating the structure, function and toxicity of alpha-synuclein: implications for Parkinson's disease pathogenesis and therapies. *Recent Advances in Parkinsons Disease: Basic Research* **183:** 115-145

Outeiro TF, Lindquist S (2003) Yeast cells provide insight into alpha-synuclein biology and pathobiology. *Science (New York, NY* **302**(5651)**:** 1772-1775

Outeiro TF, Putcha P, Tetzlaff JE, Spoelgen R, Koker M, Carvalho F, Hyman BT, McLean PJ (2008) Formation of toxic oligomeric alpha-synuclein species in living cells. *PloS one* **3**(4)**:** e1867

Paleologou KE, Oueslati A, Shakked G, Rospigliosi CC, Kim HY, Lamberto GR, Fernandez CO, Schmid A, Chegini F, Gai WP, Chiappe D, Moniatte M, Schneider BL, Aebischer P, Eliezer D, Zweckstetter M, Masliah E, Lashuel HA Phosphorylation at S87 is enhanced in synucleinopathies, inhibits alpha-synuclein oligomerization, and influences synuclein-membrane interactions. *J Neurosci* **30**(9)**:** 3184-3198

Paleologou KE, Oueslati A, Shakked G, Rospigliosi CC, Kim HY, Lamberto GR, Fernandez CO, Schmid A, Chegini F, Gai WP, Chiappe D, Moniatte M, Schneider BL, Aebischer P, Eliezer D, Zweckstetter M, Masliah E, Lashuel HA (2010) Phosphorylation at S87 is enhanced in synucleinopathies, inhibits alpha-synuclein oligomerization, and influences synuclein-membrane interactions. *J Neurosci* **30**(9)**:** 3184-3198

Paleologou KE, Schmid AW, Rospigliosi CC, Kim HY, Lamberto GR, Fredenburg RA, Lansbury PT, Jr., Fernandez CO, Eliezer D, Zweckstetter M, Lashuel HA (2008)

Phosphorylation at Ser-129 but not the phosphomimics S129E/D inhibits the fibrillation of alpha-synuclein. *The Journal of biological chemistry* **283**(24)**:** 16895-16905

Pan-Montojo F, Anichtchik O, Dening Y, Knels L, Pursche S, Jung R, Jackson S, Gille G, Spillantini MG, Reichmann H, Funk RH (2010) Progression of Parkinson's disease pathology is reproduced by intragastric administration of rotenone in mice. *PloS one* **5**(1)**:** e8762

Pankratz N, Wojcieszek J, Foroud T (2004) *Parkinson Disease Overview*: Seattle (WA): University of Washington, Seattle.

Pervushin K, Riek R, Wider G, Wuthrich K (1997) Attenuated T2 relaxation by mutual cancellation of dipole-dipole coupling and chemical shift anisotropy indicates an avenue to NMR structures of very large biological macromolecules in solution. *Proceedings of the National Academy of Sciences of the United States of America* **94**(23)**:** 12366-12371

Poirot O, O'Toole E, Notredame C (2003) Tcoffee@igs: A web server for computing, evaluating and combining multiple sequence alignments. *Nucleic acids research* **31**(13)**:** 3503-3506

Polymeropoulos MH, Lavedan C, Leroy E, Ide SE, Dehejia A, Dutra A, Pike B, Root H, Rubenstein J, Boyer R, Stenroos ES, Chandrasekharappa S, Athanassiadou A, Papapetropoulos T, Johnson WG, Lazzarini AM, Duvoisin RC, Di Iorio G, Golbe LI, Nussbaum RL (1997) Mutation in the alpha-synuclein gene identified in families with Parkinson's disease. *Science (New York, NY* **276**(5321)**:** 2045-2047

Prestegard JH, Bougault CM, Kishore AI (2004) Residual dipolar couplings in structure determination of biomolecules. *Chemical reviews* **104**(8)**:** 3519-3540

Puschmann A, Ross OA, Vilarino-Guell C, Lincoln SJ, Kachergus JM, Cobb SA, Lindquist SG, Nielsen JE, Wszolek ZK, Farrer M, Widner H, van Westen D, Hagerstrom D, Markopoulou K, Chase BA, Nilsson K, Reimer J, Nilsson C (2009) A Swedish family with de novo alpha-synuclein A53T mutation: evidence for early cortical dysfunction. *Parkinsonism Relat Disord* **15**(9)**:** 627-632

Putcha P, Danzer KM, Kranich LR, Scott A, Silinski M, Mabbett S, Hicks CD, Veal JM, Steed PM, Hyman BT, McLean PJ (2010) Brain-permeable small-molecule inhibitors of Hsp90 prevent alpha-synuclein oligomer formation and rescue alpha-synuclein-induced toxicity. *The Journal of pharmacology and experimental therapeutics* **332**(3)**:** 849-857

Rezaei-Ghaleh N, Blackledge M, Zweckstetter M (2012) Intrinsically disordered proteins: from sequence and conformational properties toward drug discovery. *Chembiochem* **13**(7)**:** 930-950

Roodveldt C, Bertoncini CW, Andersson A, van der Goot AT, Hsu ST, Fernandez-Montesinos R, de Jong J, van Ham TJ, Nollen EA, Pozo D, Christodoulou J, Dobson CM (2009) Chaperone proteostasis in Parkinson's disease: stabilization of the Hsp70/alpha-synuclein complex by Hip. *Embo J* **28**(23)**:** 3758-3770

Rospigliosi CC, McClendon S, Schmid AW, Ramlall TF, Barre P, Lashuel HA, Eliezer D (2009) E46K Parkinson's-linked mutation enhances C-terminal-to-N-terminal contacts in alpha-synuclein. *J Mol Biol* **388**(5)**:** 1022-1032

Rott R, Szargel R, Haskin J, Shani V, Shainskaya A, Manov I, Liani E, Avraham E, Engelender S (2008) Monoubiquitylation of alpha-synuclein by seven in absentia homolog (SIAH) promotes its aggregation in dopaminergic cells. *The Journal of biological chemistry* **283**(6)**:** 3316-3328

Salmon L, Nodet G, Ozenne V, Yin G, Jensen MR, Zweckstetter M, Blackledge M (2010) NMR characterization of long-range order in intrinsically disordered proteins. *Journal of the American Chemical Society* **132**(24)**:** 8407-8418

Salzmann M, Pervushin K, Wider G, Senn H, Wuthrich K (1998) TROSY in triple-resonance experiments: new perspectives for sequential NMR assignment of large proteins. *Proceedings of the National Academy of Sciences of the United States of America* **95**(23)**:** 13585-13590

Sancenon V, Lee SA, Patrick C, Griffith J, Paulino A, Outeiro TF, Reggiori F, Masliah E, Muchowski PJ (2012) Suppression of alpha-synuclein toxicity and vesicle trafficking defects by phosphorylation at S129 in yeast depends on genetic context. *Human molecular genetics* **21**(11)**:** 2432-2449

Satake W, Nakabayashi Y, Mizuta I, Hirota Y, Ito C, Kubo M, Kawaguchi T, Tsunoda T, Watanabe M, Takeda A, Tomiyama H, Nakashima K, Hasegawa K, Obata F, Yoshikawa T, Kawakami H, Sakoda S, Yamamoto M, Hattori N, Murata M, Nakamura Y, Toda T (2009) Genome-wide association study identifies common variants at four loci as genetic risk factors for Parkinson's disease. *Nature genetics* **41**(12)**:** 1303-1307

Sattler M, Schleucher J, Griesinger C (1999) Heteronuclear multidimensional NMR experiments for the structure determination of proteins in solution employing pulsed field gradients. *Progress in Nuclear Magnetic Resonance Spectroscopy* **34**(2)**:** 93-158

Schanda P, Brutscher B (2005) Very fast two-dimensional NMR spectroscopy for real-time investigation of dynamic events in proteins on the time scale of seconds. *Journal of the American Chemical Society* **127**(22)**:** 8014-8015

Schanda P, Kupce E, Brutscher B (2005) SOFAST-HMQC experiments for recording two-dimensional heteronuclear correlation spectra of proteins within a few seconds. *Journal of biomolecular NMR* **33**(4)**:** 199-211

Schapira AH, Bezard E, Brotchie J, Calon F, Collingridge GL, Ferger B, Hengerer B, Hirsch E, Jenner P, Le Novere N, Obeso JA, Schwarzschild MA, Spampinato U, Davidai G (2006) Novel pharmacological targets for the treatment of Parkinson's disease. *Nature reviews* **5**(10)**:** 845-854

Scheidt HA, Morgado I, Huster D (2012) Solid-state NMR Reveals a Close Structural Relationship between Amyloid-beta Protofibrils and Oligomers. *The Journal of biological chemistry* **287**(27)**:** 22822-22826

Schlichting I, Almo SC, Rapp G, Wilson K, Petratos K, Lentfer A, Wittinghofer A, Kabsch W, Pai EF, Petsko GA, et al. (1990) Time-resolved X-ray crystallographic study of the conformational change in Ha-Ras p21 protein on GTP hydrolysis. *Nature* **345**(6273)**:** 309-315

Schwarzinger S, Kroon GJ, Foss TR, Chung J, Wright PE, Dyson HJ (2001) Sequence-dependent correction of random coil NMR chemical shifts. *J Am Chem Soc* **123**(13)**:** 2970-2978

Schwarzinger S, Kroon GJ, Foss TR, Wright PE, Dyson HJ (2000) Random coil chemical shifts in acidic 8 M urea: implementation of random coil shift data in NMRView. *Journal of biomolecular NMR* **18**(1)**:** 43-48

Simon-Sanchez J, Schulte C, Bras JM, Sharma M, Gibbs JR, Berg D, Paisan-Ruiz C, Lichtner P, Scholz SW, Hernandez DG, Kruger R, Federoff M, Klein C, Goate A, Perlmutter J, Bonin M, Nalls MA, Illig T, Gieger C, Houlden H, Steffens M, Okun MS, Racette BA, Cookson MR, Foote KD, Fernandez HH, Traynor BJ, Schreiber S, Arepalli S, Zonozi R, Gwinn K, van der Brug M, Lopez G, Chanock SJ, Schatzkin A, Park Y, Hollenbeck A, Gao J, Huang X, Wood NW, Lorenz D, Deuschl G, Chen H, Riess O, Hardy JA, Singleton AB, Gasser T (2009) Genome-wide association study reveals genetic risk underlying Parkinson's disease. *Nature genetics* **41**(12)**:** 1308-1312

Sklenar V, Bax A (1987) Spin-Echo Water Suppression for the Generation of Pure-Phase Two-Dimensional Nmr-Spectra. *Journal of Magnetic Resonance* **74**(3)**:** 469-479

Skora L, Cho MK, Kim HY, Becker S, Fernandez CO, Blackledge M, Zweckstetter M (2006) Charge-induced molecular alignment of intrinsically disordered proteins. *Angewandte Chemie (International ed* **45**(42)**:** 7012-7015

Smith WW, Margolis RL, Li X, Troncoso JC, Lee MK, Dawson VL, Dawson TM, Iwatsubo T, Ross CA (2005) Alpha-synuclein phosphorylation enhances eosinophilic cytoplasmic inclusion formation in SH-SY5Y cells. *J Neurosci* **25**(23)**:** 5544-5552

Soper JH, Kehm V, Burd CG, Bankaitis VA, Lee VM (2011) Aggregation of alpha-synuclein in S. cerevisiae is associated with defects in endosomal trafficking and phospholipid biosynthesis. *J Mol Neurosci* **43**(3)**:** 391-405

Souza JM, Giasson BI, Chen Q, Lee VM, Ischiropoulos H (2000) Dityrosine cross-linking promotes formation of stable alpha -synuclein polymers. Implication of nitrative and oxidative stress in the pathogenesis of neurodegenerative synucleinopathies. *The Journal of biological chemistry* **275**(24)**:** 18344-18349

Spillantini MG, Goedert M (2000) The alpha-synucleinopathies: Parkinson's disease, dementia with Lewy bodies, and multiple system atrophy. *Annals of the New York Academy of Sciences* **920:** 16-27

Spillantini MG, Schmidt ML, Lee VM, Trojanowski JQ, Jakes R, Goedert M (1997) Alpha-synuclein in Lewy bodies. *Nature* **388**(6645)**:** 839-840

Stefani M, Dobson CM (2003) Protein aggregation and aggregate toxicity: new insights into protein folding, misfolding diseases and biological evolution. *Journal of molecular medicine (Berlin, Germany)* **81**(11)**:** 678-699

Steiner JA, Angot E, Brundin P A deadly spread: cellular mechanisms of alpha-synuclein transfer. *Cell death and differentiation* **18**(9)**:** 1425-1433

Stenmark H (2009) Rab GTPases as coordinators of vesicle traffic. *Nature reviews* **10**(8)**:** 513-525

Sugeno N, Takeda A, Hasegawa T, Kobayashi M, Kikuchi A, Mori F, Wakabayashi K, Itoyama Y (2008) Serine 129 phosphorylation of alpha-synuclein induces unfolded protein response-mediated cell death. *The Journal of biological chemistry* **283**(34)**:** 23179-23188

Taschenberger G, Garrido M, Tereshchenko Y, Bahr M, Zweckstetter M, Kugler S (2012) Aggregation of alphaSynuclein promotes progressive in vivo neurotoxicity in adult rat dopaminergic neurons. *Acta neuropathologica* **123**(5)**:** 671-683

Tofaris GK, Kim HT, Hourez R, Jung JW, Kim KP, Goldberg AL (2011) Ubiquitin ligase Nedd4 promotes alpha-synuclein degradation by the endosomal-lysosomal pathway. *Proceedings of the National Academy of Sciences of the United States of America* **108**(41)**:** 17004-17009

Tofaris GK, Layfield R, Spillantini MG (2001) alpha-synuclein metabolism and aggregation is linked to ubiquitin-independent degradation by the proteasome. *FEBS letters* **509**(1)**:** 22-26

Tofaris GK, Razzaq A, Ghetti B, Lilley KS, Spillantini MG (2003) Ubiquitination of alpha-synuclein in Lewy bodies is a pathological event not associated with impairment of proteasome function. *The Journal of biological chemistry* **278**(45)**:** 44405-44411

Touchot N, Zahraoui A, Vielh E, Tavitian A (1989) Biochemical properties of the YPT-related rab1B protein. Comparison with rab1A. *FEBS letters* **256**(1-2)**:** 79-84

Uversky VN (2009) Intrinsic disorder in proteins associated with neurodegenerative diseases. *Front Biosci* **14:** 5188-5238

Uversky VN, Oldfield CJ, Dunker AK (2008) Intrinsically disordered proteins in human diseases: introducing the D2 concept. *Annual review of biophysics* **37:** 215-246

van Raaij ME, Segers-Nolten IMJ, Subramaniam V (2006) Quantitative morphological analysis reveals ultrastructural diversity of amyloid fibrils from alpha-synuclein mutants. *Biophysical Journal* **91**(11)**:** L96-L98

Vilar M, Chou HT, Luhrs T, Maji SK, Riek-Loher D, Verel R, Manning G, Stahlberg H, Riek R (2008) The fold of alpha-synuclein fibrils. *Proceedings of the National Academy of Sciences of the United States of America* **105**(25)**:** 8637-8642

Visanji NP, Wislet-Gendebien S, Oschipok LW, Zhang G, Aubert I, Fraser PE, Tandon A Effect of Ser-129 phosphorylation on interaction of alpha-synuclein with synaptic and cellular membranes. *The Journal of biological chemistry* **286**(41)**:** 35863-35873

Visanji NP, Wislet-Gendebien S, Oschipok LW, Zhang G, Aubert I, Fraser PE, Tandon A (2011) Effect of Ser-129 phosphorylation on interaction of alpha-synuclein with synaptic and cellular membranes. *The Journal of biological chemistry* **286**(41)**:** 35863-35873

Volles MJ, Lansbury PT, Jr. (2003) Zeroing in on the pathogenic form of alpha-synuclein and its mechanism of neurotoxicity in Parkinson's disease. *Biochemistry* **42**(26)**:** 7871-7878

Volpicelli-Daley LA, Luk KC, Patel TP, Tanik SA, Riddle DM, Stieber A, Meaney DF, Trojanowski JQ, Lee VM Exogenous alpha-synuclein fibrils induce Lewy body pathology leading to synaptic dysfunction and neuron death. *Neuron* **72**(1)**:** 57-71

Wüthrich K. (1986) NMR of Proteins and Nucleic Acids. Wiley.

Wang L, Eghbalnia HR, Bahrami A, Markley JL (2005) Linear analysis of carbon-13 chemical shift differences and its application to the detection and correction of errors in referencing and spin system identifications. *Journal of biomolecular NMR* **32**(1)**:** 13-22

Waxman EA, Giasson BI (2011) Characterization of kinases involved in the phosphorylation of aggregated alpha-synuclein. *J Neurosci Res* **89**(2)**:** 231-247

Weinreb PH, Zhen W, Poon AW, Conway KA, Lansbury PT, Jr. (1996) NACP, a protein implicated in Alzheimer's disease and learning, is natively unfolded. *Biochemistry* **35**(43)**:** 13709-13715

Wider G, Dreier L (2006) Measuring Protein Concentrations by NMR Spectroscopy. *Journal of the American Chemical Society* **128:** 2571-2576

Wilson BS, Nuoffer C, Meinkoth JL, McCaffery M, Feramisco JR, Balch WE, Farquhar MG (1994) A Rab1 mutant affecting guanine nucleotide exchange promotes disassembly of the Golgi apparatus. *The Journal of cell biology* **125**(3)**:** 557-571

Winklhofer KF, Tatzelt J, Haass C (2008) The two faces of protein misfolding: gain- and loss-of-function in neurodegenerative diseases. *The EMBO journal* **27**(2)**:** 336-349

Wu KP, Baum J Detection of transient interchain interactions in the intrinsically disordered protein alpha-synuclein by NMR paramagnetic relaxation enhancement. *Journal of the American Chemical Society* **132**(16)**:** 5546-5547

Zarranz JJ, Alegre J, Gomez-Esteban JC, Lezcano E, Ros R, Ampuero I, Vidal L, Hoenicka J, Rodriguez O, Atares B, Llorens V, Gomez Tortosa E, del Ser T, Munoz DG, de Yebenes JG (2004) The new mutation, E46K, of alpha-synuclein causes Parkinson and Lewy body dementia. *Ann Neurol* **55**(2)**:** 164-173

Zheng G, Stait-Gardner T, Anil Kumar PG, Torres AM, Price WS (2008) PGSTE-WATERGATE: an STE-based PGSE NMR sequence with excellent solvent suppression. *J Magn Reson* **191**(1)**:** 159-163

Zibaee S, Jakes R, Fraser G, Serpell LC, Crowther RA, Goedert M (2007) Sequence Determinants for Amyloid Fibrillogenesis of Human alpha-Synuclein. *Journal of molecular biology* **374**(2)**:** 454-464

Zweckstetter M (2008) NMR: prediction of molecular alignment from structure using the PALES software. *Nature protocols* **3**(4)**:** 679-690

Appendix

I. Backbone assignment of Rab1b(1-175)-GDP

RES	N	HN	CO	CA	CB
GLY_1					
HIS_2					
MET_3					
PRO_4					
GLU_5	120.9	8.492	175.3	57.1	30.24
TYR_6	113.7	7.042	173.6	55.72	38.81
ASP_7	119.3	8.964	175.4	56.74	43.51
TYR_8	114.8	7.703	172.7	56.45	
LEU_9	125	8.325		54.04	43.92
PHE_10	123.9	8.662	174.1	51.08	40.71
LYS_11	128.5	11.64	175.8	55.8	
LEU_12	127.4	9.556		52.63	46.07
LEU_13	119.1	8.064		53.51	
LEU_14					
ILE_15					
GLY_16					
ASP_17	122.4	9.038	176.9	55.85	40.81
SER_18	115.5	8.805	176.1	60.33	63.44
GLY_19	116.4	11.17	174.5	45.82	
VAL_20	123.8	10.43	178.3	61.04	29.68
GLY_21					
LYS_22					
SER_23	117.8	8.333		61.49	55.27
CYS_24	120.9	9.648	179.1	64.64	26.84
LEU_25	125.9	9.286	177.9	59.47	42.7
LEU_26	119.3	7.979		59.01	41.84
LEU_27	119	8.82	180.1	58.47	41.3
ARG_28	119	8.514	178	57.77	27.42
PHE_29	119	8.198	178.4	60.17	40.52
ALA_30					
ASP_31	113.9	7.734		53.95	42.75
ASP_32	120.5	7.751	174.6	55.24	40.01
THR_33	106.9	7.048	173	59.59	71.75
TYR_34	119	8.062	173.3	58.88	41.61
THR_35	122.7	7.447	171	58.96	70.13
GLU_36	122.8	8.251	177	56.36	29.53
SER_37	117.2	7.934	173	58.64	63.6

TYR_38	123.3	8.314	175.7	58.78	38.3
ILE_39	129.8	8.554	175.2	60.05	38.95
SER_40					
THR_41					
ILE_42					
GLY_43	111.6	8.511	172.7	45.74	
VAL_44	113.7	7.21	175.1	59.66	35
ASP_45					
PHE_46	109.5	6.54	173.7	54.27	40.47
LYS_47	116.4	8.451	174.6	53.87	36.53
ILE_48	118.9	8.534	176.1	58.54	40.72
ARG_49	125	8.464	174.1	55.63	34.1
THR_50	123.2	8.733		62	69.21
ILE_51	121	9.223	173.3	59.16	42.29
GLU_52	121.2	8.31		54.66	32.07
LEU_53	124.5	8.734	176	54.44	45.95
ASP_54	124.6	9.385		55.16	39.88
GLY_55	104.2	8.87	173.9	45.47	
LYS_56	119.9	8.048	175.4	52.74	33.7
THR_57	119.6	9.87	174.6	63	69.41
ILE_58	129.7	9.416		59.62	40.2
LYS_59	128.9	8.812		55.81	33.74
LEU_60	125.4	8.743		52.95	43.01
GLN_61	124.7	8.971		54.66	30.96
ILE_62	126.8	9.185		61.28	39.44
TRP_63	128	9.199		58.2	
ASP_64	120.7	8.155		52.17	45.15
THR_65					
ALA_66					
GLY_67					
GLN_68					
GLU_69					
ARG_70					
PHE_71					
ARG_72					
THR_73					
ILE_74					
THR_75					
SER_76	129.7	9.375		59.55	
SER_77	113.4	7.653		59.11	
TYR_78					
TYR_79	129.3	9.103		60.96	31.93
ARG_80					
GLY_81					
ALA_82	120.2	7.129	177.2	52.68	18.04
HIS_83	122.1	9.697	175.8	59.8	33.37
GLY_84	103.4	7.679	171.3	45.4	

ILE_85	122.9	8.876	173.2	60.26	41.42
ILE_86					
VAL_87					
VAL_88	127.1	8.84	175.3		
TYR_89	122.3	9.094	170.5	55.55	40.01
ASP_90	121.5	8.856		51.31	43.41
VAL_91	118.5	8.722	176.3	64.24	30.82
THR_92	113	9.481	173.4	61.9	70.05
ASP_93	124	8.288		52.51	43.14
GLN_94	126.8	9.175	178	59.04	28.33
GLU_95	120.6	8.291		59.62	28.61
SER_96	116.1	7.959	176.2	61.27	63.46
TYR_97	123	7.188	178.5	60.13	39.21
ALA_98	126.4	8.666	181.2	55.28	17.55
ASN_99	113.9	8.374	177.4	54.14	38.15
VAL_100	123.2	7.946		67.77	30.9
LYS_101	116	7.378	178.7	60.62	31.99
GLN_102	119.2	7.265	179.1	58.64	27.84
TRP_103	121.5	7.83	178.8	60.46	29.43
LEU_104	117.7	8.758	179.1	58.36	40.79
GLN_105	118.6	7.49	178.6	58.96	28.39
GLU_106	121.1	7.753	178	59.99	29.76
ILE_107	118.8	7.984		65.88	38.25
ASP_108	118.2	7.72		56.99	40.39
ARG_109	117.1	7.385	178.3	58.55	30.54
TYR_110	113.9	7.488	176.3	57.7	41.31
ALA_111	121.8	8.629	176.6	51.2	21.61
SER_112	115	8.707	175.6	59.16	64
GLU_113	123.8	8.995	176.8	58.59	29.48
ASN_114	115.4	8.304	174.3	52.83	38.18
VAL_115	118.7	7.057	174.2	62.44	31.98
ASN_116	124.2	7.717	174.6	55.84	41.01
LYS_117	120.1	8.418		55.13	37.06
LEU_118	120.4	7.673	172.8	55.18	47.26
LEU_119	128.2	8.656		53.74	45.03
VAL_120	125.7	9.325	174	59.55	36.06
GLY_121	112.3	8.105	171.9	44.42	
ASN_122	123.1	9.075	174	51.52	41.47
LYS_123	111.8	7.232	177.6	57.56	29.26
SER_124	113.9	8.933	173.8	60.7	63.15
ASP_125	116.1	8.495	176.8	54.36	41.18
LEU_126	120.7	7.829			
THR_127	112.4	7.809	177.6	65.87	68.4
THR_128					
LYS_129	119.2	7.278	175.1	54.75	33.61
LYS_130	121.2	7.01	176.2	58.89	33.56
VAL_131	119.7	8.768	175.2	61.34	33.8

VAL_132	123.4	7.548		61.69	31.66
ASP_133	129.3	8.582	176.6	54.75	42.02
ASN_134					
THR_135	115.6	8.396	176.5	66.18	68.09
THR_136	120.1	7.365	176.1	66.05	68.73
ALA_137	125.1	7.186	178.5	54.74	20.21
LYS_138	109.4	7.712		59.35	
GLU_139	118.4	7.835	179.8	59.68	29.21
PHE_140	121.6	7.788	178.2	59.88	38.97
ALA_141	125.4	8.877	180.3	56.11	18.15
ASP_142	118.5	9.335		57.29	39.74
SER_143	118.2	8.003		61.51	62.46
LEU_144	121.5	7.167	177.4	54.51	43.79
GLY_145	109.7	7.989	174.9	46.27	
ILE_146	116	7.81	172.8	58.02	39.56
PRO_147					
PHE_148	119.7	7.877	174.7	55.31	43.89
LEU_149	128.2	8.015	173.5	54.7	47.07
GLU_150	117.3	7.992	177.5	54.39	32.31
THR_151	113.3	9.256	175.1	60.01	73.74
SER_152	111.4	8.19	175.8	56.8	64.47
ALA_153	133.3	9.043	178.1	56.15	18.16
LYS_154	117.8	7.104	176.8	58.46	33.91
ASN_155	114.2	7.956	175.2	52.21	38.05
ALA_156	118.8	7.744	176.2	55.08	17.31
THR_157	117.3	8.083	174.9	64.44	68.96
ASN_158	120.9	9.358	174.5	54.48	37.01
VAL_159	121.9	7.664	177.1	68.48	30.75
GLU_160	119.4	8.746	178.8	60.57	29.17
GLN_161	116.8	8.483	178.5	59.23	27.58
ALA_162	124.2	8.172	177.9	55.82	16.55
PHE_163	113.9	7.014	178.2	62.92	39.95
MET_164	117.8	8.831	179.2	58.22	31.12
THR_165	118.2	8.557		67.12	68.35
MET_166	119.8	7.465	176.9	58.28	32.33
ALA_167	119.6	8.384	178.1	55.73	18.82
ALA_168	119.2	8.338	180.9	55.25	18.33
GLU_169	119.1	8.165	179.3	59.14	29.39
ILE_170	120.8	7.917	178.3	64.66	38.64
LYS_171	118.9	8.208		60.22	32.2
LYS_172	117.9	7.721	178	59.31	32.55
ARG_173	117.2	7.466	177.4	57.36	30.38
MET_174	118.2	8.003		56.12	32.94
GLY_175	113.8	7.861	179.3	46.49	

II. Backbone assignment of Rab8a-GDP

RES	N	HN	CA	CB
GLY_1				
HIS_2	120.7	8.173	54.97	
MET_3				
ALA_4				
LYS_5	130.4	8.835	56.18	33.34
THR_6	125.7	8.811	61.83	68.69
TYR_7	122.6	8.958	58.91	
ASP_8	122.1	8.327	54.7	39.95
TYR_9				
LEU_10				
PHE_11				
LYS_12				
LEU_13				
LEU_14				
LEU_15	124.9	8.874	52	39.97
ILE_16	125.5	9.179	60.08	40.68
GLY_17				
ASP_18	122.9	9.033	55.6	40.56
SER_19	116.5	8.873	60.31	63.23
GLY_20	116.9	11.21	45.72	
VAL_21	113.7	7.543	62.7	32.03
GLY_22				
LYS_23				
THR_24				
CYS_25				
VAL_26	126.3	9.384	68.92	31.22
LEU_27	121.2	8.361	58.58	
PHE_28	121.1	9.115	62.35	38.82
ARG_29	121.8	8.699	57.88	27.71
PHE_30				
SER_31	110.7	8.444	61.42	64.06
GLU_32	119.1	7.697	55.36	30.97
ASP_33	120.8	7.631	55.14	39.6
ALA_34	118.9	7.035	50.86	23.34
PHE_35	119.4	8.39	57.96	
ASN_36				
SER_37				
THR_38	128.2	8.956	61.18	
PHE_39				
ILE_40	122.8	7.645	60.89	38.89
SER_41				
THR_42				
ILE_43	122.9	7.775	61.52	38.53

GLY_44	114	8.486	45.68	
ILE_45	121.3	7.775	59.84	38.38
ASP_46	125.4	8.259	55.43	42.06
PHE_47				
LYS_48	125.1	8.318	56.35	33.8
ILE_49				
ARG_50				
THR_51				
ILE_52				
GLU_53				
LEU_54				
ASP_55	124.1	9.305	55.12	39.73
GLY_56	104.5	8.756	45.46	
LYS_57	120.4	7.979	52.77	34.21
ARG_58	122.5	9.749	55.76	
ILE_59	129	9.456	59.35	38.73
LYS_60				
LEU_61				
GLN_62				
ILE_63				
TRP_64				
ASP_65				
THR_66				
ALA_67				
GLY_68				
GLN_69				
GLU_70				
ARG_71				
PHE_72				
ARG_73				
THR_74				
ILE_75				
THR_76				
THR_77				
ALA_78	118.4	8.409	55.66	18.73
TYR_79				
TYR_80	125.5	8.699	60.08	40.5
ARG_81				
GLY_82				
ALA_83	121.7	7.718	53.13	18.17
MET_84	119.9	9.069	56.17	
GLY_85	106.4	7.561	45.18	
ILE_86	124.3	9.024	60.11	
MET_87	124.8	8.671	53.16	
LEU_88				
VAL_89	123.5	8.701	60.78	33.51
TYR_90	123.5	9.057	55.38	39.52

ASP_91				
ILE_92	121.3	8.817	64.78	
THR_93	114.5	9.379	61.82	69.89
ASN_94	120.3	8.194	51.14	39.48
GLU_95	128.1	9.549	59.56	29.94
LYS_96				
SER_97	115.6	7.458	61.12	63.99
PHE_98	125.4	7.083	59.7	40.11
ASP_99	123.2	8.629	57.45	40.29
ASN_100	114.8	7.916	54.15	38.41
ILE_101	124.5	8.008	62.72	34.06
ARG_102				
ASN_103				
TRP_104				
ILE_105	119.5	8.534	65.82	37.13
ARG_106	113.2	7.452	61.85	
ASN_107				
ILE_108				
GLU_109	120.2	7.236	59.17	29.46
GLU_110	116.9	7.573	58.46	30.05
HIS_111	114	7.308	57.41	33.34
ALA_112	122.9	8.466	50.98	20.59
SER_113	115.5	8.417	58.59	63.75
ALA_114	127.1	8.68	54.21	18.68
ASP_115	114.9	8.042	53.5	40.77
VAL_116	121	7.138	62.7	32.52
GLU_117	127.4	7.435	55.42	31.46
LYS_118	122.6	8.611	54.68	35.95
MET_119				
ILE_120	118.6	8.319	58.5	40.99
LEU_121				
GLY_122				
ASN_123	123.1	8.697	52.28	40.97
LYS_124	111.1	7.044	57.7	
CYS_125	115.3	8.716	59.77	27.05
ASP_126	117.4	8.713	54.12	40.98
VAL_127	123.4	7.877	60.45	28.82
ASN_128				
ASP_129	112.3	6.923	54.9	40.6
LYS_130	129.7	7.689	56.56	
ARG_131				
GLN_132				
VAL_133	120.6	7.537	61.01	33.35
SER_134	125.7	8.462	58.17	63.8
LYS_135	127.3	9.017	60.24	32.49
GLU_136	116.6	8.6	59.82	28.83
ARG_137	120.8	7.648	59.74	30.56

GLY_138	109.9	7.287	47.92	
GLU_139				
LYS_140	125.3	9.38	58.54	31.95
LEU_141	121.7	7.473	58.44	41.48
ALA_142	119.6	7.655	55.66	19.03
LEU_143	120.4	8.108	58.09	41.86
ASP_144	121.9	8.327	57.24	
TYR_145	116	7.437	59.07	
GLY_146	112.8	8.176	46.85	
ILE_147	115.6	8.018	59.73	40.91
LYS_148				
PHE_149				
MET_150				
GLU_151	119.8	8.261	55.78	30.57
THR_152				
SER_153	112.1	8.761	57.27	65.09
ALA_154	134.1	9.023	55.34	18.87
LYS_155	120	7.07	58.85	34.58
ALA_156	118.3	8.123	51.14	19.04
ASN_157	116.8	7.208	53.18	36.26
ILE_158	119.1	8.239	60.55	40
ASN_159				
VAL_160	113.9	6.975	69.17	
GLU_161				
ASN_162	118	7.156	55.59	37.54
ALA_163	125.2	8.149	56.48	18.34
PHE_164	114.9	7.203	63.19	40.96
PHE_165	118.9	9.079	62.25	37.94
THR_166	117	8.169	67.47	
LEU_167				
ALA_168				
ARG_169	119.5	8.395	60.39	29.88
ASP_170	123	8.081	57.49	39.04
ILE_171	122.4	8.199	65.56	
LYS_172				
ALA_173	120.2	8.268	55.1	18.09
LYS_174	118	7.205	59.16	32.16
MET_175				
ASP_176	120.8	8.884	56.77	39.72
LYS_177	119.7	7.493	58.1	32.41
LYS_178	120.1	7.651	58	
LEU_179	120.8	7.887	55.92	42.12
GLU_180	120.8	7.958	57.38	30.1
GLY_181	109.1	8.147	45.52	
ASN_182				
SER_183				
PRO_184				

GLN_185				
GLY_186				
SER_187				
ASN_188				
GLN_189				
GLY_190				
VAL_191				
LYS_192	126.5	8.352	56.03	
ILE_193	124	8.195	60.72	42.03
THR_194	121.3	8.221	59.7	
PRO_195				
ASP_196				
GLN_197				
GLN_198				
LYS_199				
ARG_200				
SER_201				
SER_202				
PHE_203	120.6	8.061	55.72	
PHE_204				
ARG_205				
CYS_206				
VAL_207				
LEU_208				
LEU_209				

Publications

Mbefo MK, Paleologou KE, Boucharaba A, Oueslati A, Schell H, Fournier M, Olschewski D, **Yin G**, Zweckstetter M, Masliah E, Kahle PJ, Hirling H, Lashuel HA, Phosphorylation of synucleins by members of the Polo-like kinase family., *J. Biol. Chem.* 285:2807-22. 2010.

Di Giovanni S, Eleuteri S, Paleologou KE, **Yin G**, Zweckstetter M, Carrupt PA, Lashuel HA., Entacapone and tolcapone, two catechol O-methyltransferase inhibitors, block fibril formation of alpha-synuclein and beta-amyloid and protect against amyloid-induced toxicity, *J. Biol. Chem.* 285, 14941-53, 2010.

Salmon L, Nodet G, Ozenne V, **Yin G**, Jensen MR, Zweckstetter M, Blackledge M., NMR characterization of long-range order in intrinsically disordered proteins, *J Am Chem Soc.* 132: 8407-18. 2010.

Paleologou KE*, Mbefo MK, **Yin G***, Oueslati A, Fares MB, Zweckstetter M, Lashuel HA. The PD mutant E46K, but not A30P or A53T, enhances alpha-Synuclein phophorylation at S129, *Submitted*. *Equal contribution